Marquette University
e-Publications@Marquette

Dissertations (2009 -)

Dissertations, Theses, and Professional Projects

Investigation of the Mechanisms Governing Carrier Domain Translocation in S. Aureus Pyruvate Carboxylase

Joshua Hakala
Marquette University

Follow this and additional works at: https://epublications.marquette.edu/dissertations_mu

 Part of the Biology Commons

Recommended Citation

Hakala, Joshua, "Investigation of the Mechanisms Governing Carrier Domain Translocation in S. Aureus Pyruvate Carboxylase" (2019). *Dissertations (2009 -)*. 894.
https://epublications.marquette.edu/dissertations_mu/894

Investigation of the Mechanisms Governing Carrier Domain Translocation in *S. aureus* Pyruvate Carboxylase

by

Joshua H. Hakala

A Dissertation submitted to the Faculty of the Graduate School,
Marquette University,
in Partial Fulfillment of the Requirements for
the Degree of Doctor of Philosophy

Milwaukee, Wisconsin

December 2019

ABSTRACT
INVESTIGATION OF THE MECHANISMS GOVERNING CARRIER DOMAIN TRANSLOCATION IN *S. AUREUS* PYRUVATE CARBOXYLASE

Joshua H. Hakala, B.S., B.A.

Marquette University, 2019

A central debate in protein biochemistry focuses on the mechanism by which ligands contribute to conformational changes in proteins. Two primary hypotheses describe this process: the induced-fit hypothesis and the conformational ensembles hypothesis. In contrast to the induced-fit hypothesis, the conformational ensembles hypothesis states that the protein pre-exists in multiple conformational states, with ligand binding shifting the equilibrium towards a preferred conformation. The contribution of ligand binding to large-scale conformational changes is particularly relevant to multi-domain "swinging-arm" enzymes, for which pyruvate carboxylase (PC) serves as a well characterized paradigm system. PC catalyzes the ATP-dependent carboxylation of pyruvate to oxaloacetate. The biotin cofactor on the biotin carboxyl carrier protein (BCCP) domain is carboxylated via a MgATP-dependent reaction in the biotin carboxylase (BC) domain. The BCCP domain then travels to the carboxyltransferase (CT) domain where the carboxyl group is transferred from the biotin cofactor to pyruvate, generating oxaloacetate. There have been conflicting proposals for how ligand binding governs carrier domain translocation in PC but, to date, there have been no attempts to directly observe the positioning of the carrier domain independent of catalytic turnover. To directly observe the equilibrium positioning of the BCCP carrier domain, site-specific cross-linking was used to trap the BCCP domain in two separate orientations during translocation. This approach enabled a detailed analysis of how BCCP domain positioning responds to substrates and allosteric effectors. These studies show that carrier domain positioning is governed by conformational selection, with the carrier domain accessing intermolecular positions irrespective of the presence or identity of the ligand(s). Further, interactions between biotin and several conserved active site residues in both the BC and CT domains serve to shift the carrier domain positioning equilibrium. These studies offer the first compelling evidence that carrier domain positional equilibrium in PC is governed by conformational selection and offer new insights into the molecular level interactions contributing to these conformational changes.

ACKNOWLEDGEMENTS

Joshua H. Hakala

To my loving wife, Rachel Hakala, I cannot possibly express how grateful I am to you for all of your hard work and sacrifices to enable me to survive graduate school. Your love, support, cleaning, cooking, caring for the children, working your own full-time job and attending school in the early years was all noticed and sincerely appreciated, even though I did not express that enough. I could not have gotten through this without you, I love you so much.

To my parents, I am very appreciative of your sacrifices and hard work while raising me to be the man I am today. I don't know how you knew to continue to buy me a constant stream of science-related books, but those acts helped to shape me into who I am today. I am also very grateful for the example you set with your hard work ethics and decency toward everyone.

To my brothers, thank you for a memorable life growing up and a plethora of entertaining shared events. I know that no matter what happens in life, I'll have your support.

To Britt Wyatt-Mende, I also would have a difficult time expressing how grateful I am to you for everything you have taught me about teaching and being the best educator possible. I am sincerely in your debt thanks to all of the knowledge and passion for teaching that you have shared with me. I hope you land your dream teaching position after you finish up your post-doc so that you can inspire the next generation. I have also sincerely appreciated our friendship and your valuable advice throughout the years.

To Yumeng Liu, I have never had a friend like you that I could talk to about my work and interests. It was so enriching to be able to share my thoughts about my project with you and get your frank and insightful feedback. Your friendship, generosity, and always positive demeanor will never be forgotten and is sorely missed.

To my committee members, thank you for your wisdom, insights, and frank assessment of my work over the years. These contributions have all helped me to become a better student and scientist.

To Martin, there's so much an advisor and mentor does for a graduate student, I couldn't hope to adequately capture it all here. Thank you for your fairness in all interactions and support throughout the early, rough years. Thank you also for endeavoring to have a student take on this moon-shot of a project that ended up panning out better than either of us probably expected. Your boundless enthusiasm for teaching helped shape me into the educator I am and hope to be in the future as I transition to becoming a faculty member.

This dissertation is dedicated to the loving memory of my grandparents who gave me so much of their time and patience in my childhood and were so influential in shaping me into the person I am today.

TABLE OF CONTENTS

LIST OF TABLES

LIST OF FIGURES

LIST OF ABBREVIATIONS

ACoA ..... acetyl-coenzyme A
ADP..... adenosine diphosphate
ATP .....adenosine triphosphate
BC .....biotin carboxylase
BCCP ..... biotin carboxyl carrier protein
BirA..... biotin protein ligase
BMOE .....Bismaleimidoethane
CoA ..... coenzyme A
CT ..... carboxyltransferase
DEBS ..... 6-deoxyerythronolide B synthase
DQ..... D907C/Q1118C
DQE D907C/Q1118C/E243A
DQT D907C/Q1118C/T876A
DQY D907C/Q1118C/Y621A
DTT.....dithiothreitol
E-64..... epoxysuccinyl-L-leucylamido (4-guanido) butane
EGTA .....ethylene glycol tetraacetic acid
IPTG.....isopropyl 1-thio-β-D-galacto-pyranoside
ITF.....intrinsic tryptophan fluorescence
k_{cat}.....turnover rate
K_d.....dissociation constant
KNF.....Koshland, Nemethy, and Filmer
K_m ..... Michaelis constant
MWC..... Monod, Wyman, and Changeux
NAD^+ .....nicotinamide adenine dinucleotide (oxidized)
NADH .....nicotinamide adenine dinucleotide (reduced)
OAA ..... oxaloacetate
PC..... pyruvate carboxylase
PDB.....Protein Data Bank
PKS .....polyketide synthase
PMSF .....phenylmethylsulfonyl fluoride
QN..... Q891C/N1102C
QNE Q891C/N1102C/E243A
QNT Q891C/N1102C/T876A
QNY Q891C/N1102C/Y621A
*Re*PC .....*Rhizobium etli* pyruvate carboxylase
*Sa*PC .....*Staphylococcus aureus* pyruvate carboxylase
SDS-PAGE ..... sodium dodecyl sulfate polyacrylamide gel electrophoresis
TCA..... tricarboxylic acid
Tris 2-amino-2hydroxymethyl-propane-1,3-diol
v_i ..... initial velocity

I. INTRODUCTION

Chemical and physical interactions are necessary for the maintenance of life. The regulation of these interactions is critical to cellular maintenance, proper development, the prevention of disease, and successful reproduction. For example, the TCA cycle that is central to cellular metabolism must maintain a proper equilibrium of intermediates to ensure an appropriate metabolic flux into the numerous biosynthetic pathways that branch out from the main cycle. When the concentration of TCA cycle intermediates are low, they must be replenished to maintain metabolic flux and prevent deleterious outcomes. Pyruvate carboxylase (PC; E.C. 6.4.1.1), which converts pyruvate to oxaloacetate, is present in nearly all life forms, where it plays a critical role in maintaining proper flux through the TCA cycle. Aberrant PC activity is a hallmark of diseases such as Type-II diabetes and cancer (Han and Liu, 2010; Phannisil, et al., 2015).

PC has been intensely studied since its initial discovery and purification in the 1960s. Subsequent kinetic studies determined that the pyruvate carboxylation reaction occurs in two separate steps catalyzed by the same enzyme (Utter and Keech, 1960; Utter and Keech, 1963; Keech and Utter, 1963; Scrutton, Keech, and Utter, 1965). By 1981, it had been established that PC consisted of two separate active sites, like other biotin-dependent carboxylases, with a biotin cofactor tethered to a carrier domain responsible for transferring CO_2 from the first subsite to the second (Goodall, et al., 1981). Many early kinetic studies were interpreted to suggest that carrier domain translocation was induced by the binding of substrate to the second active-site (Easterbrook-Smith, et al., 1976; Goodall, et al., 1981; Attwood and Wallace, 1986). These early studies revealed

that acyl-CoA derivatives activated pyruvation carboxylation, specifically acetyl-CoA (Scrutton, Keech, and Utter, 1965). The first X-ray crystal structure of PC, from *Rhizobium etli*, clearly showed the existance of two spatially distinct active sites (St. Maurice, et al., 2007). The carrier domain with tethered biotin was also captured in a conformation between the intramolecular first active site and intermolecular second active site, suggesting an intermolecular translocation pathway for catalysis. When describing interactions between the carrier domain and another domain throughout this dissertation, the term "intramolecular" will be used when the carrier domain is interacting with a domain on its own polypeptide chain. The term "intermolecular" will be used when the carrier domain is interacting with a domain across the face of the PC tetramer on a separate polypeptide chain.

Studies over the past decade have continued to interpret results in light of an induced conformational change mechanism for carrier domain translocation, despite the lack of any direct experimental observations of carrier domain positioning. In this model, the carrier domain is proposed to remain in the vicinity of the first active site until a substrate binds in the second active site. Binding of a substrate in the second active site induces a conformational change that causes carrier domain translocation to the second active site.

This dissertation describes a series of biophysical studies designed to elucidate the effect of ligands on carrier domain positioning and to understand the mechanism that governs carrier domain positioning in PC. This enables the proposal of a new model for carrier domain translocation in PC and offers a detailed description of how ligands and

active site residues alter carrier domain positioning in this complex, multi-domain enzyme.

1. Fundamental Principles and Mechanisms of Ligand Binding to Proteins

At the core of many biological processes is a binding interaction between two or more units. Whether the target is a receptor, a strand of DNA, or an enzyme, at least two units must bind together in order for a signal to be transmitted, transcription to begin, or a reaction to be catalyzed. When considering this phenomenon in enzymes, a fundamental challenge has been to understand the mechanism that couples ligand binding with the conformational changes that result in catalysis. In 1894, Emil Fischer was the first to attempt a description of this phenomenon using the "lock-and-key" model, which views the protein as a rigid structure that must precisely fit the shape of the ligand. A second model, published by Daniel Koshland in 1958, became a lasting, canonical description of ligand binding in proteins. This model, commonly called the "induced conformational change" model, considers that the protein exists in a single conformation, similar to the "lock-and-key" model, but allows that a conformational change can occur as a result of ligand binding. Finally, in the last few decades, a model has been evolving that takes into account observed conformational heterogeneity in protein populations as well as the energy landscape theory of proteins. This model, called "conformational selection", views proteins as conformationally flexible entities and takes into account thermodynamic laws when considering conformational behavior. This section will trace the evolution of models that have been developed to explain the relationship between

ligand binding and conformational change in proteins and will apply these models to enzyme systems.

1.1 Evolution of the Ligand Binding Models

Emil Fischer's "lock and key" model was the first attempt to explain ligand binding to proteins (Fischer, 1894). In this model, the enzyme is viewed as a rigid construct that contains a binding pocket of a specific size and shape. To accommodate ligand binding, this binding pocket, the "lock", must precisely match the shape of the ligand, "the key". While this model was successful in explaining why an enzyme has specificity for a certain substrate, a failing of this model is that it does not consider conformational changes that occur throughout the enzyme and that give rise to regulatory properties. This model also does not explain how the unstable transition state is stabilized by the enzyme during catalysis.

In 1958, Daniel Koshland proposed his theory of ligand binding, commonly referred to as the "induced conformational change" model. In this model, the protein is considered to be flexible, in contrast to the rigidity that is assigned by Fischer's model. Binding of the ligand to the enzyme is allowed, even if the binding site does not perfectly fit the shape of the ligand. Upon binding, the ligand interacts with nearby residues, resulting in conformational changes that further strengthen the binding interaction. Some years later, this initial model was further expanded in a classic paper by Koshland, Némethy, and Filmer to describe cooperativity in hemoglobin, and became known as the KNF model (Koshland, et al., 1966). Hemoglobin consists of two heterodimers ($\alpha\beta$) that together form a homodimer ($\alpha_2\beta_2$), with one binding site for molecular oxygen in each

subunit, as observed in the first crystal structure of hemoglobin obtained by Perutz (Perutz, et al. 1960). Molecular oxygen binding to hemoglobin obeys a sigmoidal binding behavior. The shape of the curve indicates positive cooperativity within hemoglobin, such that when one oxygen molecule binds to one subunit of hemoglobin, a conformational change occurs, facilitating the subsequent binding of molecular oxygen to the remaining, non-oxygen-bound subunits.

Hemoglobin subunits exist in two dominant conformations, the "T" state, which has low oxygen affinity, and the "R" state, which has high oxygen affinity. When oxygen binds to the T state, a conformational change occurs that shifts the hemoglobin conformation from the T state to the R state. This relationship led to the concept of oxygen-binding cooperativity, with the affinity for oxygen of hemoglobin increasing as oxygen binds. The KNF model predicts that in the absence of oxygen, all subunits exist in the T state. Upon oxygen binding, the oxygen-bound subunit adopts the R state and induces adjacent subunits to also adopt the higher affinity R-state. Ultimately, all subunits of hemoglobin will adopt the R state in the presence of oxygen, proceeding via a sequential transition of the individual subunits (Figure I-1).

A competing model was proposed to explain cooperativity in hemoglobin by Monod, Wyman, and Changeux, referred to as the "MWC" model (Monod, Wyman, Changeux, 1965). This model relies on three assumptions that set it apart from the KNF model: (1) Hemoglobin can exist in one of only two states, T or R; (2) the state of the protein (T or R) is governed by the overall quaternary structure of the protein; (3) all of the subunits switch between states simultaneously, such that the tetramer exists either entirely in the T state or entirely in the R state. Regardless of the presence/absence of

ligands, the hemoglobin population would exist in an equilibrium with some percentage existing in the T state and some percentage existing in the R state (Figure I-1).

A major difference between these two models becomes clear when considering the conformational flexibility of the protein. According to the KNF model, the protein subunits uniformly exist in the T state in the absence of ligands. According to this model, hemoglobin cannot access the R state in the absence of oxygen. In the KNF model, conformational changes take place only as a consequence of ligand binding. Conversely, in the MWC model, the protein always exists in an equilibrium between the T and R states, so that each state is populated to some degree. In the MWC model, conformational changes precede ligand binding, shifting the population equilibrium between T and R states (Figure I-1).

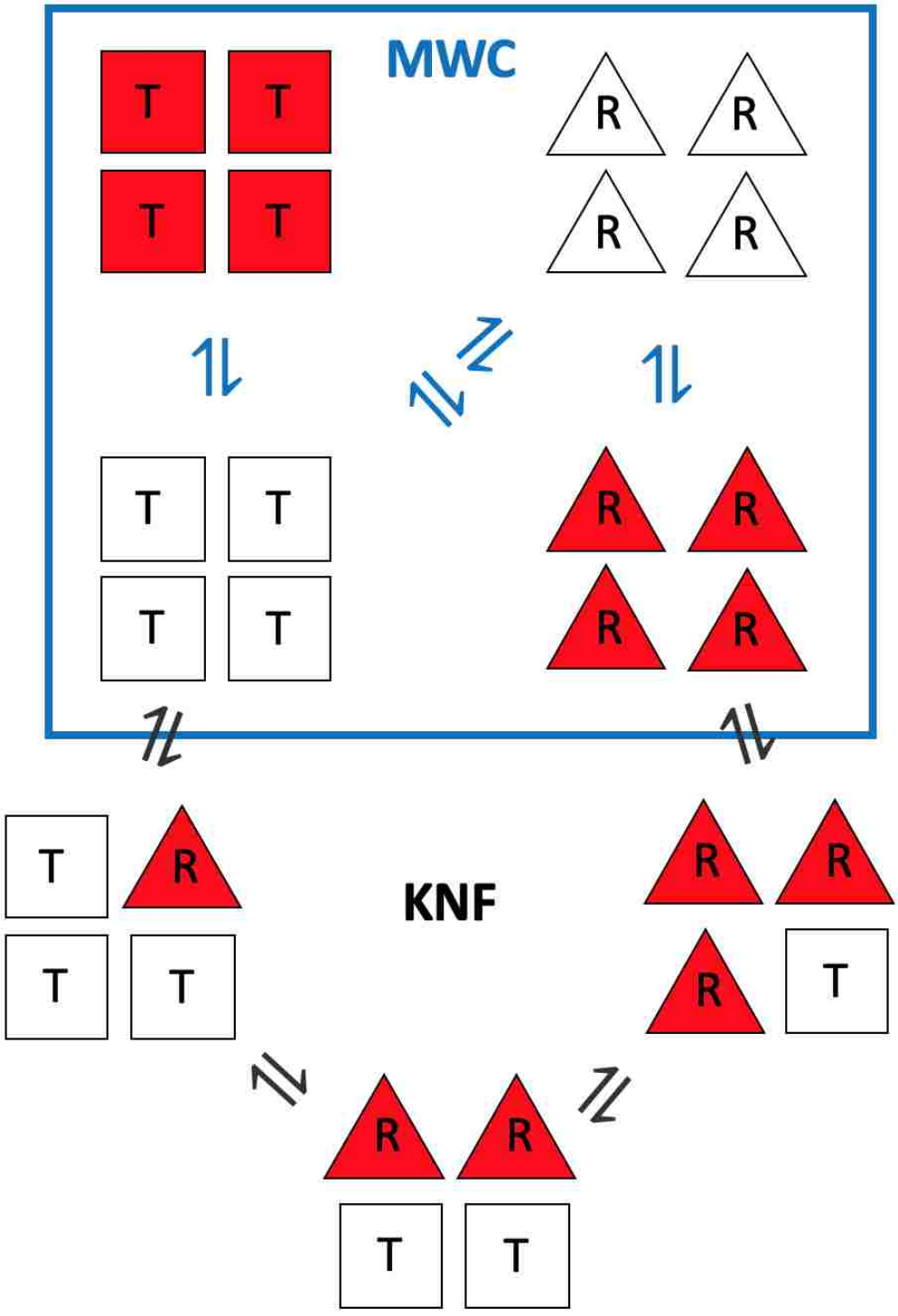

Figure I-1. Comparison between KNF model and MWC model
The low-oxygen affinity T state is represented by squares while the high-oxygen affinity R state is represented by triangles. Red fill represents the oxygen-bound state. The MWC model is contained in the blue rectangle with all subunits of hemoglobin changing conformation together and existing as a population in an equilibrium between the T and R states. The KNF model displays the sequential conformational change steps as oxygen binding induces a conformational change to the R state.

As the mechanisms underlying the thermodynamics of protein folding were coming into focus, the energy landscape theory of protein folding began to take shape. The energy landscape theory is often represented by a "protein folding funnel". According to this model, each conformation that a protein adopts has an associated free energy, with a lower free energy being more stable than a conformation with a higher free energy. As a protein folds, its free energy generally flows down the energy funnel, ultimately reaching a free energy minimum that represents the final, stable conformation of the protein. Along the path from the high-energy unfolded state to the low-energy folded state, there can be many local energy wells that stabilize the protein for a period of time. These wells can reside at energy levels far above the energetic minimum and may be deep enough to become "kinetic traps", where time and/or energy input is required for the protein to emerge and continue down the folding pathway. This protein folding landscape has also been applied to the conformational changes that take place during enzyme catalyzed turnover.

Recent models of protein conformational change have combined principles of the MWC model and the energy landscape theory into what is known as the "conformational selection" model. According to this model, a population of enzymes will exist in an ensemble of conformations, including (but not limited to) the "free" state and the "ligand-bound" state, according to a thermodynamic distribution that is driven by thermal fluctuations; those conformations with a lower free energy will be more populated (Kumar, et al., 2000, Boehr, et al., 2009). In this model, a ligand preferentially binds to a pre-existing conformation of an enzyme that has the highest affinity for the ligand, much like the lock and key model. However, ligand-binding generally results in a lowering of

the free energy for the ligand-bound state, leading to a shift in the enzyme population towards this conformation.

Since the initial studies on hemoglobin, the KNF / induced conformational change model has been applied to a range of systems, including enzymes (Michel, 2016; Corbett, P.T., et al., 2005). This model starkly contrasts with the conformational selection model in not considering flexible oscillations in enzymatic conformation prior to the ligand-binding event. More recently, many enzyme systems have been described using the conformational selection model. For example, the MWC/conformational selection model better accounts for conformational changes in aspartate transcarbamylase (Changeaux, et al., 1968; Changeaux and Rubin, 1968; Velyvis, et al., 2007), nicotinic acetylcholine receptors (Colquhoun and Sakmann, 1985; Jackson, 1984; Bertrand, et al., 1992), and G-protein coupled receptors (Lefkowitz, et al., 1993; Choe, et al., 2011; Xu, et al., 2011), while the induced conformational change model best explains conformational change in hexokinase (Bennett and Steitz, 1978) and kinesin (Kull and Endow, 2013).

1.2 Applying Ligand-Binding Models in Enzymes

The role of an enzyme in living systems is to accelerate the rate of a chemical reaction. This rate enhancement is primarily achieved through the stabilization of the high-energy transition state for the chemical reaction. In addition, an enzyme active site must bind the substrate(s) such that the substrate is optimally oriented for catalysis. Active site residues often play a dual-role: they must bind the substrate in the ground state, but they must also preferentially stabilize the high energy transition state as the substrate is converted into product. There are three major steps in any enzyme-catalyzed

reaction: the binding of substrate(s), the chemical conversion of substrate(s) into product(s), and the release of product(s). The binding affinity of an enzyme (E) with a substrate is represented by the dissociation constant, K_d but this is often difficult to measure kinetically. In most treatments, all of the microscopic rate constants that represent the formation and breakdown of the enzyme-substrate complex (ES) are collected into what is called the Michaelis constant, K_m. Finally, the maximum turnover rate, which is calculated by dividing the maximum velocity by the total enzyme concentration, is represented by k_{cat}.

The lock and key model can be described by the simple expression E + L ⇌ EL, in which the conformation of the enzyme (E) does not change throughout the binding process. In the induced conformational change model, a conformational change occurs as a result of interactions between the ligand and active site, such that the expression can be written E + L ⇌ EL ⇌ E*L, in which E* represents a different conformation of the enzyme that has a high affinity for the ligand. Finally, in the conformational selection model, a population of an enzyme would contain an ensemble of conformations with the ligand preferentially binding to the conformation with highest affinity for the ligand. This can be written E + L ⇌ E* + L ⇌ E*L (Vogt, et al., 2014). Therefore, the conformational state E* exists in the absence of ligands in the conformational selection model, while existing only in the presence of ligands in the induced conformational change model. An observation of multiple enzyme conformational states in the absence of ligands serves to experimentally support the conformational selection model in an enzymatic system.

When considering the thermodynamics of enzyme catalyzed reactions, the energetic difference between the enzyme-substrate (ES) complex at the ground-state

energy level and the high-energy transition state ($[ES]^{\ddagger}$) is represented by Gibbs free energy of activation ($\Delta G^{\ddagger}$) (Figure I-2A). Catalysis is generally accompanied by an overall reduction in $\Delta G^{\ddagger}$ for a reaction. These concepts can be applied to protein folding as well, with a distribution of conformations existing in solution, each with an associated Gibbs free energy. Generally, the lower-energy conformations will be more heavily populated than a higher-energy conformation. The free energy of a conformation can shift upon ligand binding, generally to a lower energy state which leads to an increase in the population of that state (Figure I-2B) (Boehr, et al., 2009).

This section has presented the development of ligand-binding theories and their relationship to conformational changes in proteins and enzymes. The conformational selection model embraces the thermodynamic principles and concepts of protein conformational fluidity introduced here. Rather than considering substrates and products, the free energies of interacting domains can be considered, with kinetic barriers separating the transition from one interaction to another. The thermodynamic and kinetic barriers associated with conformational changes accompanying ligand binding events can reveal fundamental information regarding the free energy landscape of an enzyme.

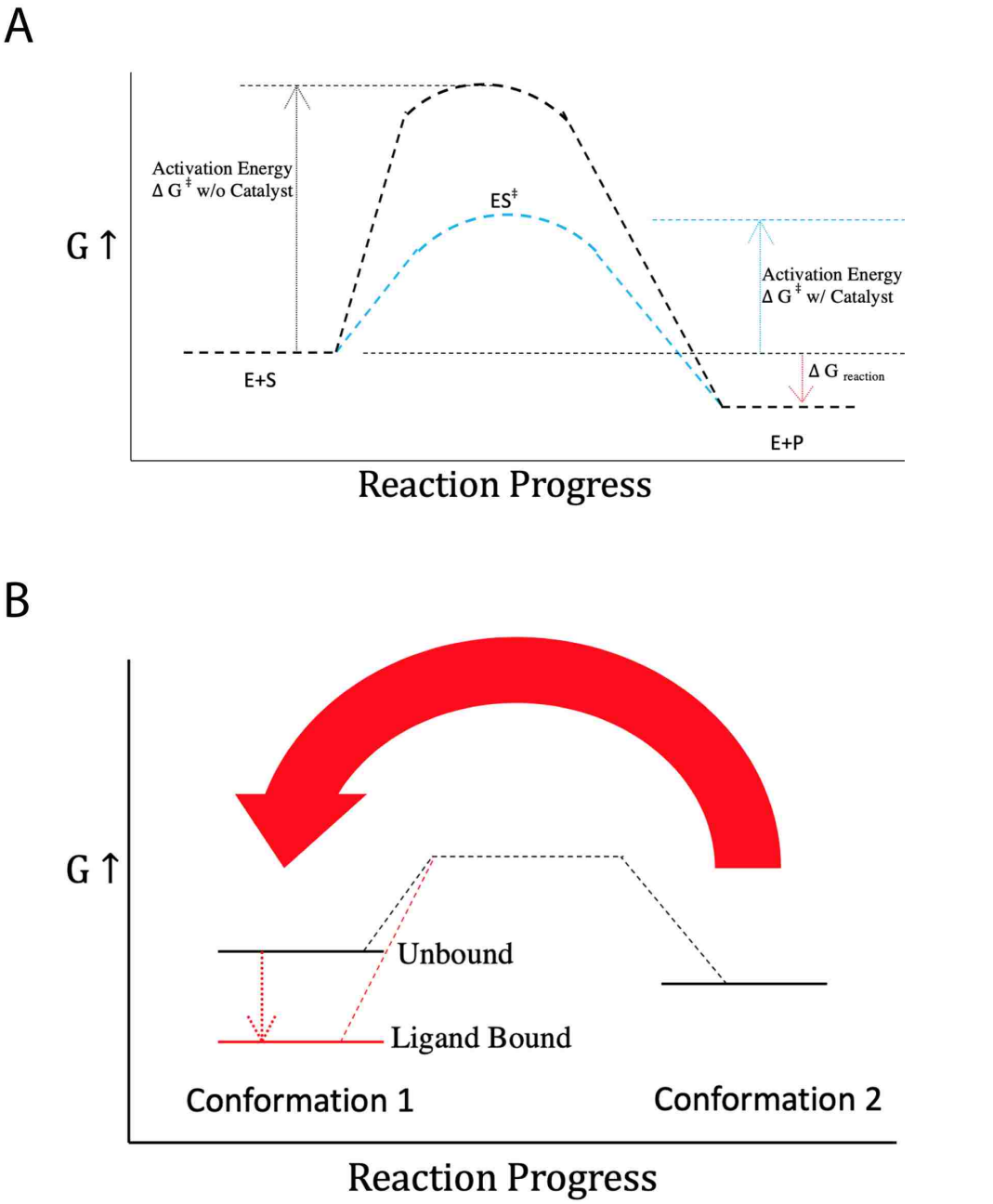

Figure I-2 Thermodynamic representation of enzymatic reactions and conformational changes. Gibbs free energy is plotted on the y-axis while reaction progress is plotted on the x-axis. **A.** The free enzyme in the presence of substrates state (E+S), high-energy transition state ($ES^{‡}$), and free enzyme in the presence of product state (E+P) are shown. The dashed lines indicate the changes in Gibbs free energy between the states with the blue line representing the enzyme catalyzed reaction and the black line the uncatalyzed reaction. **B**. The Gibbs free energy associated with two empty active sites is shown by solid horizontal black lines. Ligand binding results in a change in free energy (red). The dashed lines represent the kinetic barrier for the conformational change from Conformation 1 to Conformation 2. The thermodynamic change depicted by the decreased Gibbs free energy of the ligand bound state of Conformation 1 results in a shift in the conformational equilibrium, represented by the large red arrow.

2. PYRUVATE CARBOXYLASE

Carrier domain enzymes present a unique system in which to study the effect of ligand binding on enzyme conformation. In many enzymes, the carrier domain must translocate a relatively large distance during catalysis. However, the mechanism governing this translocation to ensure efficient transfer of intermediates between active sites is an area of active study (Perham, 2000; Lowry, et al., 2016; Khosla, et al., 2014; Zeczycki, et al., Menefee and Zeczycki, 2014). PC is a multi-domain enzyme that can serve as a model to study the relationship between ligand binding and conformational changes. It is an enzyme with a relatively simple construction, containing just two active sites and a carrier domain that bridges the individual half reactions. PC forms a tetramer of ~500 kDa, which is smaller and more easily studied than many other carrier domain systems that are often composed of larger oligomeric structures that can be more than 1 MDa in mass. PC has also been well characterized kinetically and structurally, making it an ideal system for these studies.

PC catalyzes the carboxylation of pyruvate to oxaloacetate, which serves as an anaplerotic input to the TCA cycle. The first half-reaction, which occurs in the biotin carboxylase (BC) domain, carboxylates the biotin cofactor that is tethered to the carrier domain, using bicarbonate as the carboxyl donor concomitant with the cleavage of ATP. The carrier domain translocates to the second active site in the carboxyltransferase (CT) domain, where the second half-reaction occurs. In this domain, the carboxyl group is transferred from biotin to pyruvate, forming oxaloacetate. The translocation of biotin, which covers ~70 Å, is responsible for coupling these reactions. The substrate and product of this reaction, pyruvate and oxaloacetate, are both important molecules in

metabolism. Pyruvate is the final product of glycolysis and can be funneled into several different metabolic pathways while oxaloacetate serves as one of the major inputs into the TCA cycle, which is a central pathway for oxidative metabolism. The metabolic role of PC will be briefly introduced, along with the structure and function of the individual domains of PC.

2.1 The Role of Pyruvate Carboxylase in Metabolism and Disease

Pyruvate serves as a central metabolite in what may be the most crucial crossroads in all of metabolism. It is best known as the final product of glycolysis, but it is derived from many catabolic pathways including amino acid catabolism, and lactic acid oxidation. Pyruvate can have several fates, including being shuttled into the mitochondria (in organisms containing this organelle) for entry into the TCA cycle as acetyl-CoA under aerobic conditions, fermentation into lactate or ethanol under anaerobic conditions, or transamination to the amino acid alanine (Gray, et al., 2014). When one or more biosynthetic pathways are upregulated to draw intermediates away from the TCA cycle, levels of TCA cycle intermediates decrease, which deleteriously impacts the flux in and out of the cycle. The primary role of pyruvate carboxylase is to replenish the TCA cycle intermediate oxaloacetate through the biotin-dependent carboxylation of pyruvate, thereby balancing the withdrawal of intermediates from the TCA cycle.

TCA cycle intermediates are drawn out through several biosynthetic pathways including lipogenesis, amino acid generation, nucleotide synthesis, and porphyrin biosynthesis. Citrate can be transported out of the mitochondria for conversion back to acetyl-CoA which can be used for fatty acid synthesis or the formation of the lipid

cholesterol. Succinyl-CoA is a key component in the synthesis of porphyrins, which themselves are used for the construction of hemes and other metal-binding structures. Several amino acids, including glutamate and glutamine, are derived from the TCA cycle intermediate α-ketoglutarate. Not only is glutamine incorporated into proteins, it also serves as a key precursor for the synthesis of both purine and pyrimidine nucleotides and acts as the major nitrogen carrier in vertebrates. While pyruvate is the major metabolite used in gluconeogenesis, glutamine, alanine, lactate, and glycerol can also be converted for use in gluconeogenesis (Gerich, et al., 2001). PC catalyzes the first step of gluconeogenesis with the conversion of pyruvate to oxaloacetate, which is then shuttled out of the mitochondria as malate.

Given the crucial role of PC in central metabolism, a disruption in PC expression and/or activity has been linked to a number of disease states. Pyruvate carboxylase deficiency, for example, is an autosomal, recessive disorder that ranges from benign to severe (Marin-Valencia, et al., 2010). In mice, a correlation between PC activity, pancreatic islet cell size and mass, as well as the presence of hyperglycemia has been observed, highlighting the role of PC in metabolic health (Han and Liu, 2010). PC expression is upregulated in human breast cancer tissue, where an increase in PC expression has been associated with tumor size and proliferation (Phannisil, et al., 2015). The higher metabolic demand on PC in many cancers is explained by the need for increased anaplerotic input to compensate for a higher flux through the biosynthetic pathways needed to support cellular growth and division in cancer cells (Phannisil, et al., 2015).

PC is broadly distributed among bacteria, plants, invertebrates and vertebrates (Wallace, et al., 1998). At least one microbial species, *Listeria monocytogenes* is particularly dependent on the anaplerotic role of pyruvate carboxylase. *L. monocytogenes* does not encode 2-oxoglutarate dehydrogenase, leaving *L. monocytogenes* with an incomplete, branched TCA cycle. Consequently, *L. monocytogenes* is highly dependent upon PC (encoded by *pycA* in *L. monocytogenes*) to replenish oxaloacetate, which is the only route to malate and fumarate in this incomplete TCA cycle. It has been observed that in *pycA* mutants, *L. monocytogenes* has decreased virulence in mice and cannot replicate in mammalian hosts (Schär, et al., 2010).

2.2 Structure of Pyruvate Carboxylase

In most PC enzymes, all functional domains are encoded on a single polypeptide chain (Figure I-3). The biotin carboxylase (BC) domain, site of the first half-reaction, is located at the N-terminus of the polypeptide and is linked to the carboxyltransferase (CT) domain by a helical region that forms the core of the allosteric domain. The CT domain threads back into a half beta barrel that completes the allosteric domain, which then terminates in the biotin carboxyl carrier protein (BCCP) domain.

2.2.1 Tetrameric Structure

PC forms tetramers at high concentrations, which dissociate to dimers and monomers at concentrations below 4 EU/mL (~0.13 mg/mL) (Khew-Goodall, et al., 1991; Attwood and Geeves, 2002). This process of dilution inactivation can be rescued,

to varying degrees, by the addition of the allosteric activator, acetyl-CoA, as well as by ATP and/or Mg^{2+}, both of which bind in the BC domain (Attwood, et al., 1993; Attwood and Geeves, 2002). The PC homotetramer is stabilized by contacts at each corner of the tetramer, where homodimerization interfaces stabilize identical domains to form two perpendicular faces of the tetramer, as observed in the first X-ray crystal structures of PC from *Rhizobium etli* (*Re*PC) and *Staphylococcus aureus* (*Sa*PC) (Figure I-4) (St. Maurice, et al., 2007; Xiang and Tong, 2008). These first structures revealed that the distance between active sites is ~70 Å, too far apart for biotin to reach both active sites without involving significant carrier domain translocation. A pathway of carrier domain translocation was hinted at in the *Re*PC structure with the carrier domain positioned between the intramolecular BC domain and intermolecular CT domain. After the structure was obtained, it was then experimentally confirmed that the carrier domain travels across the face of the tetramer to the CT domain on a separate polypeptide chain (St. Maurice, et al., 2007). This was further supported by the first *Sa*PC structure in which the carrier domains were observed to be interacting with the CT domain of the opposing polypeptide chain on the same face of the tetramer (Xiang and Tong, 2008).

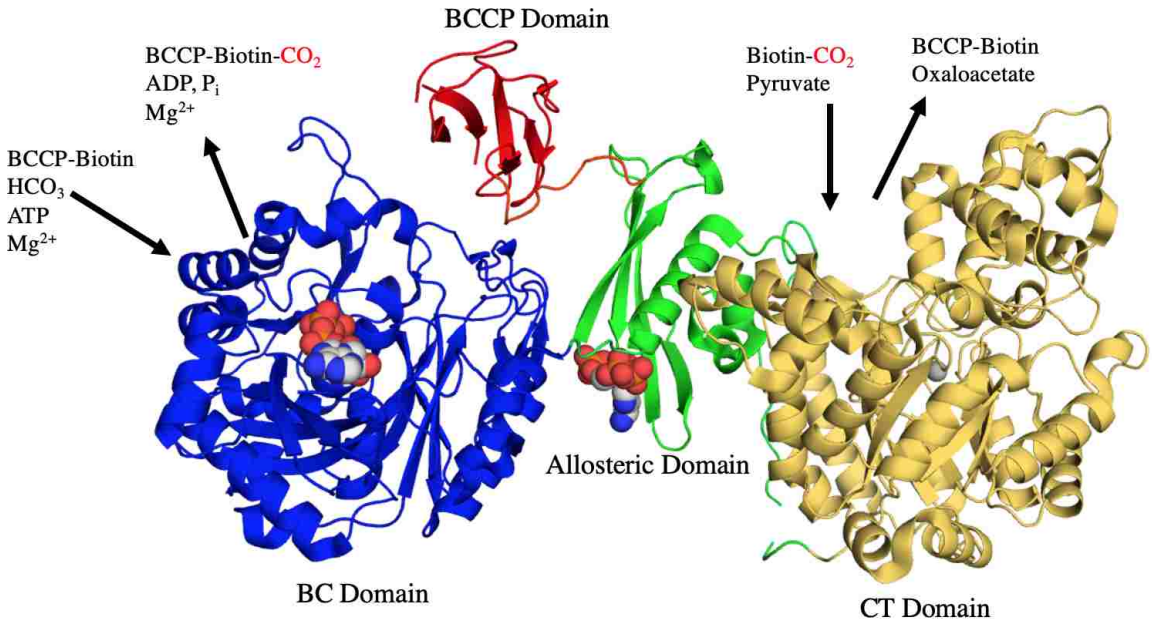

Figure I-3 *Rhizobium etli* pyruvate carboxylase monomeric structure.
Shown is the monomeric structure of *Rhizobium etli* PC. The biotin carboxylase (BC) domain is blue, the allosteric domain is green, the carboxyltransferase domain (CT) is yellow, and the biotin carboxyl carrier protein (BCCP) domain is green. The resolved nucleotide portion of ethyl-CoA is shown bound in the allosteric domain and a non-hydrolyzable ATP analog is shown bound in the BC domain.

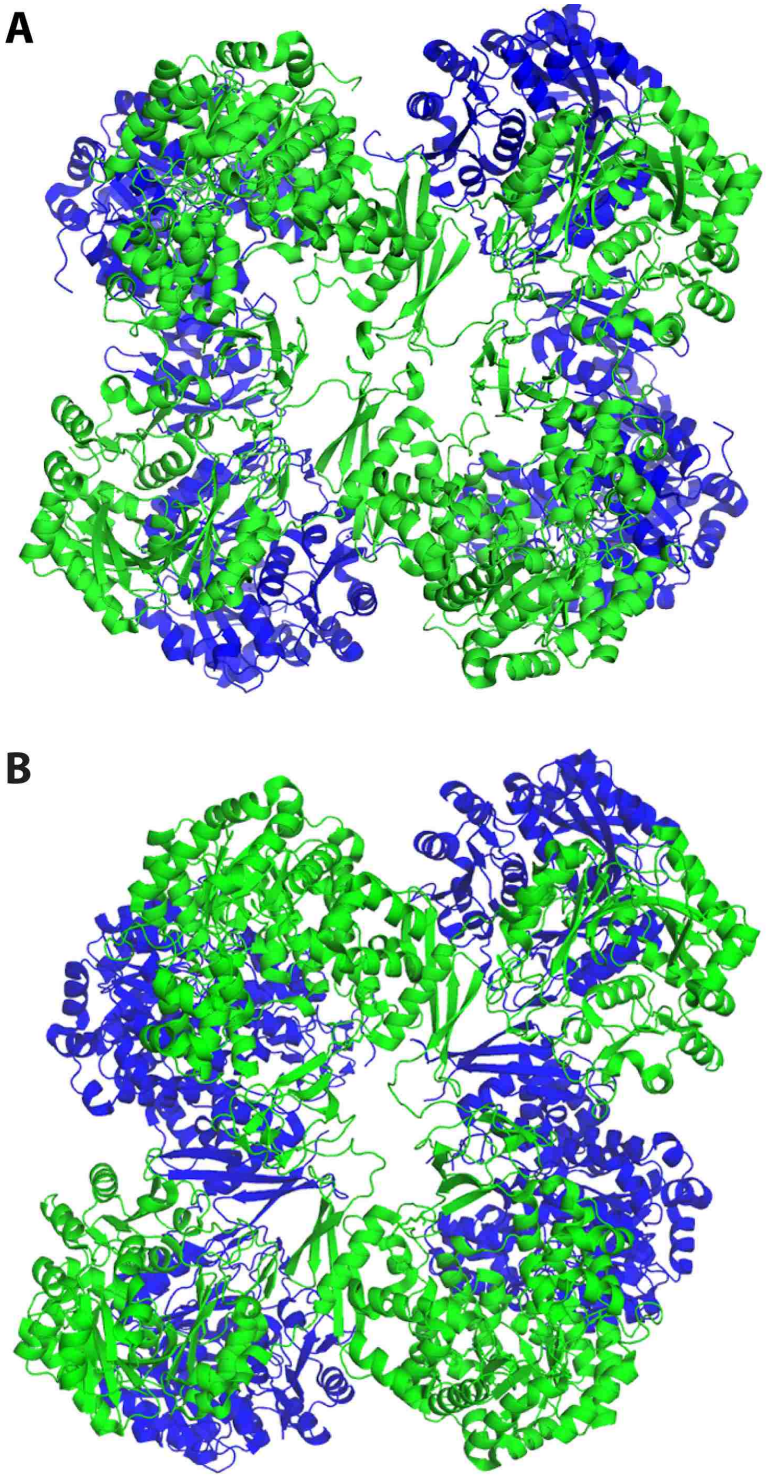

Figure I-4 Pyruvate carboxylase tetrameric structures from *R. etli* and *S. aureus*.
Shown is the tetrameric structures of *Rhizobium etli* PC (PDB ID: 2QF7) A difference between the asymmetric (*Re*PC) and symmetric (*Sa*PC) conformations are visible with the interaction of allosteric domains between faces in the symmetric conformation. (**A**) and *Staphylococcus aureus* (PDB ID: 3BG5) (**B**). The top face is colored green while the bottom face is blue.

2.2.2 Biotin Carboxylase (BC) Domain Structure

The biotin carboxylase (BC) domain is common across all biotin-dependent carboxylase enzymes. The active site in the BC domain binds Mg-ATP, with the aid of an additional magnesium ion, and bicarbonate, which donates the CO_2 for carboxylation of biotin. The structure of the BC domain is comprised of three subdomains: A, B, and C (Waldrop, et al., 1994; Broussard, et al., 2015; Tong, 2017). The A and C subdomains contribute the bulk of the BC domain, while the B-subdomain acts as a highly flexible lid that closes down on the active site in the presence of substrates (Thoden, et al., 2000). The B subdomain interacts with substrates through a glycine-rich P-loop that positions itself over the phosphate groups of ADP/ATP. In the presence of the nucleotide and Mg^{2+}, the B-subdomain combines with the C-subdomain to form the complete binding interface for the carrier domain (Thoden et al., 2000; Lietzan et al., 2011; Kondo, et al., 2004; Chou, et al., 2009; Chou, et al., 2011; Menefee and Zeczycki, 2014). Interestingly, only two specific interactions between non-conserved residues have been identified between the BC and BCCP domains (Lietzan, et al., 2011), suggesting that the interface itself between the B-subdomain lid and C-subdomain makes the most important contribution to carrier domain docking.

2.2.3 Carboxyltransferase (CT) Domain Structure

The carboxyltransferase (CT) domain of PC is less broadly distributed among the biotin-dependent enzymes, where different domains have evolved to accommodate the carboxylation of different substrates. The CT domain is composed of two subdomains: an

$\alpha_8\beta_8$ TIM-barrel core capped by a C-terminal funnel-like subdomain composed of nine α-helices that leads to the CT domain active site located at mouth of the TIM-barrel. At the near-edge of the TIM barrel, a dicationic metal ion, Zn^{2+} or Mn^{2+}, is bound that aids in the coordination and binding of pyruvate (St. Maurice, et al., 2007; Xiang and Tong, 2008; Yu, et al., 2009). The TIM barrel is a conserved structure present in members of the DRE-TIM superfamily which contains a wide range of enzymes that require the breaking or formation of C-C bonds (Frantom, et al., 2014).

The presence of pyruvate has a dramatic impact on the conformation of a flexible loop (Arg621-Asn630) within the CT domain active site (PDB ID: 4JX5) (Lietzan, et al., 2013A) (Figure I-5). In the presence of pyruvate, Arg621 (*Re*PC numbering) forms a salt bridge with the carboxyl moiety of pyruvate (Figure I-5B). Whereas, in the absence of pyruvate, Arg621 is disordered (Figure I-5A). This Arg621-pyruvate interaction corresponds with movement of the loop into a closed conformation, which rotates Tyr628 from an outward facing conformation to one where it is oriented into the active site and within hydrogen-bonding distance of Asp590 (Figure I-5B) (PDB ID: 4JX4) (Lietzan, et al., 2013A). The positioning of Asp590 is further stabilized by an interaction with the side chain of nearby Arg594. This chain of interactions directly contributes to active site conformational rearrangements upon pyruvate binding.

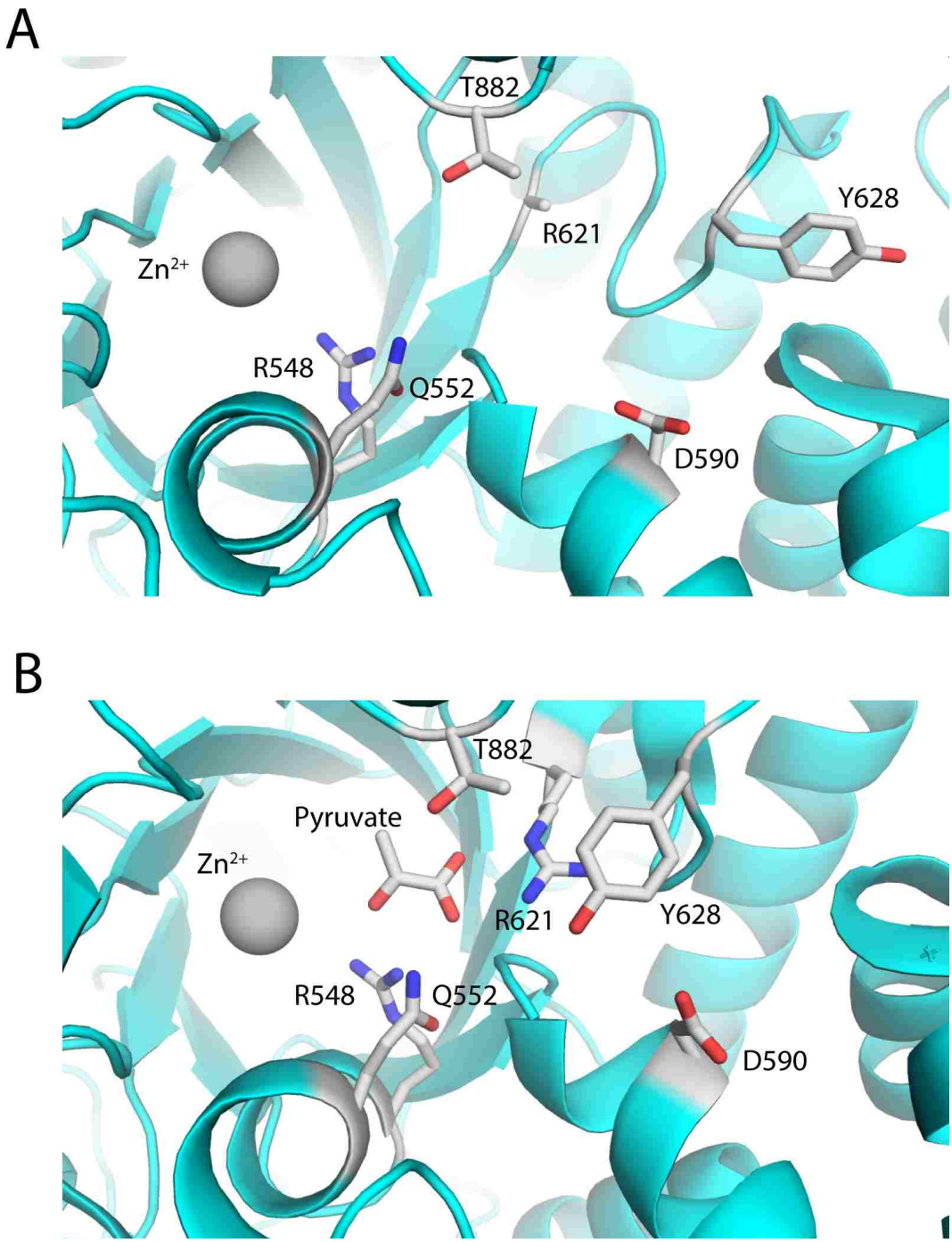

Figure I-5 *Re*PC CT domain active site structure rearrangement in the presence of pyruvate.
A. *Re*PC X-ray crystal structure in the absence (**A) (**PDB ID: 4JX4) and presence (**B**) (PDB ID: 4JX5) of pyruvate. Y628 rotates into the active site in the presence of pyruvate, providing a binding platform for biotin.

The repositioning of Tyr628 upon pyruvate binding stabilizes biotin binding in the CT domain active site through a sulfur-pi interaction between the thiophene ring of biotin and the aromatic ring of Tyr628 (Lietzan, et al., 2013A). Such interactions are predicted to contribute 1-2 kcal/mol of stabilization energy (Reid, et al., 1985; Maveyraud, et al., 1996; Zauhar, et al; 2000). The importance of these residues (Tyr628, Arg594, Asp590) to catalysis were confirmed by the near-complete loss of catalytic activity in Y628A and D590A *Re*PC mutants (Lietzan, et al., 2013A). The structure of the pyruvate binding pocket also supports the observation that α-keto acid analogues can induce carboxybiotin decarboxylation (Attwood and Wallace, 1986). Several small α-keto acids analogs bind in an identical manner to pyruvate in the active site (Lietzan and St. Maurice, 2013), stabilizing the Tyr628 biotin-binding platform and favoring the placement of carboxybiotin in the active site. Conversely, analogs lacking either the α-keto group or carboxyl group do not induce carboxybiotin decarboxylation (Attwood and Wallace, 1986).

2.2.4 Carrier Domain Structure

The crystal structure for the carrier domain from *E. coli* acetyl-CoA carboxylase, which is homologous to the PC carrier domain, was first determined in 1995 (Athappily and Hendrickson, 1995). The BCCP domain is composed of two stacked β-sheets which are each composed of four antiparallel β-strands. Located roughly midway through this domain, and projecting out from a β-hairpin turn, is the conserved biotinylated lysine. This lysine is one of four conserved residues (M<u>K</u>ME) that make up a common

biotinylation motif across all biotin-dependent enzymes (Samols, et al., 1998; Duval, et al., 1994). The carrier domain is positioned at the C-terminus of PC and is connected to the allosteric domain by a relatively long, flexible arm.

2.2.5 Allosteric Domain Structure and Function

The first X-ray crystal structure of *Re*PC, co-crystallized with ethyl-CoA, revealed the existence of the allosteric domain, which is positioned between the BC and CT domains and at the base of the carrier domain (PDB ID: 2QF7) (Figure I-3) (St. Maurice, et al., 2007). The allosteric domain has a simple composition in PC, consisting of a central α-helix covered by four antiparallel β-strands partially wrapping around it. The α-helix and β-strands are non-contiguous, with the helix originating from the C-terminal end of the BC domain and the four antiparallel β-strands located C-terminal to the CT domain. In the symmetric tetrameric conformation captured in the *Sa*PC structure, the allosteric domains of the top face of the tetramer formed a dimerization interface with the allosteric domains on the bottom face of the tetramer. Thus, this domain has also been named the PC tetramerization domain (Xiang and Tong, 2008). This domain has no strong sequence conservation in other biotin-dependent enzymes, though a very similar structural motif has been observed in several other biotin-dependent enzymes. The BT domain of acyl-CoA carboxylases is one example of a similarly structured domain that resembles the PC allosteric domain. However, rather than containing four β-strands like the PC allosteric domain, the BT domain has eight β-strands that wrap around the central α-helix (Tong, 2017)

Since the discovery and initial characterizations of PC, it was known that acyl-CoA derivatives activated PC (Scrutton, et al., 1965). Acetyl-CoA is commonly the most effective activator of PC and has been the most extensively studied, along with allosteric inhibitors such as L-aspartate. The first crystal structure of *Re*PC showed ethyl-CoA (a nonhydrolyzable analogue of acetyl-CoA) bound in the allosteric domain (Figure I-3). Acetyl-CoA is stabilized in the binding site by hydrogen bonding with two conserved arginine residues, Arg427 and Arg472 in *Re*PC (St. Maurice, et al., 2007). Mutations to these residues have an impact beyond simply affecting acetyl-CoA binding. For example, the K_m for ATP is increased by mutations to these residues. (Adina-Zada, et al., 2012). Many site-specific mutations have been made in this domain to elucidate the mechanism of allosteric activation by acetyl-CoA.

Activation by Acetyl-CoA. Soon after PC was initially purified, it was discovered that acetyl-CoA acted as an activator (Scrutton, et al., 1965). Acetyl-CoA is generated cellularly by the pyruvate dehydrogenase complex for entry into the TCA cycle or by fatty acid oxidation. As acetyl-CoA enters into the TCA cycle, it condenses with oxaloacetate, forming citrate. This is a logical feedback mechanism, in which a higher concentration of acetyl-CoA, perhaps derived from an increased flux through glycolysis, requires an increased concentration of oxaloacetate with which to condense.

Several kinetic studies have determined that the BC domain is the locus of action for acetyl-CoA. Acetyl-CoA was observed to increase the magnitude of the dissociation rate constant for fluorescent analogues of both ATP and ADP (Geeves, et al., 1995). One initial study suggested that acetyl-CoA accelerates the formation of the carboxyphosphate intermediate and ATP cleavage. ATP cleavage was also better coupled to carboxybiotin

formation in the presence of acetyl-CoA, as well (Legge, Branson, Attwood, 1996). This was supported by a more recent study in which chimeric PC enzymes constructed from two isoforms of yeast PC (PYC1 and PYC2) were investigated for their regulatory properties. Despite having different degrees and characteristics of activation by acetyl-CoA, it was determined that the BC domain was the locus of acetyl-CoA activation (Jitrapakdee, et al., 2007).

Several recent studies have suggested that the role of acetyl-CoA is not simply confined to the BC domain. A 2011 study by Zeczycki, et al. showed that, under ideal conditions, acetyl-CoA enhanced the coupling between the BC domain and CT domain reactions, reducing non-productive ATP cleavage (Zecycki, et al., 2011). Succeeding this study was a thermodynamic and kinetic study conducted in *Sa*PC to investigate the activation of acetyl-CoA. Acetyl-CoA was proposed to not only constrain the movements of the carrier domain, but also to kinetically and thermodynamically couple MgATP and pyruvate. The authors suggested that acetyl-CoA may even regulate the quaternary conformation and domain motions of PC (Westerhold, et al., 2018). This is consistent with suggestions by Sirithanakorn, et al. that acetyl-CoA may stabilize the symmetric conformation in PC, which involves a conformational change in the quaternary structure and corresponds to a repositioning of the carrier domain (Sirithanakorn, et al., 2016). However, direct observations of the effects of acetyl-CoA on carrier domain positioning or conformational dynamics of PC in response to acetyl-CoA are currently lacking.

Inhibition by L-aspartate. As a product of the TCA cycle, L-aspartate displays classic feedback inhibition of PC. Studies of L-aspartate inhibition have generally been performed in conjunction with acetyl-CoA in which L-aspartate has been observed to

reduce the degree of activation by acetyl-CoA. However, studies of PC cloned from three different species revealed that acetyl-CoA and L-aspartate binding are mutually exclusive, suggesting that they share a common binding site (Cazzulo and Stoppani, 1968*;* Osmani, et al., 1981; Sirithanakorn, et al., 2014). Supporting this, Osmani, et al. suggested the binding site to be outside of the BC active site, as its inhibition with respect to MgATP is non-competitive in *Aspergillus nidulans* PC whereas an observation of competitive inhibition would have suggested a shared binding site between MgATP and L-aspartate (Osmani, et al., 1981). Despite being mutually exclusive, the two effectors appear to have distinct binding sites: mutation of the acetyl-CoA binding site does not affect L-aspartate inhibition in *Re*PC (Adina-Zada, et al., 2012). No crystal structure has yet revealed the L-aspartate binding site, preventing a complete understanding of how L-aspartate competes with acetyl-CoA and inhibits BC domain activity.

The locus of action of L-aspartate is the BC domain and not the CT domain (Sirithanakorn, et al., 2014). L-aspartate does not affect the coupling between BC and CT domain reactions whereas acetyl-CoA greatly affects half-reaction coupling (Sirithanakorn, et al., 2014; Zeczycki, et al., 2011B). Finally, L-aspartate was observed to similarly affect all carrier domain translocation pathways in *Re*PC while acetyl-CoA preferentially activated the translocation pathway between the intramolecular BC domain and intermolecular CT domain (Liu, et al., 2018). The mechanism by which L-aspartate inhibits PC catalytic activity remains unresolved and direct observations of the effect of L-aspartate on carrier domain translocation have not been made.

2.3 Catalysis in Pyruvate Carboxylase

The carboxylation of pyruvate requires two active sites working in concert. The cleavage of ATP in the presence of bicarbonate leads to the carboxylation of the carrier domain-tethered biotin. The carrier domain must then translocate to the CT domain where it transfers the carboxyl group from biotin to pyruvate, forming oxaloacetate (Figure I-6). Each domain must stabilize biotin in the active site while preventing the abortive decarboxylation of carboxybiotin. Abortive decarboxylation can occur if pyruvate isn't present to accept the carboxyl group in the CT domain or if carboxybiotin returns to the BC domain active site and decarboxylates in the reverse reaction. The catalytic reactions and the BC domain mechanism for controlling biotin access will be introduced here. The mechanism of stabilizing biotin in the CT domain active site was discussed above.

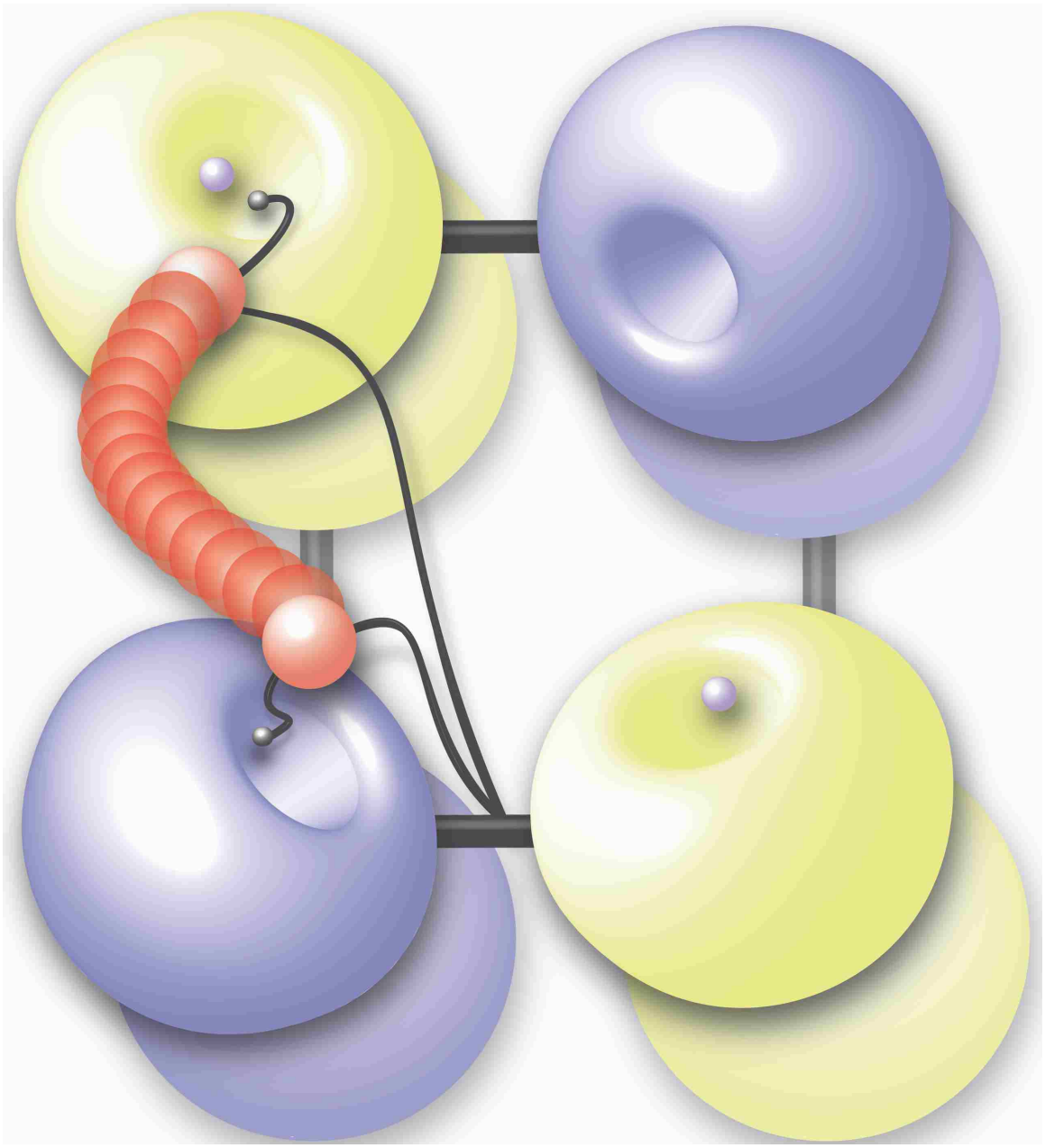

Figure I-6 Illustration of SaPC carrier domain translocation.
The *Sa*PC tetramer is shown with BC domains in blue, CT domains in yellow, and a BCCP domain in pink. Biotin is represented as a grey sphere tethered by a flexible black linker. The CT domain active site Mn^{2+} is represented by a light grey sphere. Carrier domain translocation is shown from the BC domain of its own polypeptide chain to the CT domain of the opposing polypeptide chain. Other carrier domains have been omitted for clarity. Illustration by Anya Lei Koza with creative and scientific input by Joshua H. Hakala.

2.3.1 BC Domain Function

The first step in the *Re*PC BC domain reaction occurs when Mg^{2+} and MgATP bind in the BC domain active site, which may occur in either an ordered binding process or through a rapid random equilibrium (Attwood and Graneri, 1992). To aid in proper orientation of the nucleotide, Lys245 interacts with the γ-phosphate of ATP with the positively charge Lys stabilizing the negatively charge phosphate group of ATP (Zeczycki, et al., 2011A). In turn, the positioning of Lys245 is stabilized by the formation of a hydrogen bond between the side chain of Glu218 and the amino group of Lys245 (Zeczycki, et al., 2011A). After bicarbonate binds, the first chemical step is the deprotonation of bicarbonate. Glu305 acts as a general base in the deprotonation of bicarbonate, which is promoted by hydrogen-bonding to Glu218 (Zeczycki, et al. 2011A). This highlights the dual-purpose of Glu218, which was further supported when the E218A mutation in *Re*PC resulted in a complete loss of catalytic activity (Zeczycki, et al., 2011A). The γ-phosphate of ATP undergoes a nucleophilic attack by the "activated" bicarbonate. This is proposed to form a carboxyphosphate intermediate, along with ADP (Ogita and Knowles, 1988). This highly unstable carboxyphosphate intermediate breaks down to CO_2 and inorganic phosphate (PO_4^{3-}). However, at this stage, the N_1 position of biotin would still be protonated and unable to react with CO_2. The phosphate liberated from ATP cleavage has been proposed to deprotonate the N_1 position of biotin, priming it for the final electrophilic attack by CO_2 (Menefee and Zeczycki, 2014). The proposed mechanism for the BC domain reaction is summarized in Figure I-7.

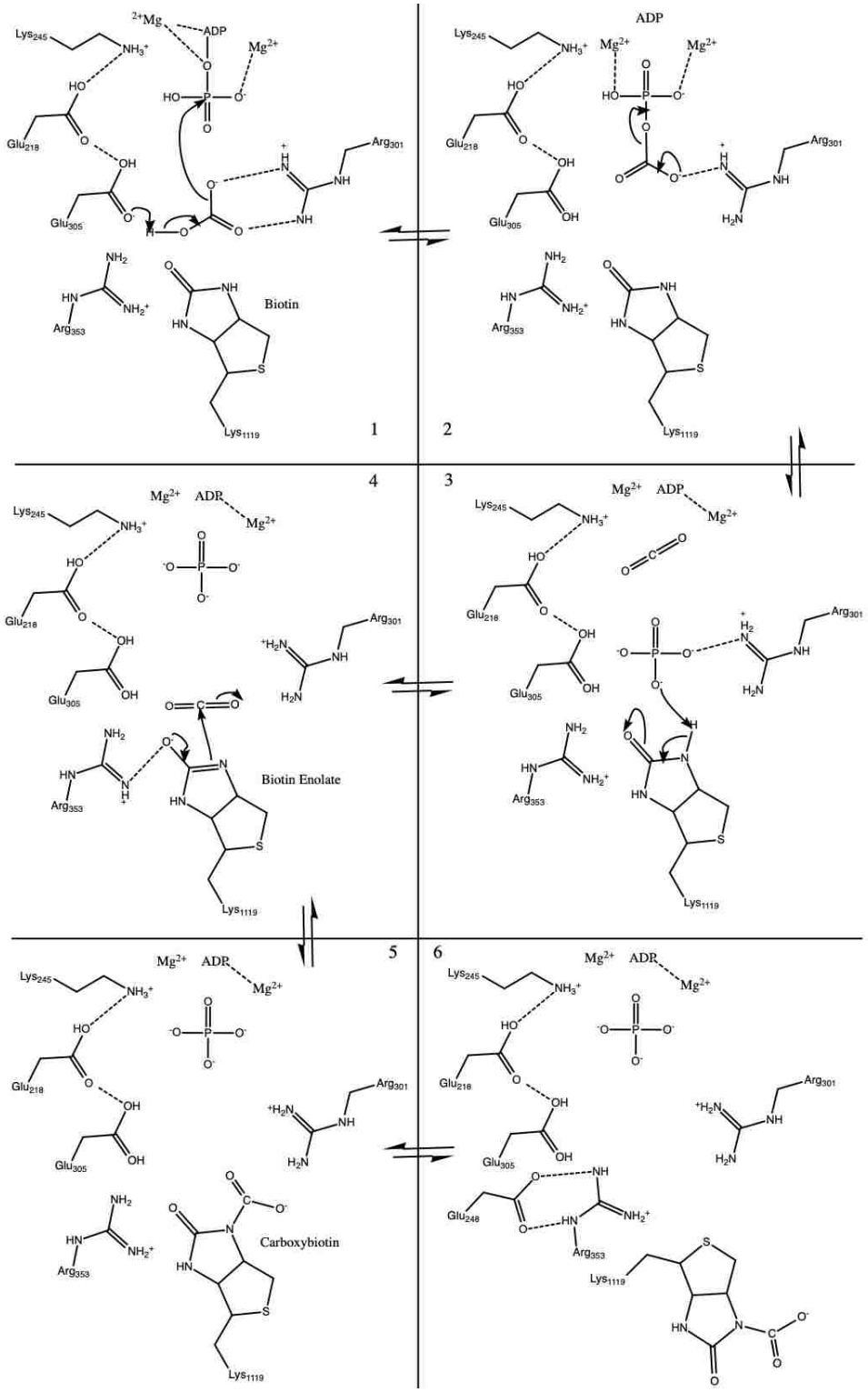

Figure I-7 BC Domain Mechanism
Shown is the proposed mechanism of the BC domain. Adapted from Zeczycki, et al., 2011A.

To aid in the positioning of the inorganic phosphate in close proximity to biotin, Arg301 has been proposed to behave as a general base catalyst in promoting the proton transfer from the N_1 position of biotin to the phosphate. The deprotonation of the N_1 of biotin results in the formation of a biotin enolate, which is stabilized by Arg353 (Zeczycki, et al., 2011A). This mechanism was further supported by the dramatically reduced ability of the R353M *Re*PC mutant to catalyze the formation of carboxybiotin (Zeczycki, et al., 2011A). When the biotin enolate breaks down, a nucleophilic attack is initiated on the electrophilic carbon of CO_2, resulting in the final carboxybiotin product.

A mechanism to control carboxybiotin access to the BC domain active site has also been proposed. A T882A *Re*PC X-ray crystal structure co-crystallized with ADP and phosphonoacetate shows the carrier domain docked with the BC domain (PDB ID: 3TW6) (Lietzan, et al., 2011). In this structure, biotin does not project into the active site. Instead, biotin is removed and pointing away from the active site. In this structure, Glu248 and Arg353 interact through a salt bridge, forming a "gate" that appears to block the entry of biotin to the active site. This Glu248-Arg353 interaction has been proposed to prevent the abortive decarboxylation of biotin. This proposal was supported by the observation that, when these residues were mutated, it led to increased rates of ADP phosphorylation, increased rates for the reverse BC domain reaction, and decreased coupling efficiency between the BC and CT domain reactions (Lietzan, et al., 2011; Lietzan et al., 2013B; Zeczycki, et al., 2013).

2.3.2 CT Domain Function

The CT domain is responsible for properly orienting and binding carboxybiotin in the active site, stabilizing the formation of the biotin enolate during the decarboxylation of biotin, binding pyruvate, and stabilizing the formation of the enol-pyruvate intermediate as pyruvate carboxylation is underway. To accomplish this, there are two separate regions in the vicinity of the active site. The N-terminal subdomain provides all residues necessary for pyruvate binding and enolization while the C-terminal subdomain provides the residues that bind carboxybiotin and stabilize the biotin enolate.

In *Re*PC, after carboxybiotin is bound in the active site, biotin decarboxylates, leading to the formation of a biotin enolate intermediate (Figure I-8). The developing negative charge on the ureido oxygen is stabilized by Gln844, Ser885, and the polypeptide backbone amide of Lys866 (Zeczycki, et al., 2009). In the next step, Thr882 donates a proton to the N_1 position of biotin which then, in a concerted manner, abstracts a proton from the methyl group of pyruvate (Sheng and Liu, 2014). This action leads to the generation of the pyruvate-enol intermediate, which is stabilized by the positively-charged active site Zn^{2+}. Finally, the enol-pyruvate breaks down to promote a nucleophilic attack on the carbon of CO_2, completing the carboxylation of pyruvate (Zeczycki, et al., 2009).

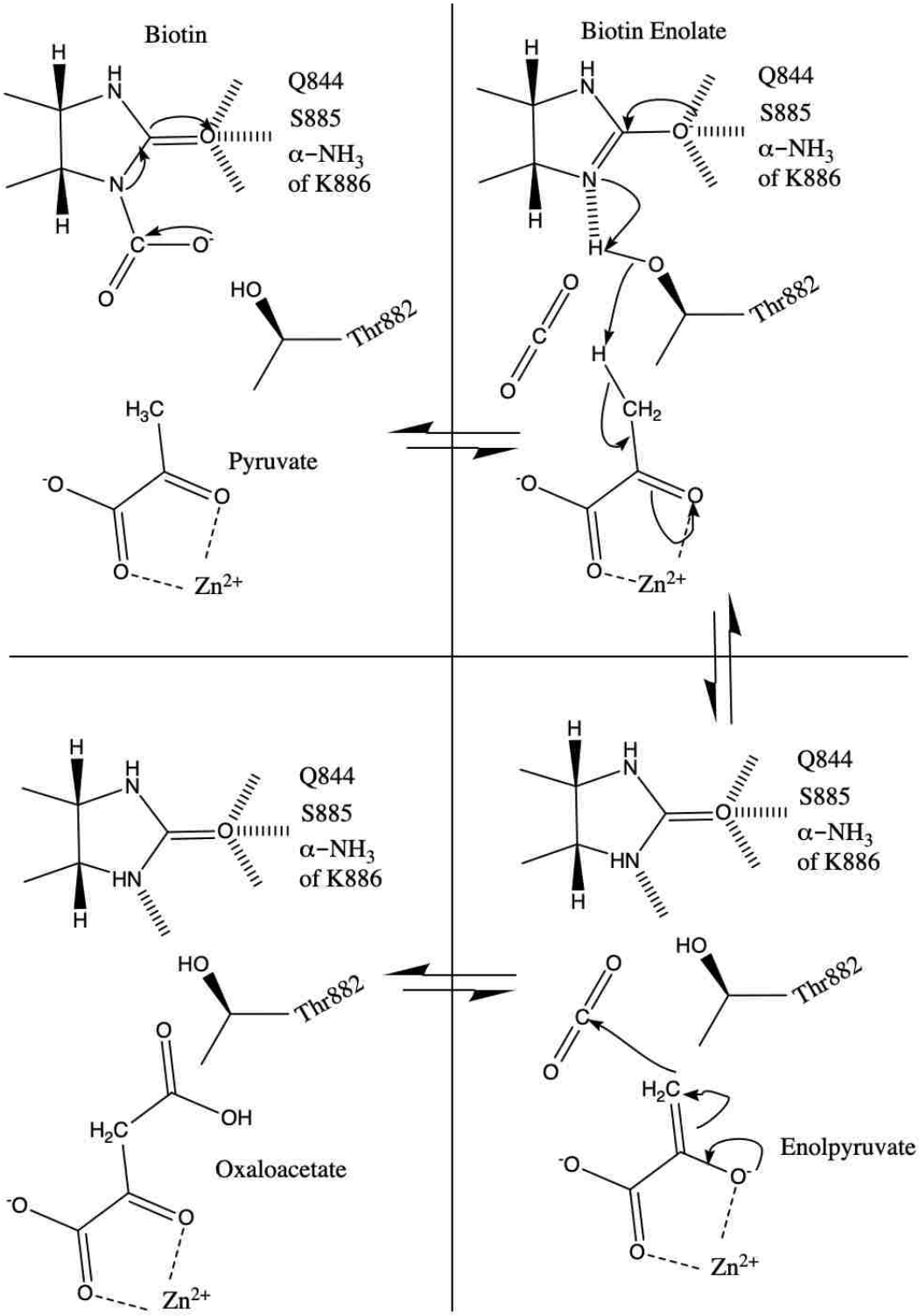

Figure I-8 CT Domain Mechanism
Shown is the proposed CT domain mechanism. Adapted from Zeczycki, et al., 2009.

2.4 Conformational Changes in PC Associated with Catalysis

Many kinetic studies on PC have attempted to provide insights into how carrier domain positioning contributes to catalytic turnover. Based on increased rates of carboxybiotin decarboxylation in the presence of CT domain ligands, it was suggested that CT domain ligands induce the translocation of the carrier domain from the BC domain to the CT domain (Easterbrook-Smith, et al. 1976; Goodall, et al., 1981; Attwood and Wallace, 1986). This led to a model in which the carrier domain was proposed to occupy two different positional states in or near the BC domain in the absence of CT domain ligands, with a third state representing carboxybiotin translocation to the CT domain for rapid decarboxylation (Easterbrook-Smith, et al., 1976; Goodall, et al., 1981; Attwood and Wallace, 1986). These initial models assumed that the carrier domain did not translocate to the CT domain or occupy any other conformations near the CT domain in the absence of a CT domain ligand. More recent structural and kinetic studies have revealed a high inherent flexibility to the carrier domain (Adina-Zada, et al., 2019, Liu, et al., 2018), suggesting that this assumption may not hold to be true.

In 2011, Zeczycki, et al. observed that, in the presence of saturating pyruvate and acetyl-CoA, the ratio of phosphate release to oxaloacetate formation was 1:1 in *Re*PC. Recall that in the BC domain, ATP cleavage occurs concomitantly with biotin carboxylation, which produces ADP and inorganic phosphate, which is released after the reaction is complete. Oxaloacetate is the product of the CT domain reaction. Therefore, the observation that the ratio of phosphate release to oxaloacetate formation was near unity indicates an efficient coupling of these two reactions. In the absence of acetyl-CoA, the half-reactions become highly uncoupled, with much more P_i released than

oxaloacetate formed (Zeczycki, et al., 2011B). Thus, acetyl-CoA plays a crucial role in establishing catalytic efficiency in PC, but the mechanism for this enhancement was still unknown. Recently, a kinetic study using a system of hybrid tetramers of *Sa*PC with inactivated BC or CT domains was used to suggest that pyruvate and acetyl-CoA facilitate long-range communication throughout the tetramer and induce carrier domain translocation (Westerhold, et al., 2016). Westerhold, et al. also discovered that acetyl-CoA thermodynamically couples MgATP and pyruvate, while this coupling is abolished in the absence of acetyl-CoA, further suggesting a role for acetyl-CoA in long-range communication between active sites. In addition, acetyl-CoA decreased the activation entropy in *Sa*PC, suggesting that acetyl-CoA constrained the motions of the carrier domain (Westerhold, et al., 2017). Finally, a study of carrier domain translocation pathways demonstrated that, in *Re*PC, acetyl-CoA activates the catalytic pathway for carrier domain translocation from the intramolecular BC domain to the intermolecular CT domain whereas the allosteric inhibitor, L-aspartate, did not influence any one translocation pathway over any other (Liu, et al., 2018).

Several structural studies have been performed which have helped to understand the role of acetyl-CoA on PC structure. Initial electron microscopy studies revealed that the tetrahedral shape of PC adopts a tighter conformation in the presence of acetyl-CoA or pyruvate (Attwood, et al., 1986). *Re*PC was captured in an asymmetric conformation with the BC and CT domains on opposing polypeptide chains on one face of the tetramer 65 Å apart and 80 Å apart on the opposite face. The carrier domain in this conformation of PC was located in the vicinity of the BC domain in the presence and absence of acetyl-CoA (St. Maurice, et al., 2007). Conversely, the symmetric conformation was captured in

*Sa*PC with the opposing active sites approximately 75 Å apart. In the symmetric PC conformation, the carrier domain was positioned in the vicinity of the CT domain in the absence and presence of acetyl-CoA (Xiang and Tong, 2008; Yu, et al., 2009). When combined, these structures highlight the difficulty in assigning any specific conformation to the presence of acetyl-CoA. In 2010, a cryo-EM study of *Sa*PC observed several different conformational states of PC in the absence of active turnover. These conformational states supported suggestions that the carrier domain interacts with the BC domain on the same polypeptide chain (intramolecular) and the CT domain of the opposing polypeptide chain (intermolecular) (Lasso, et al., 2010). Finally, a cryo-EM study was performed in which *Sa*PC samples undergoing catalysis were frozen and analyzed for conformational variability (Lasso, et al. 2014). It was discovered that there were populations of *Sa*PC that adopted the symmetric conformation and populations that adopted the asymmetric conformation, demonstrating that PC can adopt both conformations during catalysis. These two conformations appeared to capture PC in the process of catalyzing the two separate half-reactions, with PC oscillating between these two states during the catalytic cycle. Each state, symmetric or asymmetric, correlated with specific carrier domain positions. Interestingly, asymmetric PC displays only two acetyl-CoA binding sites whereas symmetric PC contains four binding sites, suggesting that acetyl-CoA may regulate the adoption of these conformational states (Lasso, et al., 2014).

3. CARRIER DOMAIN ENZYMES AND CONFORMATIONAL CHANGE STUDIES

Pyruvate carboxylase belongs to a large class of multi-domain enzymes that utilize a prosthetic group aboard a carrier domain to transport an intermediate between active sites. Multifunctional enzymes and multi-enzyme complexes of this class are similar in that they catalyze multi-step reactions in spatially distinct active sites and require a carrier domain to physically couple their activities. While the prosthetic group carrying the intermediates may differ, the core function of efficiently transporting intermediates from one active site to another is conserved. The prosthetic groups participating in these reactions provide two benefits. First, the intermediate is prevented from diffusing away into solvent or being captured by a different system due to the covalent bond with the prosthetic group. Second, the flexible nature and length of these groups and the carrier domains allow the prosthetic group to reach and access distant active sites while maintaining high local concentrations for the reactive intermediates (Perham, 2000). The prosthetic groups of the enzymes discussed here and shown in Figure I-9 include biotin (biotin-dependent enzymes), phosphopantetheine (polyketide synthases), lipoic acid (pyruvate dehydrogenase complex), and the amino acid cysteine (which acts as a prosthetic group for the carrier protein in the bacterial sulfur oxidation pathway).

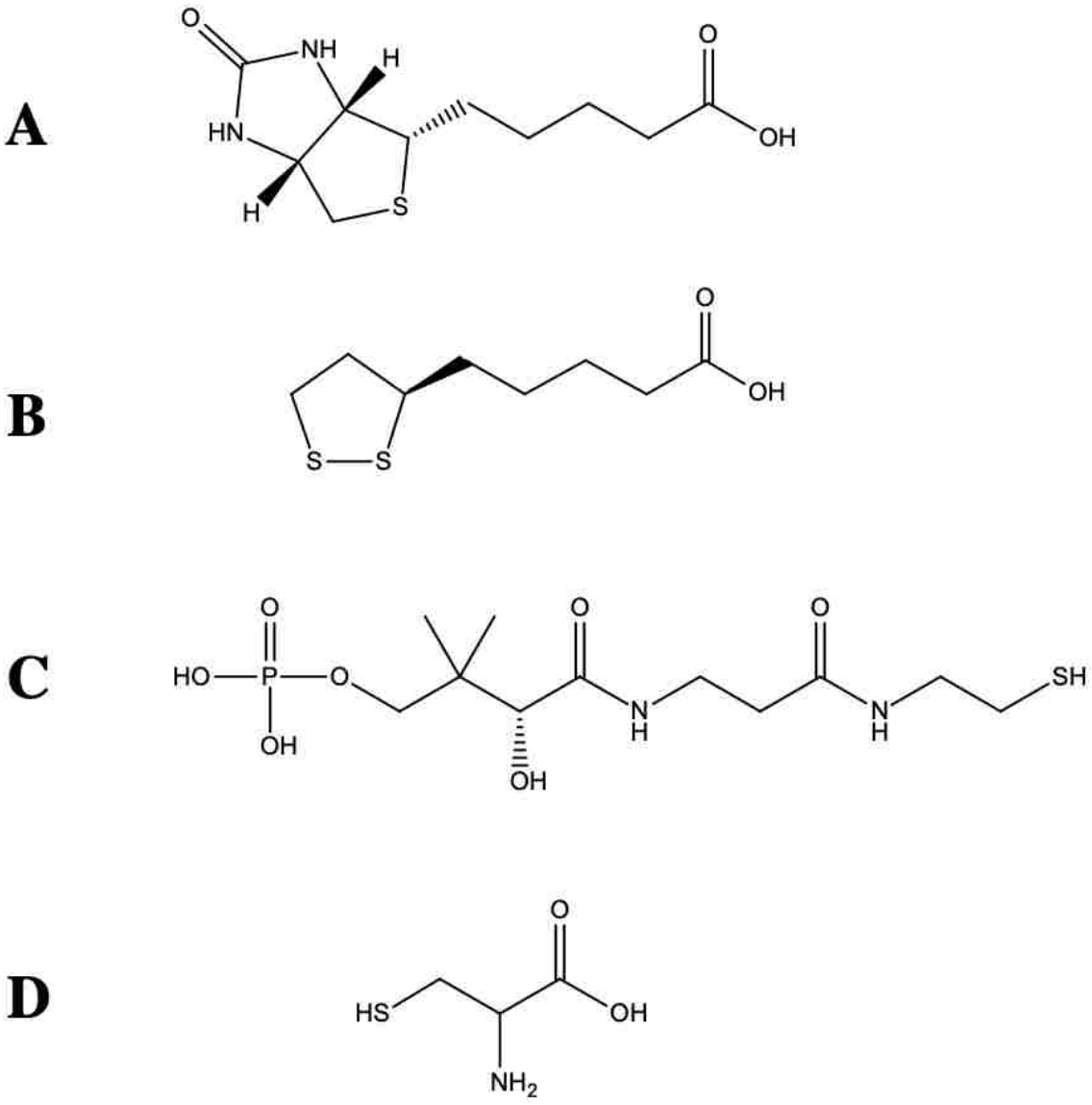

Figure I-9 Prosthetic Group Structures
Several prosthetic groups utilized by carrier domain enzymes are shown. **A.** Biotin **B.** Lipoic Acid **C.** Phosphopantetheine **D.** Cysteine

3.1 Biotin-Dependent Enzymes

Biotin was first discovered as an agent that reduced the toxicity of raw egg whites to humans in 1936. The “toxin” responsible for this toxicity was the protein avidin, which

irreversibly binds biotin. This strong interaction has proven useful, as avidin has been used in studies of biotin-dependent enzymes for decades as well as in a variety of biotechnological applications. (Waldrop, et al., 2012; Diamandis and Christopoulos, 1991). As exemplified above, the biotin cofactor is utilized by carrier domain enzymes for the transport of carbon dioxide in transcarboxylation reactions. Biotin is composed of a ureido ring fused to a tetrahydrothiophene ring with a valerate side chain. The cofactor is covalently tethered through a pseudo-peptide linkage to a specific lysine side-chain in biotin-dependent enzymes. Biotin participates in three types of enzyme-catalyzed reactions. The first reaction, exemplified by PC, is ATP-dependent carboxylation. The second reaction type occurs in a class of enzymes that couple sodium transport in anaerobes to the decarboxylation of β-keto acids (Dimroth and Hilbi, 1997). The third reaction type is catalyzed by a large assembly of polypeptides called transcarboxylase. In this unusual reaction, transcarboxylase transfers a carboxyl group to pyruvate from methylmalonyl-CoA, forming oxaloacetate and propionyl-CoA (Wood, et al., 1963). Pyruvate carboxylase was extensively described in section 1.2. This section will focus on a related, well-characterized biotin-dependent carboxylase that catalyzes the ATP-dependent carboxylation of acetyl-CoA.

Acetyl-CoA carboxylase (ACC) catalyzes the ATP-dependent carboxylation of acetyl-CoA to malonyl-CoA. The product of this reaction is a key precursor in fatty acid biosynthesis, as well as in the biosynthesis of some polyketides. Like PC, ACC is composed of at least three major domains: the BC domain, CT domain, and BCCP domain.

Prokaryotic ACCs function as assemblies of individual subunits while eukaryotic ACCs include all functional domains on a single polypeptide chain (Cronan Jr., et al., 2002). Eukaryotic ACCs also contain two additional domains: a large central domain (CD) and a BC-CT (BT) interaction domain (Wei and Tong, 2015). The BC domain of ACC catalyzes the ATP-dependent carboxylation of the biotin-cofactor and is structurally and functionally similar to the BC domain in PC and all other biotin-dependent carboxylases. More uniquely, the BC domain of ACC is also subject to regulation and conformational dynamics. In eukaryotic ACC, the BC domain is only catalytically active as a dimer. Large conformational changes have been observed in the BC domain dimer interface in crystal structures comparing the BC domain dimer and monomer (Wei and Tong, 2015; Shen, et al., 2004). During catalysis, the BC domains from two different polypeptide chains come together to form an active dimer. In the monomeric form, a flexible loop occupies part of the BC-BCCP binding interface while, in the dimer, this loop is not in a position to obstruct this binding interaction (Wei and Tong, 2015). This illustrates one mechanism of controlling biotin access to an active site. However, in either the open conformation or the dimerized BC domain conformation, the distance between BC and CT domains is greater than 110 Å. This is much larger than the observed separation of active sites in other biotin-dependent enzymes and is too large to be bridged by carrier domain translocation alone (Hunkeler, et al., 2016).

The central domain of single-chain ACCs has only recently been structurally characterized and have been found to be quite dynamic and an important point of regulation (Hunkeler, et al., 2016). This domain does not directly bind substrates or catalyze any reactions, but instead plays a large regulatory role in the dynamics of ACC.

The CD domain is positioned between the BC and CT domains and serves as the attachment point for the BCCP domain. The central domain is regulated by phosphorylation of a regulatory loop at the interface between two smaller subdomains. Phosphorylation stabilizes the loop and restricts conformational flexibility. While the regulatory role of the CD domain has been related to BC domain dimerization, its proximity and physical connection to the carrier domain may be important. However, there have been no direct attempts to relate the conformational dynamics of the BC, CD, and BCCP domains in ACC. Especially absent to date are studies of how carrier domain dynamics relate to catalysis in ACC, making this recent study on the effects of phosphorylation on conformational dynamics our best understanding of conformational dynamics in ACC.

3.2 Crosslinking Studies of Polyketide Synthase

Polyketide synthases (PKSs) are massive, multi-modular enzyme complexes that catalyze the production of a diverse range of natural products. PKSs operate like an assembly line, passing an intermediate product between multi-domain modules to catalyze very specific, ordered reactions to generate elaborately decorated natural products. Due to the complex nature of the final product, these reactions must maintain exquisite directionality. There are many open questions regarding the structure and organization of the modules, the mechanism ensuring proper reaction directionality, and the mechanism behind conformational changes in these enzymes. Given the size of these complexes, many of the standard biochemical and biophysical approaches are

inaccessible in these systems. Currently, no X-ray crystal structure of a complete PKS module has been determined.

6-deoxyerythronolide B synthase (DEBS) is a PKS that operates as an $\alpha_2\beta_2\gamma_2$ homodimer and has been extensively studied in recent years. X-ray crystal structures of individual domains and lower-resolution techniques such as cryo-EM and small angle X-ray scattering (SAXS) has contributed to a better understanding of this system in recent years (Robbins, et al., 2016). A DEBS module, which is a homodimer, is composed of at least a ketosynthase domain (KS), an acyltransferase (AT) domain, and an acyl-carrier protein (ACP). Some modules also contain a ketoreductase domain (KR) and/or a TE domain, which cyclizes the 14-membered product. An ACP domain can interact with either AT domain in the homodimer. Interestingly, the ACP domain only participates in chain elongation with the intermolecular KS domain but prefers the intramolecular KS domain during chain translocation (Robbins, et al., 2016). Previous work has demonstrated that protein-protein interactions play an important role in transporting intermediates between modules, but there is no direct evidence to explain the reason for the preferred ACP domain associations during catalysis.

While no studies have reported directly on ACP domain positioning, one recent study has shed light on a mechanism related to ACP domain translocation. This study was designed to reveal how the assembly line-style process of catalysis is synchronized to keep the directionality of reactions proceeding in the proper direction. Protein interactions between various DEBS domains were captured by crosslinking in the presence/absence of substrates. This study ultimately revealed a mechanism that prevents more than one polyketide chain from being bound to an active site of the same module.

This mechanism, dubbed the “turnstile mechanism”, prevents KS domain acylation of the next polyketide chain until the previous chain elongation product has moved downstream by virtue of the ACP domain transferring it to a downstream module. To summarize, the KS domain active site is closed until the growing polyketide chain that has just finished interacting with the KS domain is transported to the next module, ensuring proper directionality of the multi-step reaction and correct product formation. However, the molecular underpinnings of this mechanism have not been established and the role of conformational changes in this system is not yet known (Lowry, et al., 2016).

3.3 Sulfur Oxidation Enzyme Interactions Explored by Disulfide Bond Formation

The microbial oxidation of sulfide to sulfate for energy generation in bacteria can follow two pathways: the sulfide:quinone oxidoreductase pathway or the Sox pathway. The Sox pathway utilizes a heterodimeric carrier protein SoxYZ that uses a Cys residue to carry various sulfur-containing species for catalysis by multiple enzyme partners. Since SoxYZ does not co-purify with any Sox enzymes, it has been suggested that these interactions between SoxYZ and the active-site containing partners are weak and transient (Rother, et al., 2001). Prior to a 2015 study by Grabarczyk, et al., there have been no specific interactions between the carrier protein and other Sox enzymes discussed in the literature. However, a highly conserved loop on the surface of SoxYZ, termed the “Z-loop”, was proposed to play a role in interactions between SoxYZ and its partners (Sauvé, et al., 2007).

The 2015 study by Grabarczyk, et al. investigated the interactions between SoxYZ and SoxB, a Sox pathway enzyme, using crystallography, biophysical techniques,

and molecular modelling (Grabarczyk, et al, 2015). One of these techniques involved mutating an active site residue to a cysteine that would form a disulfide bond with the carrier protein cysteine, trapping the interacting pair together for further analysis. SoxYZ interacts with SoxB at several places on the surfaces of each protein. When the SoxY carrier arm is inserted into the tunnel leading to the active-site of the SoxB enzyme, hydrogen-bonding interactions occur in the active-site tunnel and at the base of the carrier arm. In this scenario, a surface loop on SoxB is positioned to rest in a pocket on the SoxZ surface through stabilizing hydrophobic and electrostatic interactions. While a description of these interactions contributed to a greater understanding of the molecular interface between SoxB and SoxZ, they did not provide an explanation for how the dissociation of the carrier arm facilitates interactions with other Sox enzymes. Structural and kinetic data suggest that Arg416 in the SoxB active site undergoes an induced conformational change in the presence of the sulfonate-containing substrate. In the absence of substrate, Arg416 forms an ion pair with a mobile loop near the active site. This mobile loop sterically clashes with SoxY insertion into the active site, disfavoring binding in the absence of substrate. When SoxY-substrate binds, the mobile loop is displaced, freeing Arg416 to interact with the sulfonate-group on the carrier domain, further disfavoring interaction with the mobile loop. After catalysis, the sulfonate-group is lost, favoring the return of the Arg416-mobile loop interaction. This disfavors SoxY binding, freeing the carrier domain to dissociate and interact with other Sox enzymes. This protein-protein interaction resembles the Tyr621-biotin interaction proposed in the CT domain of PC as a way to stabilize the carrier domain in a catalytically-relevant conformation.

3.4 A FRET Investigation of a Nonribosomal Peptide Synthetase

Nonribosomal peptide synthetases (NRPSs) produce peptide-based natural products such as the antibiotic vancomycin or the immunosuppressant cyclosporin A. The genes for these enzymes are typically arranged in an operon in bacteria and as a gene cluster in eukaryotes. NRPSs operate as a series of modules, much like polyketide synthases, with each module containing multiple domains to catalyze various chemical steps and the addition of amino acids to the growing peptide. The aminoacyl or peptidyl intermediate is transferred between domains or modules using a central peptidyl-carrier-protein (PCP) domain. The PCP domain has a 4'-phosphopantetheine with a terminal sulfhydryl group which covalently binds the aminoacyl or intermediate for transport. Crystal structures have shown that only one catalytic site is within range of the prosthetic group, indicating that the PCP domain must translocate. However, prior to 2017, no observations of PCP domain translocation had been made, nor was it clear how carrier domain positioning is governed.

In 2017, conformational changes within gramicidin synthetase I from *Aneurinibacillus migulanus* were investigated using FRET (Alfermann, et al., 2017). The construct of gramicidin synthetase I investigated was composed of two domains, the catalytic A domain and the PCP carrier domain. The A domain is a member of the acyl-CoA synthetase, NRPS adenylation domain, luciferase enzyme (ANL) superfamily (Marahiel, et al., 1997; Gulick, A.M., 2009). This domain catalyzes the activation of an amino acid with ATP, forming aminoacyl adenylate (amino acid-AMP) and pyrophosphate (PP_i), and covalently attaches it to the terminal cysteine of the PCP domain. In a full gramicidin synthetase I enzyme, the PCP domain would then interact

with an upstream or downstream module for peptide bond formation or chemical alterations of the intermediate peptide. The A domain is composed of two subdomains: the N-terminal A^N and C-terminal A^C, connected by a short linker (Conti, et al., 1997). In the absence of substrate, these domains do not strongly interact and adopt an open conformation. In the presence of substrate, a closed conformation is adopted with active sites forming at the interface between the domains.

In the FRET study, EGFP was fused to the C-terminal portion of the PCP domain while a cysteine was introduced in the A domain which was labeled with an appropriate fluorophore to generate a FRET signal when interacting with EGFP. It was observed that gramicidin synthetase I adopts multiple conformations in solution with the conformational equilibrium shifted by ligand binding. Large concentrations of PP_i, one of the products of the reaction catalyzed by the A domain, inhibited forward progress in catalysis by favoring the adoption of a specific conformation, disfavoring conformations required for further catalytic steps. Separately, the PCP-bound thioester intermediate was proposed to have high affinity for a downstream catalytic domain, ensuring proper direction of peptide synthesis (Linne and Marahiel, 2000; Mootz and Marahiel, 1997; Belshaw, et al., 1999). Taken together, these mechanisms offer insight into how these complex enzymatic systems may control carrier domain translocation and reaction progress.

3.5 Trapping the Acyl Carrier Protein of a Fatty Acid Synthase

Fatty acid synthesis generally refers to the production of long-chain fatty acids using acetyl-CoA and NADPH. This process is catalyzed by a series of enzymes that

perform chain elongation and chemical modifications to achieve specific end products. An acyl carrier protein is used to transport the growing fatty acid between enzyme active sites throughout the reaction cycle. This carrier protein utilizes phosphopantetheine as the prosthetic group that covalently bonds to the fatty acid chain. These enzymes are of interest for their potential to be used in biofuel synthesis, as well as antibiotic development (Finzel, et al., 2015). As in other carrier domain enzyme systems, there are many open questions regarding the mechanism that controls fatty acid length and how the acyl carrier protein (ACP) selectively binds to the "correct" downstream enzyme (Finzel, et al., 2015).

A recent study re-engineered ACPs with covalently bound substrate analogues of different lengths, for investigation with FabA, an enzyme in the microbial fatty acid synthesis pathway that performs a dehydratase reaction with a specific preference for fatty acid chains 8-12 carbons long. To investigate how this enzyme selects for a substrate of a specific length and interacts with the carrier protein, a crosslinking system was developed to trap ACP-substrate complexes bound to FabA (Finzel, et al., 2015). This study revealed three relevant regions. A positively charged area on the surface of FabA, which was proposed to form the ACP binding interface, was confirmed to play a crucial role in binding ACP. Two phenylalanines at the opening of a tunnel leading to the active site contributed favorable hydrophobic interactions with fatty acid chains of longer lengths. Finally, the morphology of the active site pocket was determined to impact the length of the fatty acid chain that selected for catalysis. Constriction of the pocket through mutagenesis of residues lining the pocket led to less interaction with longer fatty acid chains (Finzel, et al., 2015). Taken as a whole, these findings are similar to PC in

that protein-protein interactions are proposed to stabilize the carrier domain-active site complex (BC and CT domain of PC) while active site residues may restrict access of the prosthetic group to the active site (BC domain arginine and glutamate of PC).

3.6 Pyruvate Dehydrogenase Complex Lipoyl Domain Interactions Investigated by Crosslinking

The pyruvate dehydrogenase complex (PDC) catalyzes the production of acetyl-CoA and NADH from the decarboxylation of pyruvate. This is a central enzyme in metabolism, controlling the carbon flux from glycolysis into the TCA cycle and maintaining glucose homeostasis. The PDC is a massive, unwieldy complex that is composed of duplicates of three catalytic enzymes, referred to as E1, E2, and E3. There are generally multiple E1 and E3 units bound to each E2 unit. The E2 enzyme, dihydrolipoyl transacetylase, utilizes lipoic acid as the prosthetic group of the carrier domain that transfers an acetyl group to CoA, forming acetyl-CoA (Patel, et al., 2014).

A study in 2006 in which the bovine dodecahedral E2 core domain was crystallized in the absence/presence of acyl-CoA revealed a gating mechanism to control substrate access to the active site. These structures revealed that CoA binding favors a conformational change that opens up the opposite side of the active site channel, allowing a second substrate to bind (Kato, et al., 2006). Recently, the first high-resolution structure of the E2 core (*H. sapiens* E2) was obtained using cryoEM (Jiang, 2018). This structure revealed a similar gating structure to that observed in bovine E2, suggesting that these two E2 cores behave similarly.

A recent study combined crosslinking of the carrier domain to catalytic domains with mass spectrometry to analyze the interaction frequency in the absence/presence of CoA (Prajapati, et al., 2019). This study revealed that the presence of CoA increased carrier domain interaction with the E2 domain and the downstream E3 active site. The authors interpreted this to suggest that substrate binding affected the sampling of catalytic conformations. However, given the lack of high-resolution structures of the lipoyl carrier domain interacting with the E1, E2, and E3 catalytic domains, much remains to be discovered about how its translocation is controlled, such as exactly how the conformational change promoted by CoA binding affects interactions with the carrier domain, how the organization of interactions between the carrier domain and many surrounding active sites is controlled, and how substrate binding in the E1 and E3 domains might affect lipoyl domain binding (Yu, et al., 2008) (Prajapati, et al., 2019).

4. OVERVIEW

PC is an important enzyme of central metabolism, providing a critical anaplerotic input for a variety of biosynthetic reactions. PC also serves as an important paradigm in which to study mechanisms of allosteric regulation and the relationship between ligand-binding and large-scale domain movements. There have been numerous studies over the past ~50 years focused on kinetically characterizing the enzyme function, understanding the effect of acetyl-CoA on the enzyme structure and function, and describing the overall PC catalytic cycle in great detail. The results of all of these studies, at some level, are dependent on carrier domain translocation. The carrier domain bridges the individual reactions in each of the two active sites during catalysis, translocating a relatively large

distance in the process. While many studies have interpreted carrier domain behavior indirectly from kinetic or structural data, the mechanism governing the translocation of the carrier domain is perhaps the least understood phenomenon in PC. In this section, I will highlight the major questions related to carrier domain translocation in PC and outline how this dissertation will contribute to clarifying the relationship between ligand binding and carrier domain positioning in PC.

In early kinetics studies of pyruvate carboxylase, CT domain ligands were shown to enhance the decarboxylation of carboxybiotin, presumably in the CT domain (Easterbrook-Smith, et al., 1976; Goodall, et al., 1981; Attwood and Wallace, 1986). These results were, understandably, interpreted to suggest that CT domain ligands induced carrier domain translocation to the CT domain and that, in the absence of these ligands, the carrier domain remained in the vicinity of the BC domain. Under ideal conditions, acetyl-CoA was observed to efficiently couple the BC domain half-reaction with the CT domain half-reaction, suggesting that acetyl-CoA plays a key role in mediating carrier domain translocation (Zeczycki, et al., 2011B). More recently, a kinetics-based study in *Sa*PC has suggested that pyruvate and acetyl-CoA facilitate long-range communication that serve to induce carrier domain translocation (Westerhold, et al., 2016). Acetyl-CoA has also been shown to reduce the activation entropy in *Sa*PC, suggesting that the conformational flexibility of the carrier domain is constrained by acetyl-CoA (Westerhold, et al., 2017) However, none of these studies have directly demonstrated that carrier domain translocation is induced by ligand binding, nor have they offered a mechanism for the role that acetyl-CoA plays in affecting carrier domain translocation. Meanwhile, various structural studies have proposed an alternative to the

induced conformational change mechanism in PC, where local conformational changes are sufficient to alter the domain positioning (Lietzan, et al., 2011; Lietzan, et al., 2013A).

This dissertation describes a detailed effort to investigate the mechanism governing carrier domain translocation. I have focused on *directly* observing the positioning of the carrier domain through the use of crosslinking traps, in order to capture the carrier domain in two distinct intermolecular conformations. The effects of substrates and effectors on carrier domain positioning are also investigated to more thoroughly investigate the mechanism governing carrier domain positioning and to better understand the molecular interactions responsible for shifting the positional equilibrium. Decades of prior studies have interpreted carrier domain translocation using the induced conformational change model, which was developed prior to the modern description of thermodynamics in protein folding and conformational change. Prior to the studies outlined in this dissertation, there had been no attempts to directly observe carrier domain positioning in PC. Crystal structures suggest an alternative to the induced conformational change model for controlling carrier domain positioning by revealing potential interactions between active site residues and biotin which may favor/disfavor biotin access to these active sites (Lietzan, et al., 2011; Lietzan, et al., 2013A). However, these static structures do not capture the dynamic interplay between ligand binding and shifts in the carrier domain positional equilibrium. While there is clear evidence to support that CT domain ligands stimulate carboxybiotin decarboxylation, the induced conformational change model is not required to explain these observations. Similarly, while acetyl-CoA has been observed to accelerate the rate of reactions catalyzed in the BC domain, the

relationship between this allosteric activator and carrier domain positioning has not been explored. This dissertation will outline research that is focused on directly determining the mechanism behind carrier domain translocation and the role of ligands in shifting carrier domain positioning.

This study was performed entirely with PC cloned from *Staphylococcus aureus* PC (*Sa*PC). This was considered an ideal choice since several X-ray crystal structures exist with the carrier domain positioned in two different intermolecular interactions: one with biotin positioned in the CT domain active site and the other structure with biotin positioned in the exo-binding site (Xiang and Tong, 2008). *Sa*PC is also responsive to acetyl-CoA activation (Yu, et al., 2009) has been studied kinetically (Yu, et al., 2009) and has recently been used to study the kinetic and thermodynamic effects of acetyl-CoA on *Sa*PC activation (Westerhold, et al., 2016; Westerhold, et al., 2017).

Based on the studies described in this dissertation, I propose that carrier domain positioning in PC is governed by the conformational selection model. Regardless of the presence or absence of ligand(s), the carrier domain repositions itself into various intermolecular conformations. This is in direct opposition to the induced conformational change model. Ligands shift the equilibrium positioning of the carrier domain, with biotin playing the primary role in the sensitivity of the carrier domain to these ligands. Residues that have been proposed to interact with biotin and which serve to favor/disfavor positioning of biotin in either the CT or BC domain active sites are observed to shift carrier domain positioning and alter the kinetic barriers to carrier domain translocation. Acetyl-CoA favors carrier domain positioning away from the BC domain by reducing a kinetic barrier to translocation in the presence of substrates and by

thermodynamically favoring this intermolecular repositioning. BC domain substrates have a kinetic and thermodynamic effect on carrier domain translocation, shifting carrier domain positioning towards the BC domain, while pyruvate has the opposite effect, thermodynamically and kinetically favoring translocation of the carrier domain to adopt an intermolecular position. These combined studies revolutionize our understanding of carrier domain translocation in PC by offering the first direct observations of carrier domain translocation and positioning, offering alternative explanations to several previous interpretations of carrier domain behavior. This work highlights the great potential for PC to serve as a paradigm system in which to study the relationship between ligand binding, catalytic turnover and large-scale domain rearrangements in complex enzyme systems.

II. MATERIALS AND METHODS

Acetyl-CoA was purchased from Crystal Chem, Inc. (Elk Grove Village, IL) and CoALA Biosciences (Austin, TX). Sodium phosphate (mono- and di-basic), potassium phosphate (mono- and di-basic), ammonium chloride, Tris buffer, L-arabinose, D-glucose, glycine, bis-tris propane, DL-dithiothreitol (DTT), sodium dodecyl sulfate (SDS), ethylene glycol-bis(β-aminoethyl ether)-N,N,N′,N′-tetraacetic acid (EGTA), chloramphenicol, glycerol, and granulated Luria broth were purchased from Research Products International Corp. (Mount Prospect, IL). Kanamycin sulfate was purchased from VWR (Dublin, Ireland) and Gold Biotechnologies (Olivette, MO). D-biotin was purchased from VWR (Dublin, Ireland). Epoxysuccinyl-L-leucylamido(4-guanido) butane (E-64) was purchased from Research Products International Corp. (Mount Prospect, IL) or Gold Biotechnologies (Olivette, MO). Pepstatin A and dimethyl sulfoxide was purchased from Fisher Scientific (Waltham, MA). Sodium chloride, malic dehydrogenase, and lactate dehydrogenase were purchased from Sigma Aldrich (St. Louis, MO). 30% acrylamide/bis solution, tetramethylethylenediamine (TEMED), Coomassie Brilliant Blue G-250 and R-250 were purchased from Bio-Rad (Hercules, CA). 4× Laemmli SDS loading buffer and triethanolamine hydrochloride were purchased from Alfa Aesar (Haverhill, MA). Glacial acetic acid was purchased from MilliporeSigma (Burlington, MA). Methanol was purchased from Avantor (Radnor, PA). *Staphylococcus aureus* (*Sa*PC) PC was previously cloned into a modified pET-27b vector and was generously supplied by Dr. Liang Tong, Columbia University (12). The masses of reagents used were measured by Mettler Toledo XS2002S or Mettler Toledo XS105 balances (Columbus, OH).

SaPC Mutagenesis, Expression, and Purification. All *Sa*PC genes were expressed and purified in an identical manner. Mutations in *Sa*PC were generated according to the Agilent Quikchange II Site-Directed Mutagenesis protocol. Primers were obtained from Integrated DNA Technologies. All constructs used in this study were confirmed by DNA sequencing of the gene in its entirety by Functional Biosciences, Inc. (Madison, WI). The primers used for mutagenesis are shown in Appendix A, Figure VIII-1 and were synthesized by Integrated DNA Technologies (Coralville, IA). Each PCR reaction tube for mutagenesis had a total reaction volume of 28 µL with consisted of 2.5 µL of 10× ammonium buffer, 0.5 µL each of a 10 µM stock of the forward and reverse primer, 5 µL DNA template (50-100 ng/µL plasmid DNA), 0.5 µL dNTP (from 10 mM stock), 0.5 µL Premium Bullseye PR DNA polymerase obtained from Midwest Scientific (Valley Park, MO), and 19 µL of sterile, distilled and deionized water. The PCR reaction for mutagenesis was performed in several steps. Step 1: 95 °C for 3 minutes, Step 2: 95 °C for 50 sec., Step 3: 3-5 °C below lowest T_M of primers for 50 sec., Step 4: 72 °C for 14 min., and Step 5: 72 °C for 7 min. Steps 2-4 were repeated 18 times before Step 5 was initiated. After mutagenesis, 1 µL of Dpn1, obtained from New England Biolabs (Ipswich, MA), was reacted with the PCR reaction product for 3 hours at 37 °C to digest the original DNA template before transformation. Electro-competent *E. coli* Top10 cells were used for transformation by electroporation. 50-100 ng of plasmid was added to the 50 µL of Top10 cells on ice. This mixture was transferred to a frozen electroporation cuvette with a 1 mm electroporation gap and electroporated at 1600V in an Eppendorf Electroporator 2510. 1 mL of Luria broth was added immediately after transformation, transferred to a sterile tube, and the cells were allowed to recover at 37 °C for 45 mins. –

1 hour before plating on a Luria Broth agar plate with 25 µg/mL kanamycin. DNA was purified from the Top10 cells using the Promega Wizard *Plus* SV Miniprep Kit following the included spin purification protocol obtained from Promega (Fitchburg, WI).

Glycerol stocks were created by mixing 700 mL of overnight culture, incubated at 37 °C, with 300 µL of 50 % (v/v) sterile glycerol and stored at -80°C.

All PC clones were co-transformed and co-expressed with the pCY216 vector encoding *Escherichia coli* biotin protein ligase A (BirA) to ensure complete biotinylation of PC. Transformed *E. coli* BL21 (DE3) cells were cultured in M9 minimal media with 25 µg/mL kanamycin and 30 µg/mL chloramphenicol at 37 °C to an optical density (OD_{600}) of 0.8 - 1.0, after which protein expression was induced by the addition of isopropyl 1-thio-β-D-galactopyranoside (IPTG) and L-arabinose to a final concentration of 0.5 mM and 25 mM, respectively. The culture was also supplemented with D-(+)-biotin at a final concentration of 3 mg/L. Induced cells were incubated at 16 °C for 16 - 24 hours before harvesting by centrifugation at 6000 rpm for 15 min. at 4 °C.

All *Sa*PC enzymes were purified using sequential Ni^{2+}-affinity and anion exchange chromatography. Harvested cell paste (20 – 30 g) was re-suspended in 200 mL lysis buffer (20 mM Tris-HCl pH 7.8; 200 mM NaCl; 0.5 mM EGTA; 5 mM imidazole; 6 mM β-mercaptoethanol; 1 mM PMSF; 1 µM pepstatin A; and 5 µM E-64). Cells were lysed by sonication for 10 minutes at a temperature, monitored by a thermoprobe in the lysate, between 4-10 °C and pelleted by centrifugation at 20,000 rpm for 30 mins at 4 °C. A Branson Model 450 Digital Sonifier with a model 102-c converter and a ½" diameter Tapped Bio Horn was used for the sonication. The supernatant was loaded on a 5 mL Ni^{2+}-nitrilotriacetic acid profinity resin column (Bio-Rad, Hercules, CA). The column

was washed with 12× column volume of wash buffer (20 mM Tris-HCl pH 7.8; 200 mM NaCl; 0.5 mM EGTA; 20 mM imidazole; 6 mM β-mercaptoethanol) and the protein was eluted with a gradient from 20 mM to 250 mM imidazole using wash buffer and elution buffer (20 mM Tris-HCl pH 7.8; 200 mM NaCl; 0.5 mM EGTA; 250 mM imidazole; 6 mM β-mercaptoethanol). Purified protein was pooled and dialyzed against a buffer compatible with anion-exchange chromatography (20 mM triethanolamine, pH 8.0; 50 mM NaCl; 1 mM EGTA; and 2 mM dithiothreitol (DTT)) at 4 °C overnight. The dialyzed protein was loaded onto a 10 mL Q-Sepharose Fast Flow resin column (GE Healthcare), washed with 10x column volumes of dialysis buffer and eluted from the column in dialysis buffer with a gradient from 50 mM to 1 M NaCl. SaPC typically elutes between 400 - 800 mM NaCl. The purified protein was pooled and dialyzed against storage buffer (20 mM Bis-Tris Propane, pH 7.2; 15 mM NaCl; 10 mM $MgCl_2$, and 1 mM TCEP) for three successive changes of 4 hours or more. The protein was concentrated to a final concentration of 4 mg/mL − 10 mg/mL and was drop frozen in liquid nitrogen prior to storage at -80 °C. Concentration was achieved by using Amicon Ultra-15 100K centrifugal filters from MilliporeSigma. Centrifugation was conducted at 4,000 rpm and All protein concentrations were determined using the predicted extinction coefficient corresponding to absorbance at 280 nm.

Mutagenesis Rationale. The Q891/N1102 and D907/Q1118 pairs were chosen for mutagenesis to cysteines for crosslinking due to their proximity (< 8 Å) for crosslinking based on the 3BG5 *Sa*PC crystal structure, as well as their general lack of conservation (Xiang and Tong, 2008). Y621, E243, and T876 were mutated all mutated to alanine to ensure consistency with previous studies of these mutations in literature (Lietzan, et al.,

2013A, Lietzan, et al., 2011, Zeczycki, et al., 2009). V1062 was determined from the 3BG5 crystal structure of *Sa*PC to represent an amino acid near the base of the carrier domain suitable for truncation of the carrier domain. TAG was chosen for the stop codon introduced as it required the least number of nucleotides to be mutagenized of the three available stop codons (TAG, TAA, TGA). W808 was mutated to a phenylalanine as this amino acid represented the most structurally and biochemically conservative choice. K1112 was mutated to a glutamine as this is also a structurally conservative choice and this mutation had been successfully performed in the lab in PC from other species.

Enzymatic Activity Assay. A Shimadzu UV-1800 UV Spectrophotometer with an attached Shimadzu CPS Controller was used for all enzyme activity assays. The UV Probe ver. 2.62 (Shimadzu Corp., Kyoto, Japan) software was used to monitor all activity assays and calculate rates of absorbance change. The ranges for the rate measurements were selected to cover linear portions of absorbance change during the reactions with the same ranges applied to all replicates. Readings were taken for the times as described below with a cycle time of 22 sec. with a Windows XP-based computer or 30 sec. after a new Windows 10-based computer was installed.

Pyruvate carboxylation activity was measured spectrophotometrically at 340 nm by following the conversion of oxaloacetate to malate using the coupled enzyme, malate dehydrogenase (MDH). Reactions were performed in a buffer containing 0.1 M Tris-HCl (pH 7.8), and 7 mM $MgCl_2$. All substrates and coupling reagents were prepared as a 10x stock solution in this buffer that provided final reaction concentrations of 25 mM $NaHCO_3$, 2.5 mM ATP, 0.25 mM acetyl-CoA, 12 mM sodium pyruvate, 0.12 mM NADH, and 10 U/mL MDH. All measurements were performed in triplicate and the

errors are reported as the standard deviation. The final PC concentration in the assay ranged from 2.5 - 10 μg/mL per reaction. Reactions were followed until completion or 10 mins. had elapsed. Data from crosslinking inactivation assays were fit to Equation 1 using a least-squares regression in GraphPad Prism (version 8.1.1 for Windows, GraphPad Software, San Diego, California, USA). The value for k_{obs} was determined by fitting the data to Equation 1, where a represents the initial value at t = 0, b describes the limiting residual value, t is the time in seconds, and k_{obs} is the observed rate constant.

$$y = (a - b) * e^{-k_{obs} \cdot t} + b \qquad \text{(Equation 1)}$$

The PC-catalyzed rate of oxamate-induced oxaloacetate decarboxylation activity was measured spectrophotometrically at 340 nm by following the conversion of pyruvate to lactate using the coupled enzyme, lactate dehydrogenase (LDH)[5, 6, 12, 13]. Reactions were performed at 25 °C in a buffer containing 0.1 M Tris-HCl (pH 7.8), and 7 mM $MgCl_2$. All substrates and coupling reagents were prepared as a 10× stock solution that provided final concentrations of 0.12 mM NADH, 0.5 mM oxamate, 0.2 mM oxaloacetate, 0.25 mM acetyl-CoA, and lactate dehydrogenase (10 units). Reactions were initiated by the addition of *Sa*PC (60-200 μg/mL). Reactions were followed until completion or 20 mins. had elapsed.

ADP phosphorylation by carbamoyl phosphate activity was measured by following the production of ATP photometrically at 340nm using a hexokinase/glucose-6-phosphate dehydrogenase coupled assay[5, 6, 12, 14]. Specific activities were measured at 25 °C in 1-mL reaction volume containing 0.1 mM Tris, 7 mM $MgCl_2$, 3.5 mM ADP,

0.25 mM acetyl-CoA, 20 mM carbamoyl phosphate, 0.4 mM glucose, 0.36 mM NADP, glucose-6-phosphate dehydrogenase (5 units) and hexokinase (1 unit). Reactions were initiated by the addition of *Sa*PC (150-200 μg/mL). Reactions were followed until completion or 20 mins. had elapsed.

SaPC Crosslinking. BMOE was prepared in 100% DMSO at 20× the desired reaction concentration. SaPC was reacted at a final concentration of 1 mg/mL (premixed with substrates for a minimum of 10 minutes when applicable) in a buffer containing 0.1 M Tris-HCl (pH 7.8), 7 mM $MgCl_2$ with the desired concentration of BMOE (and identical concentration of substrate when applicable) at room temperature. After a defined incubation period, dithiothreitol was used to quench the reaction at a final concentration of 13 mM for 15 minutes at room temperature. Samples were then either assessed for activity using the MDH assay described above or mixed with 4× Laemmli Buffer in reducing conditions and heated to 100 °C for 3 minutes for SDS-PAGE analysis using an 8% polyacrylamide gel. Protein molecular weights were estimated using the Spectra Multicolor High Range Protein Ladder (Thermo Scientific, Waltham, MA). SDS-PAGE gels were run at 100V until the dye-front ran off the bottom of the gel. Coloration was achieved with Coomassie Brilliant Blue G-250 (Bio-Rad, Hercules, CA).

SDS-PAGE Gel Preparation. 150 mL of resolving buffer contained 27.23g Tris base dissolved in distilled, deionized water and adjusted to pH 8.8 with 6N HCl. 100mL stacking buffer contained 6g Tris base dissolved in distilled, deionized water and adjusted to pH 6.8 with 6N HCl. 1 L of 10x electrode running buffer for SDS-PAGE contained 30.3 g Tris base, 144 g glycine, and 10 g SDS dissolved in distilled, deionized water. The 8% acrylamide resolving gel was composed of 13.8 mL distilled, deionized water, 8 mL

30% acrylamide, 7.2 mL resolving buffer, and 293 µL of 10% SDS. These components were stirred together before the simultaneous addition of 154 µL of 10% ammonium persulfate and 16 µL TEMED. The mixture was stirred briefly before pouring for gel formation. This was allowed a minimum of 45 minutes for polymerization to occur. 5% stacking gel was poured on top of this to form the stacking portion of the final SDS-PAGE gel. This stacking gel was composed of 2.9 mL distilled, deionized water, 850 µL 30% acrylamide, 1.25 mL stacking buffer, 50 µL of 10% SDS. These components were mixed before the simultaneous addition of 25 µL of 10% ammonium persulfate and 5 µL TEMED. This mixture was stirred before it was poured on top of the resolving portion and the appropriate comb was inserted for well formation. This was allowed to remain undisturbed for 45 minutes for polymerization to occur. To achieve reducing conditions in the loading buffer, β-mercaptoethanol was added to the 4× Laemmli buffer to achieve a 5% β-mercaptoethanol / 95% 4× Laemmli buffer (v/v) final mixture.

Coomassie protein stain was composed of 225 mL distilled, deionized water, 225 mL methanol, 50 mL glacial acetic acid, and 0.25 g Coomassie Brilliant Blue G-250. This was stirred until the Coomassie stain was completely dissolved. Protein gel destain solution was composed of 700 mL distilled, deionized water, 200 mL methanol, and 100 mL glacial acetic acid. Staining was performed with an overnight incubation of the gel with protein stain while destaining was performed for at least 1 hour to achieve minimal background staining.

Densitometric Analysis. Densitometric analyses were performed using the LabWorks software developed by UVP, Inc. (Upland, CA). The coloration intensity of each band was determined from images of the SDS-PAGE gels. The “Area Density

Analysis Tool" function in Labworks was utilized for determination of the density of each band. A rectangle was drawn around each band with a size to include the full band but exclude nearby bands or excess background. The software includes background subtraction to minimize the effect of varying sizes of these rectangular areas. This was verified by drawing varying sizes of rectangles around a band and ensuring that the areal density remained unchanged. The normalized density of the monomer band was determined by dividing the monomer band density by the total of the band density for both the monomer and dimer bands. This software does not have any automatic feature to detect overloads in the bands when determining areal density other than to color the saturated portions of a band in red when obtaining the image. All images where obtained using exposure times to prevent this kind of saturation.

Stopped-Flow Spectroscopy. Stopped-flow spectroscopy was performed using an Applied Photophysics SX20 instrument at room temperature obtained from Applied Photophysics, Ltd. (Leatherhead, England). Intrinsic tryptophan fluorescence was observed at an excitation wavelength of 295 nm using a 350 nm emission filter. SaPC (0.35 mg/mL) was premixed with substrates for a minimum of 10 minutes when applicable and loaded in one drive syringe and mixed 1:1 with the substrate/BMOE mixture in the second drive syringe. The final concentration of substrates or ligands used was 2.5 mM ATP, 5 mM ADP, 5 mM phosphonoacetate (PPA), 0.25 mM acetyl-CoA, 12 mM pyruvate, and 10 mM L-aspartate. All solutions were prepared in a buffer containing 0.1 M Tris-HCl (pH 7.8), 7 mM $MgCl_2$. Applied Photophysics Pro-Data SX software was used to operate the instrument, interpret, and average the data. All data are the average of 4-5 replicates. Reported rates are the average value of three independent acquisitions of

these replicates. The data from each sample was normalized to start at a value of 1 to account for variability in initial fluorescence intensity. Normalization was performed to plot the fractional change in intensity: the measured intensity at every time point was divided by the initial measured intensity at t = 0. Data were fit to Equation 2, where *a* represents the amplitude, k_{obs} represents the observed rate, *t* represents time in seconds, *c* represents the slope of the linear second phase, and *d* represents the initial value at t = 0.

$$y = a * (1 - e^{k_{obs} \cdot t}) + ct + d \quad \text{(Equation 2)}$$

III. CONFORMATIONAL SELECTION GOVERNS CARRIER DOMAIN POSITIONING IN *STAPHYLOCOCCUS AUREUS* PYRUVATE CARBOXYLASE

1. Introduction

Two classical models are typically used to describe conformational changes accompanying ligand binding in biological macromolecules: the induced-fit hypothesis states that ligand binding induces a conformational change in the protein (Koshland, 1959; Koshland, et al., 1966), while the conformational selection hypothesis states that the protein pre-exists in multiple conformational states, with ligand binding shifting the population towards the ligand-bound conformation (Monod, et al., 1965; Boehr, et al., 2009). While these models have been tested and elaborated upon in many systems, the large-scale carrier domain motions associated with swinging domain enzymes provide a particularly intriguing and challenging system in which to study the influence of ligands on protein conformational change (Perham, 2000).

The mechanism by which reaction intermediates are transferred in a coordinated, unidirectional manner remains largely undefined in swinging domain enzymes. For example, assembly line polyketide synthases are built on an array of multiple modules and domains, requiring exquisite coordination as intermediates are transferred between active sites on distinct modules and domains. It has been proposed that vectorial synthesis in multimodular enzymes is dependent on conformational changes among the catalytic and carrier domains (Khosla, et al., 2014), but it remains unclear whether these conformations interchange freely at equilibrium or whether conformational changes are induced by ligand binding and catalytic turnover events. This is a particularly difficult

question to investigate in large and unwieldy systems such as polyketide synthases and their multi-domain counterparts, for which conventional structural and functional approaches do not easily apply. Instead, smaller and more tractable swinging domain enzyme systems can serve as structurally and biophysically accessible paradigms to study the relationship between ligand binding and large-scale protein conformational changes. One such enzyme, pyruvate carboxylase (PC), is a homotetrameric, swinging domain enzyme that has been well characterized structurally and kinetically (Lietzan, et al., 2014; Tong, 2013; Jitrapakdee, et al., 2008; Menefee and Zeczycki, 2014). During catalysis, the carrier domain of PC undergoes a conformational change spanning more than 70 Å, providing an ideal system to study the influence of ligand binding on large-scale conformational changes in swinging domain enzymes.

PC catalyzes the ATP-dependent carboxylation of pyruvate to oxaloacetate, with bicarbonate serving as the carboxyl group donor. The reaction proceeds through two connected half-reactions catalyzed in distinct and remote active sites (Figure II-1A). In the first half-reaction, the biotin cofactor on the biotin carboxyl carrier protein (BCCP) domain is carboxylated with the concomitant cleavage of MgATP in the biotin carboxylase (BC) domain. The second half-reaction occurs in the carboxyltransferase (CT) domain, where the carboxyl group is transferred from the biotin cofactor on the BCCP domain to pyruvate, generating oxaloacetate. These two half-reactions are coupled through the intermolecular translocation of the biotinylated carrier domain, which must translocate over 70 Å to transfer the carboxyl group between active sites on the BC domain and the CT domain (Figure III-1A) (St. Maurice, et al., 2007; Xiang and Tong, 2008; Lasso, et al., 2014).

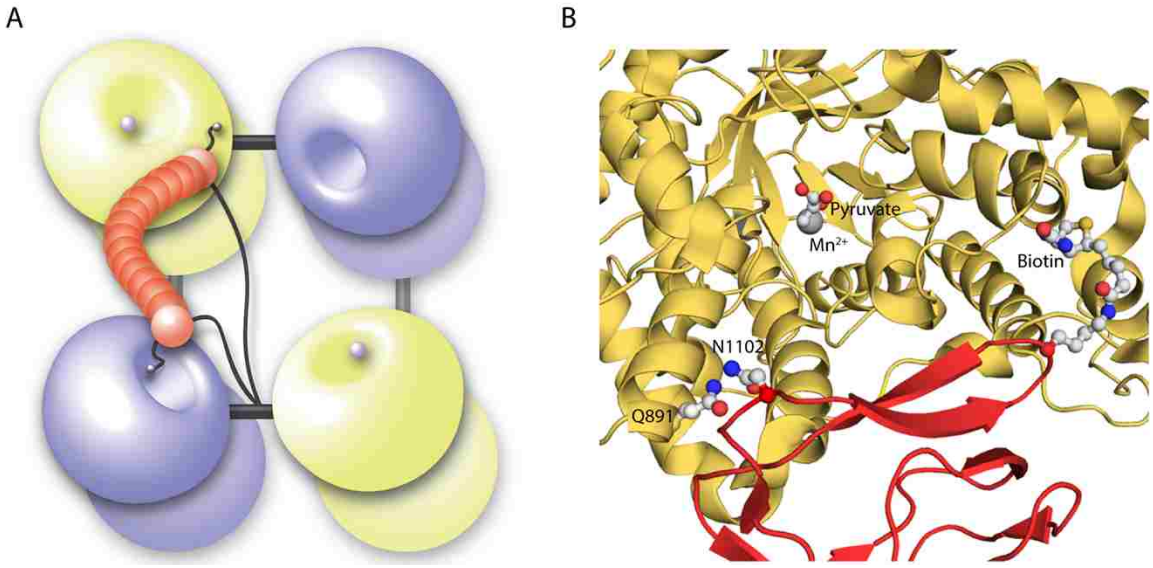

Figure III-1 SaPC carrier domain motions and conformations.
A. A schematic of the PC tetrameric structure and intermolecular carrier domain translocation. BC domains are colored in blue, CT domains in yellow, and the BCCP carrier domain in red. A hypothetical intermolecular translocation pathway is traced for a single carrier domain from the BC domain of its own subunit to the exo binding site on the CT domain of a neighboring subunit. **B.** The *Sa*PC X-ray crystal structure (PDB ID: 3BG5) showing the BCCP domain of one subunit (red) interacting at the exo binding site of the CT domain on the opposing subunit (yellow). The Mn^{2+} ion, colored as a grey sphere, and pyruvate are shown in the CT domain active site. Gln891 on the CT domain and Asn1102 on the BCCP domain were both mutated to cysteine to enable maleimide-based crosslinking to trap the BCCP domain in an intermolecular conformation.

Prior efforts to study the influence of ligand binding on carrier domain translocation in PC have largely relied on interpretations of kinetic data. For example, detailed studies of carboxybiotin decarboxylation in sheep liver PC (Easterbrook-Smith, et al., 1976; Goodall, et al., 1981) and chicken liver PC (Attwood and Wallace, 1986) were performed in the presence of various CT domain ligands and were interpreted based on a ligand-induced conformational change model, where CT domain substrates were considered to induce carrier domain translocation to the CT domain. Based on rate enhancements observed in the presence of CT domain substrates or free biotin, it was concluded that substrates and cofactors mediate communication between subunits by inducing conformational changes through the enzyme (Zeczycki, et al, 2009). More

recent kinetic analyses were also interpreted in light of an induced conformational change model to propose that both pyruvate and the allosteric activator, acetyl-CoA, facilitate long-range communications that induce carrier domain translocation (Westerhold, et al., 2016; Westerhold, et al., 2017). While these interpretations are reasonable, kinetic studies cannot directly observe carrier domain positioning and are limited to observations that conflate ligand binding, catalytic turnover and carrier domain translocation. In short, while many studies on PC have been interpreted using an induced conformational change model, they do not attempt to directly assess the conformational change model itself.

In contrast to the interpretations described above, snapshots of PC from X-ray crystallography and cryo-electron microscopy have revealed multiple conformational states and carrier domain positions that are independent of the identity or bound state of the ligand (St. Maurice, et al., 2007; Lasso, et al., 2014; Yu, et al., 2009). These structural studies suggest that the carrier domain may sample multiple positions in a ligand-independent dynamic equilibrium (Lietzan, et al., 2011; Lietzan, et al., 2013A). Ultimately, neither kinetic measurements nor structural studies are suitable to determine whether carrier domain positioning exists in a dynamic equilibrium or, instead, is governed by ligand-induced conformational changes. To address this question, alternative approaches are required that directly follow the positioning of the carrier domain, independent of catalytic turnover.

Here we directly observe positioning of the carrier domain to clarify the mechanism of ligand associated conformational changes on the carrier domain in *Staphylococcus aureus* PC (*Sa*PC). Using an intermolecular crosslinking trap, combined with a variety of analytical approaches, the positioning of the BCCP carrier domain is

directly observed as a function of substrates and allosteric effectors. These data clearly demonstrate that carrier domain positioning in PC is governed by conformational selection and also suggest that the allosteric activator, acetyl-CoA, favors the carrier domain to engage in an intermolecular interaction with the CT domain. This work clarifies the mechanism of carrier domain positioning in PC and can be extended to other carrier domain enzyme systems that function in vectorial biosynthesis.

2. Results

2.1 Crosslinkers trap the intermolecular SaPC carrier domain conformation.

To directly observe *Sa*PC carrier domain positioning, a system was designed to trap the BCCP carrier domain using maleimide-based homobifunctional crosslinkers. Specifically, the system was designed to capture the BCCP domain as it accesses an intermolecular interaction with the CT domain of an opposing subunit (Figure III-1A). The carrier domain has been observed in two intermolecular conformations in the *Sa*PC crystal structure. In one conformation, biotin is docked in the CT domain active site while, in the second conformation, biotin is docked in the so-called “exo-binding site” which is located immediately adjacent to the CT domain active site. The exo-binding site conformation of *Sa*PC was chosen as the basis for the crosslinking mutations to minimize detrimental effects on catalytic turnover. Two specific residues were targeted for mutation to cysteines, based on the X-ray crystal structure of *Sa*PC with BCCP in the exo-binding site conformation (Xiang and Tong, 2008) (PDB ID: 3BG5): Gln 891 on the CT domain and Asn 1102 on the BCCP domain were both mutated to cysteine to

generate the double mutant, Q891C/N1102C *Sa*PC (Figure III-1B). The Q891C/N1102C double mutant and the corresponding single mutants retained 30 – 50% of the wild-type pyruvate carboxylation activity, indicating that these mutations have only a modest impact on catalytic turnover (Table -1).

Table III-1 Pyruvate carboxylation activity for SaPC and mutated constructs of SaPC.

*Sa*PC	k_{cat} (min^{-1})	% Compared to WT
WT	1430 ± 100	-
Q891C	510 ± 50	36
N1102C	690 ± 20	48
Q891C/N1102C	390 ± 30	27

(n = 3; errors represent standard deviations)

To initially characterize this system, Q891C *Sa*PC, N1102C *Sa*PC, and Q891C/N1102C *Sa*PC were incubated with bismaleimidoethane (BMOE) for 15 minutes and analyzed by SDS-PAGE (Figure III-2A). BMOE was selected as the crosslinker for its relatively short spacer arm, but longer crosslinkers were also evaluated and no discernable difference was observed compared to BMOE (Figure III-3). Crosslinked samples are predicted to run at twice the subunit molecular weight (*Sa*PC monomer = 131 kDa), resulting in a ~260 kDa crosslinked dimer. No crosslinked dimers were observed in the Q891C single mutant across a wide range of BMOE concentrations, while a very small degree of crosslinked dimers developed in the N1102C mutant at low concentrations of BMOE (10 μM). A high degree of crosslinked dimers were observed in the Q891C/N1102C double mutant at 300 μM and 1 mM. Some higher molecular weight species were observed at all BMOE concentrations in both the single mutants and the Q891C/N1102C double mutant. Analytical ultracentrifugation of crosslinked wild-type *Sa*PC and Q891C/N1102C *Sa*PC confirmed that these high molecular weight species

were composed of large, aggregated protein. These species presumably arose from nonspecific crosslinking between individual protomers. A small percentage of these high molecular weight species were present across all samples incubated with BMOE and, therefore, were not considered further in this analysis.

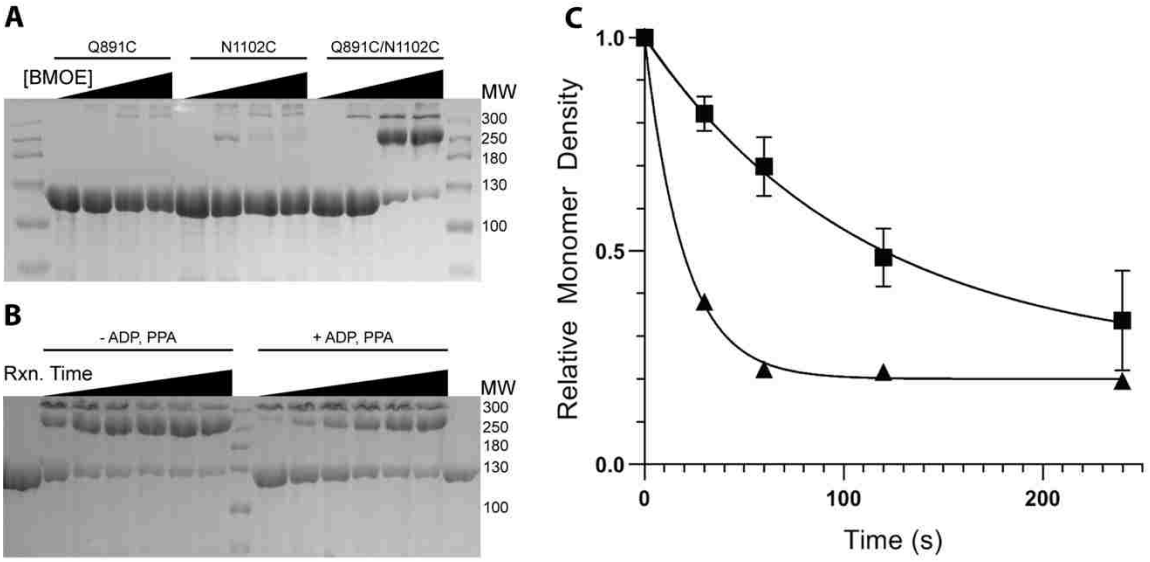

Figure III-2 Q891C, N1102C, and Q891C/N1102C SaPC crosslinked with BMOE.
A. 8% acrylamide SDS-PAGE gel of SaPC mutants at 1 mg/mL reacted with either 0 μM, 10 μM, 300 μM, or 1 mM BMOE for 15 min. Q891C SaPC and N1102C SaPC did not form crosslinked dimers at BMOE concentrations greater than 300 μM. Q891C/N1102C SaPC was primarily crosslinked into dimers at BMOE concentrations of 300 and 1000 μM. 5 μg of *Sa*PC was loaded in each lane. B. 8% acrylamide SDS-PAGE gel showing time-dependent crosslinking Q891C/N1102C SaPC with BMOE ± 5 mM ADP/phosphonoacetate for various reaction times. Q891C/N1102C SaPC at 1 mg/mL was incubated with 0 or 300 μM BMOE for the indicated times in the absence/presence of 5 mM ADP and 5 mM phosphonoacetate and then quenched with 13 mM DTT for 15 minutes. Lane 1: Q891C/N1102C SaPC reacted with 0 μM BMOE. Lane 2-7: Q891C/N1102C SaPC reacted with 300 μM BMOE for 30 s, 1 min, 2 min, 4 min, 8 min, or 15 min. Lane 8: Molecular Weight Ladder. Lanes 9-14: Q891C/N1102C SaPC preincubated with 5 mM ADP and 5 mM phosphonoacetate for 15 minutes, then reacted with 300 μM BMOE for 30 s, 1 min, 2 min, 4 min, 8 min, 15 min. Lane 15: wild-type SaPC reacted with 300 μM BMOE. 5 μg of *Sa*PC was loaded in each lane. C. Densitometric analysis of monomer bands in Figure 2B as a function of time. Either no substrates were added (▲) or 5 mM ADP and 5 mM phosphonoacetate (■) were present during crosslinking. The y-axis represents the normalized monomer density, determined as described in the methods section.

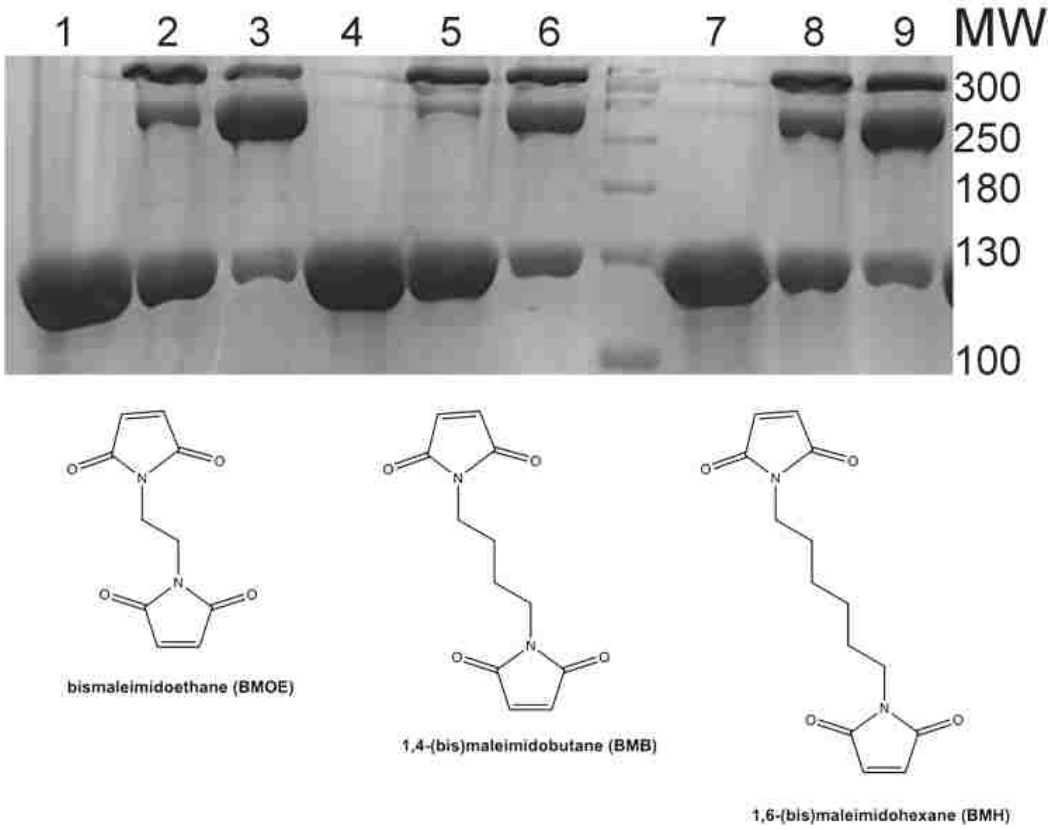

Figure III-3 Q891C/N1102C SaPC incubated with bismaleimidoethane (BMOE), 1,4-(bis)maleimidobutane (BMB), and 1,6-(bis)maleimidohexane (BMH).
Each SaPC mutant was preincubated at 1 mg/mL with the indicated concentration of crosslinker for 120 seconds. Samples were quenched with 13 mM DTT for 15 minutes. 7 μg of SaPC was loaded in each lane. 1: 0 μM BMOE; 2: 10 μM BMOE; 3: 300 μM BMOE; 4: 0 μM BMB; 5: 100 μM BMB; 6: 300 μM BMB; 7: 0 μM BMH; 8: 100 μM BMH; 9: 300 μM BMH.

In the absence of ligands, the percentage of crosslinked dimers, as measured by SDS-PAGE, rapidly approached equilibrium (Figure III-2B). The rate of approach to equilibrium was greatly reduced, however, in the presence of ADP and phosphonoacetate, an analogue of the carboxyphosphate intermediate. These ligands substantially reduced the rate of crosslinked dimer formation relative to that observed in the absence of ligands (Figure III-2B). A quantitative densitometric analysis was performed to determine the change in monomer density as a function of time (Figure III-2C). These data are described by a single exponential decay and revealed that ADP and

phosphonoacetate dramatically reduce the observed rate constant for crosslinked dimer formation (Table III-2). While this generally illustrates that BC domain ligands can perturb the carrier domain equilibrium, the rapid re-equilibration observed in the absence of substrates precluded a more detailed kinetic analysis using this approach. Although this data is promising, the bands of the gels in Figure III-2 and others throughout the following studies may be overloaded. Further, the Coomassie G-250 dye was used throughout for protein coloration while R-250 may be more optimal for use in densitometry.

Table III-2 Summary of observed first-order rate constants determined using densitometry, inactivation kinetics and intrinsic tryptophan fluorescence.

Substrate	Densitometric k_{obs} (s^{-1})*	Inactivation k_{obs} (s^{-1})*	ITF k_{obs} (s^{-1})**
None	0.051 ± 0.003	0.057 ± 0.014	0.073 ± 0.002
ADP + phosphonoacetate	0.009 ± 0.001	0.005 ± 0.001	0.026 ± 0.001
A. CoA	N/A	0.083 ± 0.17#	0.082 ± 0.001
Pyruvate	N/A	0.091 ± 0.24#	0.081 ± 0.001

* Reported errors represent the standard errors calculated from iterative non-linear curve fitting. The data were fit to Equation 1, where each data point was plotted as the average ± standard deviation of 3 independent determinations.

** Reported errors represent standard deviations from n=3 independent measurements of k_{obs}.

\# Very high errors result from manual sample handling. These values are provided as estimates only.

To complement and confirm the densitometric analysis by SDS-PAGE, inactivation kinetics were also assessed as a reporter of carrier domain crosslinking. Crosslinks between the BCCP and CT domains will immobilize the carrier domain, thereby inactivating the enzyme by preventing subsequent rounds of carboxyl group

transfer between active sites. To confirm that enzyme inactivation was specific to carrier domain crosslinking, initial velocities were evaluated for the Q891C *Sa*PC, N1102C *Sa*PC, Q891C/N1102C *Sa*PC, and wild-type *Sa*PC as a function of crosslinker incubation time (Figure III-4). The native pyruvate carboxylation activities of these mutants are shown in Table III-1. Wild-type *Sa*PC retained its full enzymatic activity over 15 minutes of incubation with 300 μM BMOE. The activity of the Q891C mutant increased slightly upon incubating with BMOE, perhaps as a consequence of masking the cysteine mutation at that position. The N1102C mutation exhibited a slight loss of activity (~8% over 15 minutes), which coincides with the small amount of dimers observed by SDS-PAGE (Figure III-2A). Compared with the wild-type and individual mutants, the Q891C/N1102C mutant exhibited a rapid and significant loss of activity upon incubation with BMOE, consistent with specific crosslinking between the carrier domain and the CT domain. The observed rate constant for inactivation was very similar to the rate of crosslinked dimer formation observed by SDS-PAGE (Table III-2).

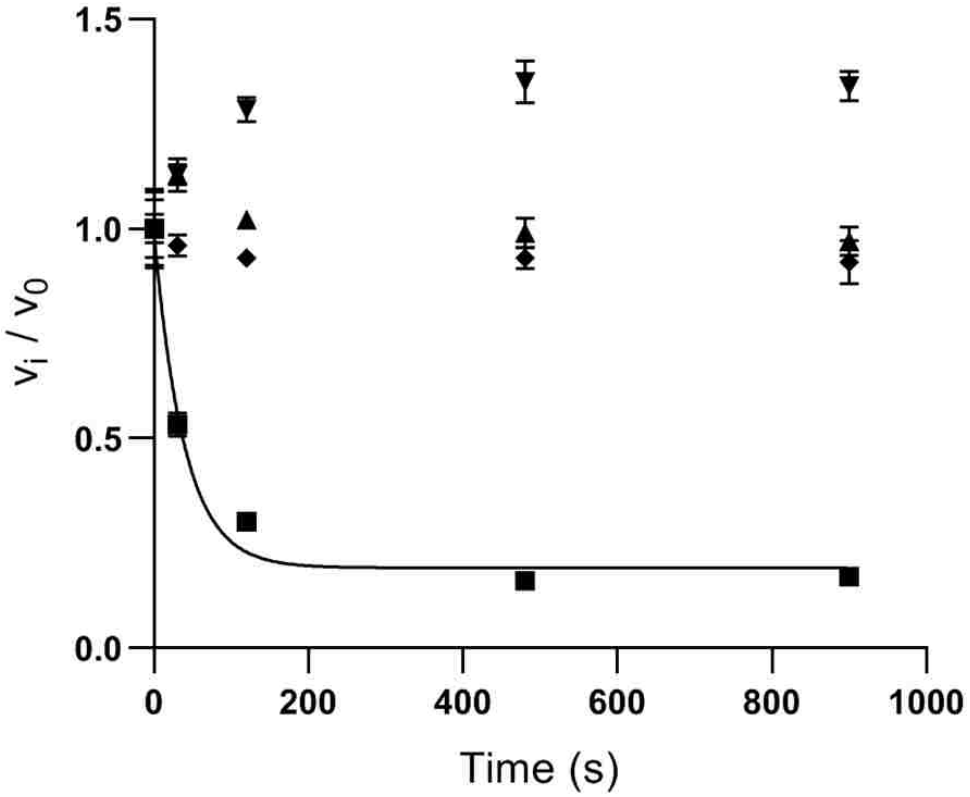

Figure III-4 Inactivation kinetics for wild-type SaPC and 3 mutated constructs of SaPC. Wild-type (▲), Q891C (▼), N1102C (◆), or Q891C/N1102C (■) SaPC were reacted with 300 μM BMOE in 5% DMSO for 30 s, 2 min, 8 min, or 15 min. All reactions were then quenched with 13 mM DTT for 15 min. The initial velocity (v_i) was determined and divided by the initial velocity determined after incubating the same enzyme with 5% DMSO for 15 min (v_o). Each sample was measured in triplicate using the malate dehydrogenase coupled enzyme assay. The error bars represent the standard deviation from three independent measurements. Error bars for Q891C/N1102C are included but are obscured by the data markers.

2.2 Intrinsic tryptophan fluorescence reports on carrier domain conformational states.

Both densitometry and inactivation kinetics are constrained by their reliance on manual sample handling, limiting these measurements to slower re-equilibration events such as those slowed by the presence of ADP and PPA. To gain greater time-resolution and accuracy, we explored whether changes in intrinsic tryptophan fluorescence (ITF) intensity could serve as a reporter on carrier domain positioning. Fortuitously, in *Sa*PC, all 5 tryptophan residues are located in the CT domain (Figure III-5). As such, we predicted that the Trp fluorescence intensity would increase when the carrier domain is

positioned near the CT domain, resulting from the altered local environment of the five CT domain tryptophan residues. Consistent with this prediction, wild-type *Sa*PC yielded distinct ITF signals in the presence of different ligands (Figure III-6A). When *Sa*PC was mixed with ATP, a BC domain substrate, a rapid decrease in the ITF signal intensity was observed. Conversely, when *Sa*PC was mixed with acetyl-CoA, an increase in the ITF signal intensity was observed.

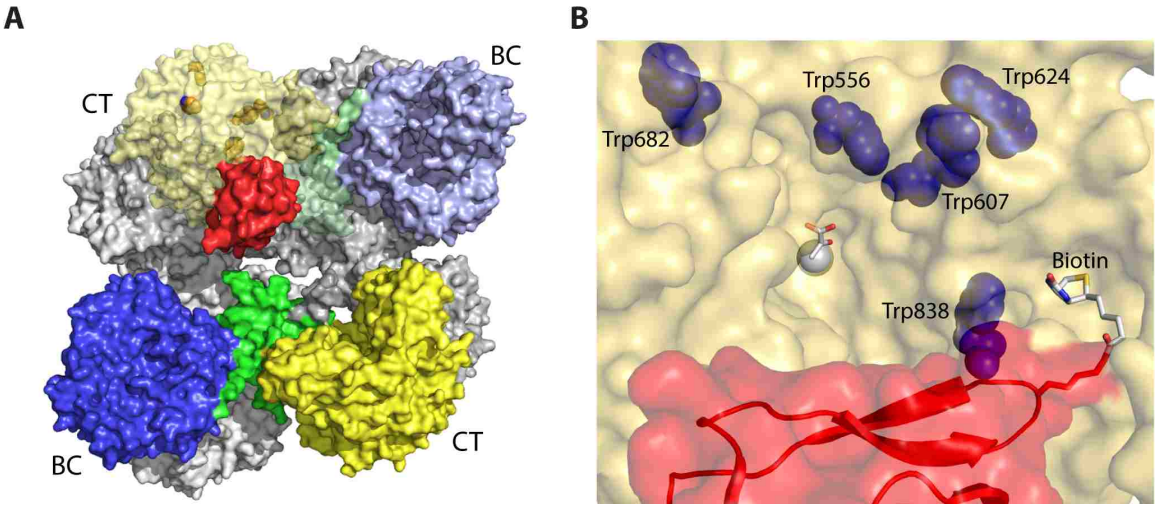

Figure III-5 Structure of SaPC (PDB ID: 3BG5) showing the location of the five tryptophan residues. **A:** The BC domains (blue), CT domains (yellow), allosteric / PC tetramerization domains (green), and BCCP domain (red) are shown. All five Trp residues (dark yellow) are located in the CT domain. **B:** A close-up view of the CT domain (yellow) with the BCCP domain (red) docked in the exo-binding site. Tryptophans (dark blue; Homo sapiens PC numbering) are highlighted, illustrating the proximity of Trp838 to biotin.

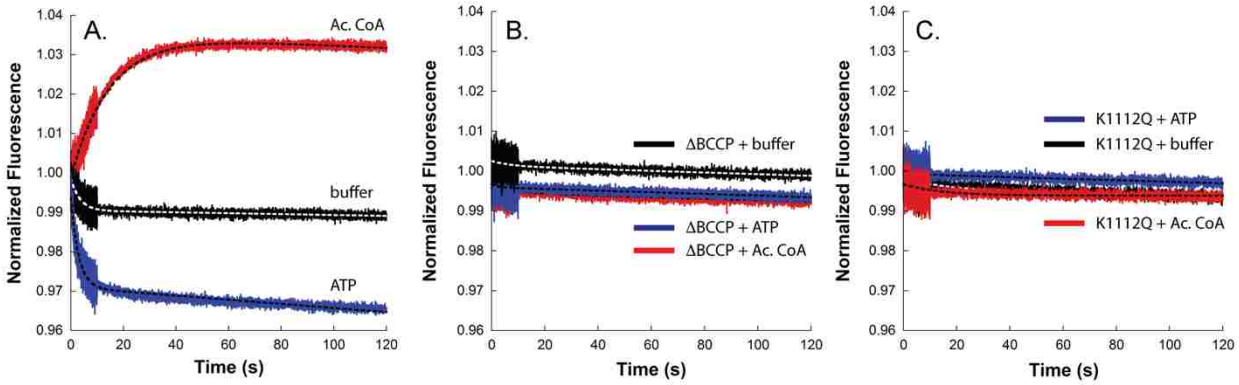

Figure III-6 The role of substrates and the biotinylated carrier domain in generating the tryptophan fluorescence signal.
A. Wild-type SaPC intrinsic tryptophan fluorescence (ITF) in the presence of substrate/effector. Wild-type SaPC (0.35 mg/mL) was mixed with 2.5 mM ATP (blue), 0.25 mM acetyl-CoA (red), or buffer (black) at 0 s in a stopped-flow instrument with tryptophan excitation at 295 nm and ITF emission measured at 350 nm. **B.** Q891C/V1062X (ΔBCCP) SaPC ITF in the presence of substrate/effector. Q891C/V1062X SaPC (final concentration of 0.175 mg/mL) was mixed with buffer (black) or final concentrations of 2.5 mM ATP (blue) or 0.25mM acetyl-CoA (red) at 0 s in a stopped-flow instrument with tryptophan excitation at 295 nm and ITF emission measured at 350 nm. **C.** Q891C/N1102C/K1112Q SaPC ITF in the presence of substrate/effector. Q891C/N1102C/K1112Q SaPC (final concentration of 0.175 mg/mL) was mixed with buffer (black) or final concentrations of 2.5 mM ATP (blue) or 0.25 mM acetyl-CoA (red) at 0 s in a stopped-flow instrument with tryptophan excitation at 295 nm and ITF emission measured at 350 nm. Dashed lines represent the fit of the data to Equation 2.

We reasoned that the presence of ATP favors one conformational state for the BCCP carrier domain that reports as a decrease in ITF signal intensity, while the presence of acetyl-CoA favors a different state for the carrier domain that reports as an increase in ITF signal intensity. To confirm that carrier domain positioning mediates the ITF signal, we produced a *Sa*PC construct with a C-terminal truncation by introducing a STOP codon (TAG) at Valine 1062, eliminating the BCCP domain (Q891C/V1062X; ΔBCCP *Sa*PC). This construct was assessed for changes in the ITF signal intensity in the presence of ligands. When this ΔBCCP *Sa*PC mutant was mixed with either substrate or allosteric effector, no change in ITF intensity was observed (Figure III-6B), confirming that changes in the ITF intensity are a consequence of interactions with the BCCP domain and are not simply a result of conformational changes upon ligand binding. The specific

contribution of biotin to the ITF signal was also investigated by mutating the biotinylated Lys 1112 to glutamine (Q891C/N1102C/K1112Q), to produce an unbiotinylated *Sa*PC. Again, the fluorescence intensity did not change in the presence of substrates (Figure III-6C), indicating that the biotin cofactor is necessary for generating the ITF signal.

Having established that the ITF signal intensity is both BCCP and biotin dependent, the behavior of the system was evaluated in the presence of BMOE crosslinker (Figure III-7). While wild-type *Sa*PC and the single mutants displayed only very small changes in signal intensity when mixed with BMOE (Figure III-7A), the crosslinking competent Q891C/N1102C *Sa*PC displayed a large increase in fluorescence intensity in the presence of BMOE, as predicted from locking the BCCP domain in proximity to the CT domain. To distinguish whether biotin contributes to the ITF signal intensity or, rather, to positioning of the BCCP domain itself, crosslinking of the unbiotinylated *Sa*PC was evaluated by SDS-PAGE in the presence of BMOE (Figure III-8). Crosslinking was observed both in the presence and absence of substrates and, while the response to substrates dramatically diminished in unbiotinylated *Sa*PC, the unbiotinylated carrier domain did not lose the ability to position itself for crosslinking. Furthermore, when Q891C/N1102C/K1112Q was reacted with 200 μM BMOE in the presence of exogenously added biotin or biocytin, the ITF signal intensity did not replicate what was observed with the biotinylated Q891C/N1102C (Figure III-7B), indicating that biotin must be properly tethered to the BCCP domain to produce large increases in the ITF intensity in the presence of BMOE. Thus, we conclude that the intrinsic fluorescence signal changes observed in *Sa*PC directly report on changes in the positioning of the carrier domain and its tethered biotin cofactor.

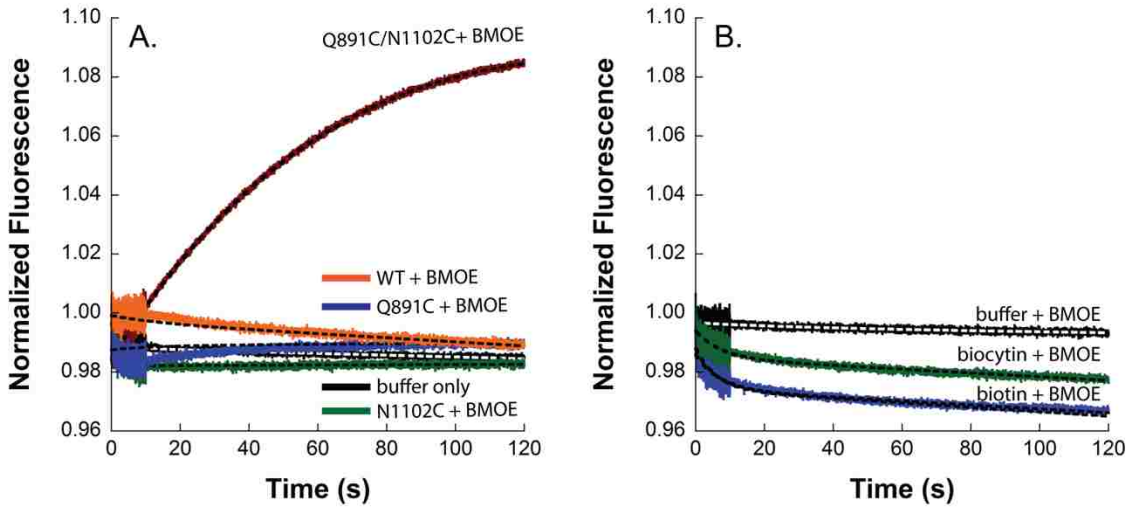

Figure III-7 SaPC ITF changes observed in the presence of crosslinker.
A. Q891C/N1102C mixed with buffer (black), Q891C SaPC reacted with 200 μM BMOE (blue), N1102C SaPC reacted with 200 μM BMOE (green), Q891C/N1102C SaPC reacted with 200 μM BMOE (maroon), and wild-type SaPC reacted with 200 μM BMOE (orange). All mixing occurred at 0 seconds in a stopped-flow instrument with excitation at 295 nm and ITF emission measured at 350 nm. **B.** Q891C/N1102C/K1112Q SaPC ITF changes observed when crosslinked in the presence of biotin or biocytin. Q891C/N1102C/K1112Q SaPC (0.175 mg/mL final concentration) was incubated with buffer (black), 5 mM final concentration of biotin (blue), or 5 mM final concentration of biocytin (green) for 15 minutes before being mixed with an equal concentration of biotin or biocytin and 200 μM final concentration of BMOE at 0 seconds in a stopped-flow instrument with excitation at 295 nm and ITF emission measured at 350 nm. Q891C/N1102C/K1112Q SaPC mixed with buffer (black) is also shown for reference. Dashed lines represent the fit of the data to Equation 2.

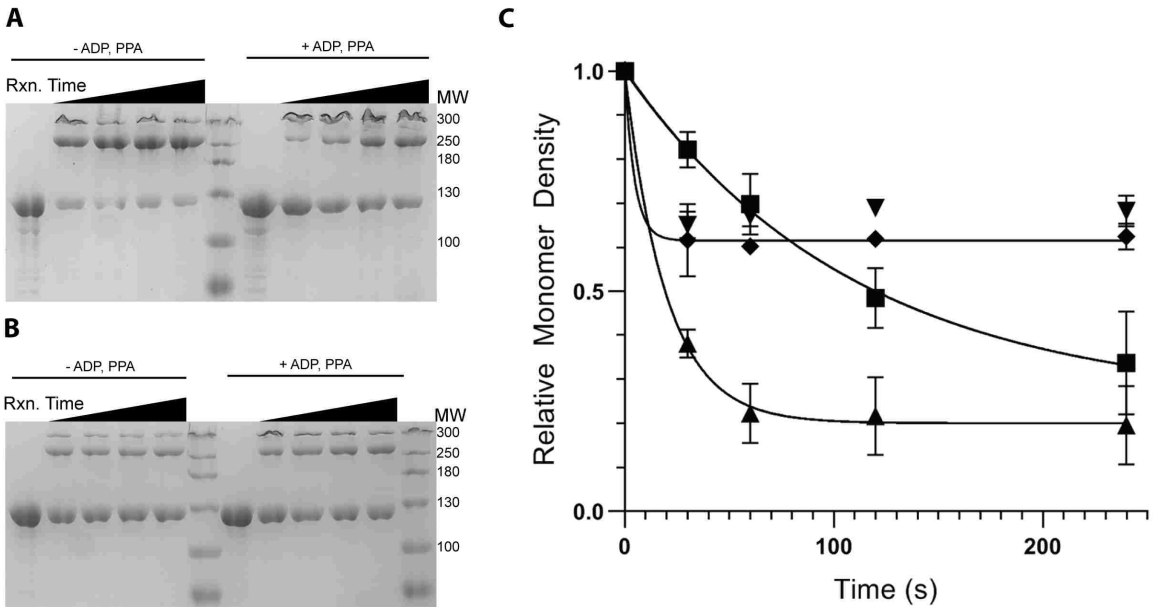

Figure III-8 Q891C/N1102C (biotinylated) SaPC and Q891C/N1102C/K1112Q (unbiotinylated) crosslinked in the presence and absence of ADP and phosphonoacetate (PPA).
Each SaPC mutant at 1mg/mL was preincubated with no ligands present or 5 mM ADP and 5 mM phosphonoacetate for 10 minutes and then reacted with 300 μM BMOE for 10 s, 30 s, 60 s, and 120 s. Samples were quenched with 13mM DTT for 15 minutes. 5 μg of SaPC was loaded in each lane. **A.** Q891C/N1102C; **B.** Q891C/N1102C/K1112Q; **C.** Densitometry analysis of relative monomer density as a function of time for Q891C/N1102C without ligands (▲), Q891C/N1102C with 5 mM ADP and 5 mM phosphonoacetate (■), Q891C/N1102C/K1112Q without ligands (◆), and Q891C/N1102C/K1112Q with 5 mM ADP and 5 mM phosphonoacetate (▼). The experiment was performed in triplicate, with the error bars representing the error propagated standard deviation of the measured band densities.

Given that biotin is necessary for mediating changes in the ITF signal intensity, we sought to determine which Trp residue(s) in the CT domain interact with biotin and contribute to the ITF signal change. The crystal structure of *Sa*PC (PDB ID: 3BG5) reveals that biotin is positioned near Trp808 in the exo-binding site of *Sa*PC (Figure III-5B). This residue was mutated to a phenylalanine (W808F) to assess the sensitivity of this mutated *Sa*PC to changes in ITF intensity. Unfortunately, the W808F mutation rendered the protein aggregation-prone and it could not be purified, precluding a clear confirmation of this prediction.

2.3 Substrates and effectors alter the carrier domain positioning equilibrium.

To assess the contribution of substrates and effectors to carrier domain positioning, the crosslinking competent Q891C/N1102C *Sa*PC was incubated with 300 μM BMOE for 2 minutes in the presence of various substrates and effectors (Figure III-9). Both pyruvate and acetyl-CoA increased the amount of crosslinked dimer in the presence of ADP and phosphonoacetate compared to dimer formation in the presence of just ADP and phosphonoacetate. This suggests that pyruvate and acetyl-CoA both shift the carrier domain positioning towards the CT domain on the opposing subunit.

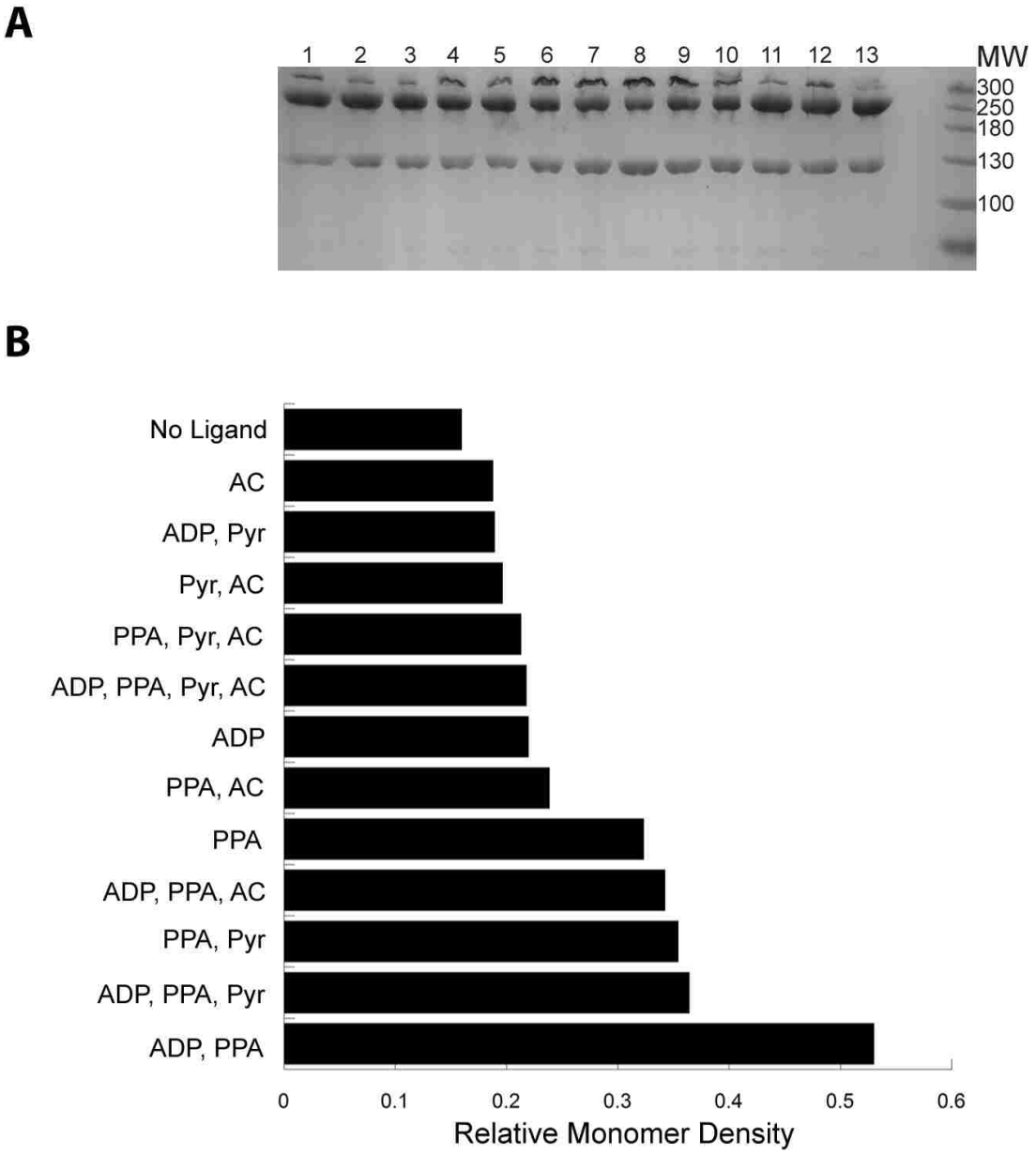

Figure III-9 Q891C/N1102C SaPC crosslinked in the presence of various substrates and effectors. **A.** Q891C/N1102C SaPC crosslinked in the presence of various substrates and effectors. Q891C/N1102C SaPC at 1 mg/mL was reacted with 300 μM BMOE for 120 s in the presence of a combination of 5 mM phosphonoacetate, 0.25 mM acetyl CoA, 12 mM pyruvate and/or 5 mM adenosine 5'-diphosphate (ADP), as listed below, then quenched with 13 mM DTT for 15 minutes. A. 5 μg was loaded in each lane. (1) No Substrates; (2) Acetyl CoA (AC); (3) Acetyl-CoA, Pyruvate (Pyr); (4) ADP; (5) ADP, Pyruvate; (6) Phosphonoacetate; (7) Phosphonoacetate, Pyruvate; (8) ADP, Phosphonoacetate; (9) ADP, Phosphonoacetate, Pyruvate; (10) ADP, Phosphonoacetate, Acetyl-CoA; (11) ADP, Phosphonoacetate, Pyruvate, Acetyl-CoA; (12) Phosphonoacetate, Acetyl-CoA; (13) Phosphonoacetate, Pyruvate, Acetyl-CoA. The molecular weights for the ladder on the right are shown in kDa. **B.** A densitometry analysis was performed with the relative monomer density shown for each ligand combination.

The rate of inactivation was determined for Q891C/N1102C *Sa*PC reacted with BMOE crosslinker in the presence of ADP and phosphonoacetate in combination with pyruvate and acetyl-CoA (Figure III-10). It was necessary to include ADP and phosphonoacetate in these measurements to reduce the inactivation rates into a measurable range. These data were fit to a single exponential decay (Equation 1), where the fastest rate of inactivation was observed in the absence of substrates (Figure III-10; Table III-3). This indicates that the BCCP domain explores an ensemble of conformations in the absence of substrates, trapping the carrier domain in an intermolecular conformation in a time-dependent manner. The presence of ADP and phosphonoacetate reduced the rate of inactivation ~7-fold, consistent with BC domain substrates drawing the carrier domain equilibrium position towards the BC domain. Conversely, the addition of acetyl-CoA increased the rate of inactivation, consistent with a reduction in the activation energy barrier for the translocation of the carrier domain from the BC to the CT domain. The combination of acetyl-CoA and pyruvate produced the fastest rates of inactivation in the presence of ADP and phosphonoacetate (Figure III-10; Table III-3).

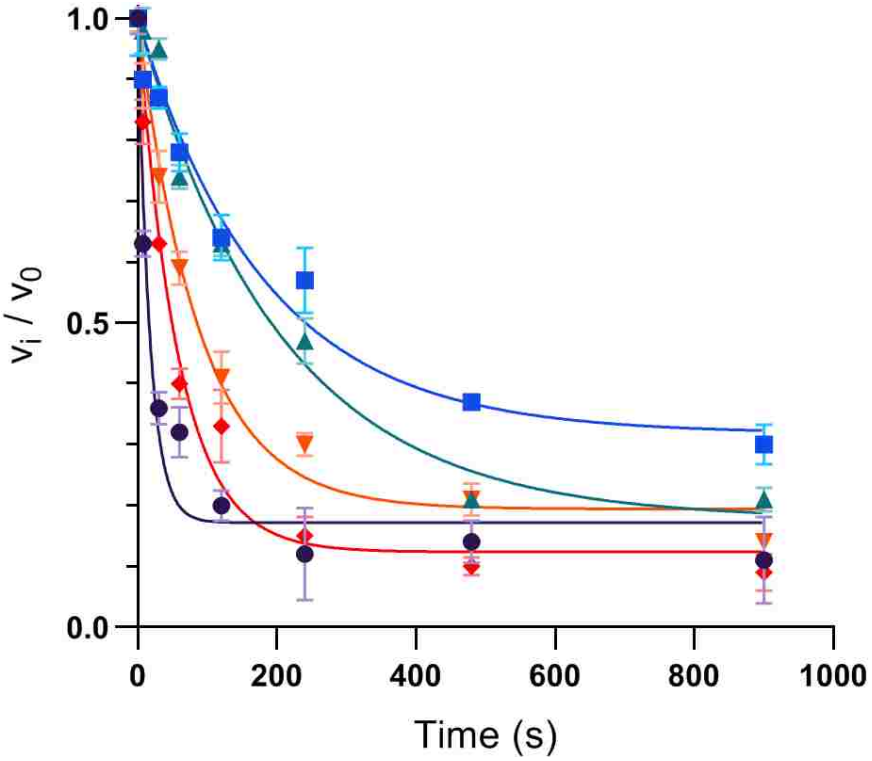

Figure III-10 Inactivation kinetics for Q891C/N1102C SaPC crosslinked with BMOE in the presence of various substrates.
Inactivation kinetics for Q891C/N1102C SaPC crosslinked with BMOE in the presence of various substrates. Q891C/N1102C SaPC was reacted with 300 μM BMOE in 5% DMSO for 10 s, 30 s, 1 min, 2 min, 4 min, 8 min, or 15 min and then quenched with 13 mM DTT for 15 min. Each sample was then assayed in triplicate for catalytic activity using the malate dehydrogenase coupled enzyme assay. The initial velocity (v_i) was determined and divided by the initial velocity determined after incubating the same enzyme with 5% DMSO for 15 min (v_o). The error bars represent the standard deviation obtained from each sample assayed in triplicate. Rates were measured in the absence of added ligands (purple circles), in the presence of 5 mM ADP and 5 mM phosphonoacetate (blue squares), in the presence of 5 mM ADP, 5 mM phosphonoacetate, and 12 mM pyruvate (green triangles), in the presence of 5 mM ADP, 5 mM phosphonoacetate, and 0.25 mM acetyl-CoA (orange inverted triangles), or in the presence of 5 mM ADP, 5 mM phosphonoacetate, 12 mM pyruvate, and 0.25 mM acetyl-CoA (red diamonds).

Table III-3 Observed rates of inactivation for the different substrate combinations used during inactivation kinetics experiments with Q891C/N1102C SaPC.

ADP	Phosphonoacetate	Pyruvate	Acetyl-CoA	k_{obs} (s^{-1})*
0	0	0	0	0.057 ± .014
5 mM	5 mM	0	0	0.005 ± .001
5 mM	5 mM	0	0.25 mM	0.011 ± .001
5 mM	5 mM	12 mM	0	0.005 ± .001
5 mM	5 mM	12 mM	0.25 mM	0.017 ± .002

* Reported errors represent the standard errors calculated from iterative non-linear curve fitting in GraphPad Prism. The data were fit to data where each data point was plotted as the average ± standard deviation of 3 independent determinations.

The effects of substrates on BCCP domain positioning were further evaluated by following changes in ITF intensity. The rapid acquisition of ITF data in a stopped-flow instrument permitted a direct analysis of the effect of substrates and effectors on BCCP domain positioning, without requiring the inclusion of ADP and phosphonoacetate in all experiments. Q891C/N1102C *Sa*PC was mixed with various substrates and the change in ITF intensity was monitored continuously for 120 seconds. The presence of ADP and phosphonoacetate decreased the observed ITF intensity, as shown in the first 120 seconds of Figure III-11, consistent with the data presented in Figure III-6A. After the system was allowed to reach equilibrium, the crosslinker was subsequently added to observe the impact of the ligand on the rate at which the system re-equilibrates to the trapped conformation. The data were fit to a single exponential equation (Equation 2). After addition of the crosslinker, ITF was followed for an additional 120 seconds. The presence of ADP and phosphonoacetate substantially reduced the rate of increase in the ITF intensity, relative to the combination of either or both acetyl-CoA and/or pyruvate with ADP and phosphonoacetate (Figure III-11). A comparison of the observed rates of carrier domain repositioning, measured by each approach, is summarized in Table III-2. This

reveals remarkable agreement between the measurements, despite the different methods used.

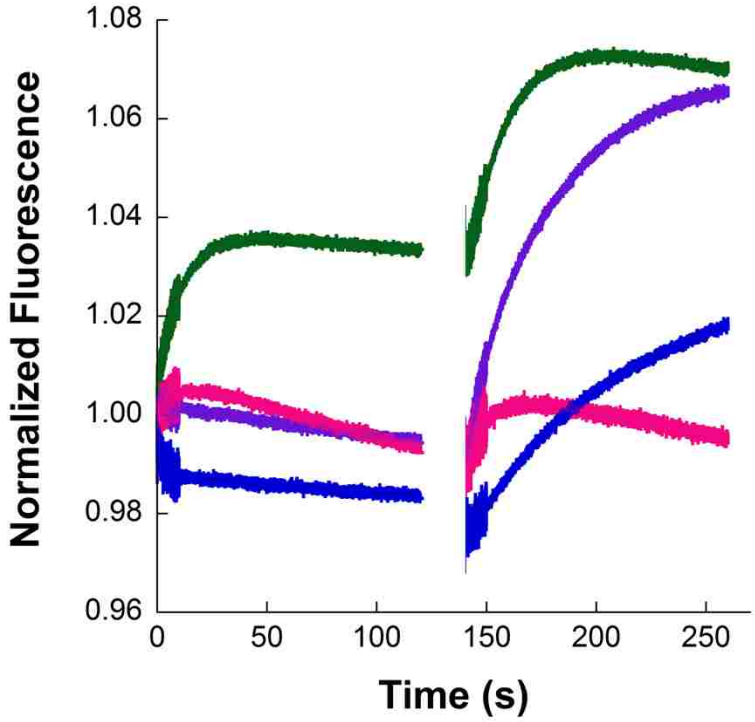

Figure III-11 SaPC ITF intensity in the presence of substrates/effector.
Q891C/N1102C SaPC was first mixed with ligand at t = 0 and the ITF intensity was recorded for 120 seconds. Q891C/N1102C SaPC, preincubated with the ligand, was then mixed with ligand and 200 μM BMOE, to the same final concentrations, and the ITF intensity was recorded for 120 seconds (denoted as beginning at 140 seconds). In all cases Q891C/N1102C SaPC was mixed to a final concentration of 0.175 mg/mL with buffer (purple), 12 mM final concentration of pyruvate (pink), 0.25 mM final concentration of acetyl-CoA (green), or 5 mM final concentrations each of ADP and phosphonoacetate (blue) in a stopped-flow instrument. Tryptophan was excited at 295 nm and ITF emission was recorded at 350 nm.

Using ITF intensity as a direct measure of carrier domain positioning, we sought to investigate the role of two allosteric effectors in carrier domain positioning: acetyl-CoA and L-aspartate. Acetyl-CoA enhances the coupling efficiency between the two half-reactions of PC (Zeczycki, et al., 2011B). Westerhold et al. proposed that the enhanced coupling efficiency in the presence of acetyl-CoA is mediated by the carrier domain (Westerhold, et al., 2017). In the present study, acetyl-CoA increased the ITF intensity,

consistent with the carrier domain positioning equilibrating to favor an intermolecular interaction with the CT domain (Figure III-11). While acetyl-CoA does not, on its own, alter the observed rate of ITF intensity change, the combination of pyruvate and acetyl-CoA leads to a 360% increase in the observed rate of ITF intensity change in the presence of BMOE (*t* test; $p < 0.01$) (Table III-4, Figure III-12). Acetyl-CoA also increased the observed rate of ITF intensity change when ATP was present in combination with BMOE. These data indicate that acetyl-CoA reduces the kinetic barrier for the translocation of the carrier domain in the presence of substrates.

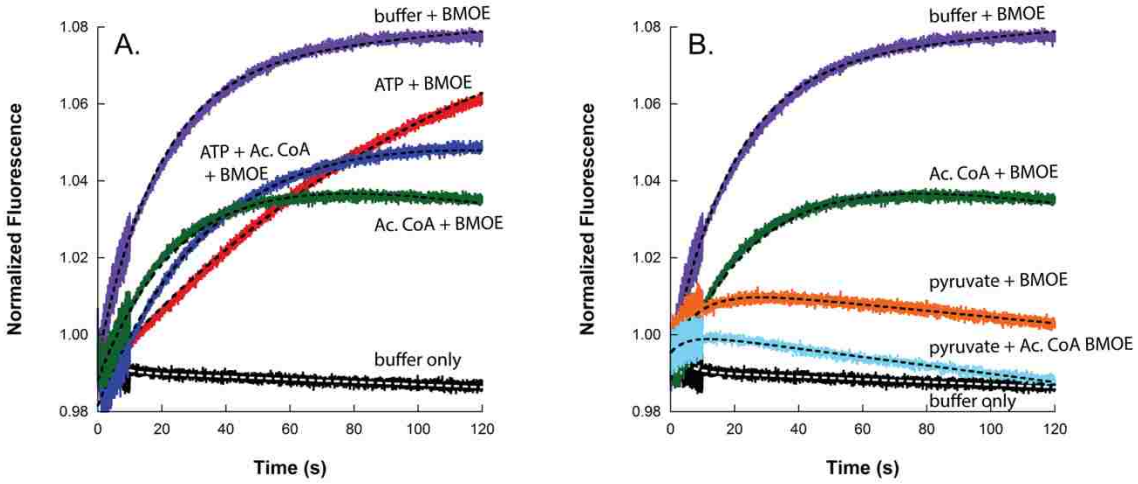

Figure III-12 Q891C/N1102C SaPC crosslinked in the presence of ligands and monitored for change in ITF intensity.
A final concentration of 0.175 mg/mL Q891C/N1102C SaPC was mixed with either buffer or various substrates at final concentrations listed in the Methods section, with 200 µM BMOE present at 0 s in a stopped-flow instrument with tryptophan excitation at 295 nm and emission measured at 350 nm. **A.** SaPC was mixed with either buffer (black), buffer + BMOE (purple), ATP + BMOE (orange), acetyl-CoA and BMOE (green), or ATP + acetyl-CoA + BMOE (blue). **B.** SaPC was mixed with either buffer (black), buffer+BMOE (purple), acetyl-CoA + BMOE (green), pyruvate + BMOE (orange), or acetyl-CoA + pyruvate +BMOE (blue). Dashed lines represent the fit of the data to Equation 2.

Table III-4 The effect of ligands on the observed rates of ITF intensity change.

substrate (+ BMOE)	Q891C/N1102C SaPC k_{obs} (s^{-1})	k_{obs} / (k_{obs} [No Substrate])
None	[4.8 ± 1.0] x 10^{-2}	-
ATP	[3.0 ± 0.3] x 10^{-2}	0.63
Acetyl-CoA + ATP	[3.6 ± 0.3] x 10^{-2}	0.75
Acetyl-CoA	[5.0 ± 0.3] x 10^{-2}	1.0
Pyruvate + Acetyl-CoA	[17.4 ± 2.6] x 10^{-2}	3.6
L-Aspartate	[3.4 ± 1.0] x 10^{-2}	0.70
None*	[7.3 ± 0.2] x 10^{-2}	-
Pyruvate*	[8.1 ± 0.1] x 10^{-2}	1.1

* Assay performed independently from above data. (n = 3; errors represent standard deviations)

L-aspartate is an allosteric inhibitor of microbial PC enzymes (Osmani, et al, 1981; Cazzulo and Stoppani, 1968; Jitrapakdee, et al., 2007; Sirithanakorn, et al., 2014). L-aspartate inhibition is competitive with respect to acetyl-CoA and its effects are independent of the coupling between MgATP cleavage and oxaloacetate formation (Sirithanakorn, et al., 2014). Sirithanakorn et al. proposed that L-aspartate may inhibit carboxybiotin formation or slow the rate of carrier domain translocation between the active sites (Sirithanakorn, et al., 2014). When L-aspartate is mixed with Q891C/N1102C *Sa*PC, no ITF intensity change is observed (Figure III-13A), in contrast to what is observed with the allosteric activator, acetyl-CoA. However, when Q891C/N1102C *Sa*PC is crosslinked in the presence of L-aspartate, the observed rate of ITF intensity change is 30% slower (*t* test; $p < 0.05$) (Table III-4, Figure III-13B) than the rate in its absence. This indicates that while L-aspartate may not alter the ground state energy of the enzyme, it has a kinetic effect that reduces the rate of carrier domain repositioning.

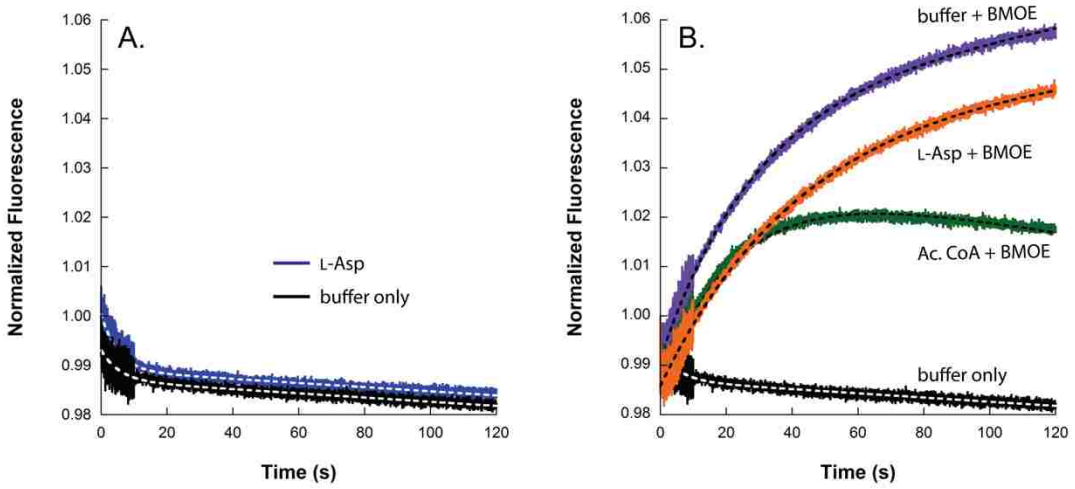

Figure III-13 Effect of L-aspartate on Q891C/N1102C SaPC carrier domain positioning and crosslinking rates.
Data was collected with a stopped-flow instrument with tryptophan excitation at 295 nm and ITF emission measured at 350 nm. **A.** SaPC was mixed with either buffer (black) or a final concentration of 10 mM L-aspartate (blue) at 0 sec. **B.** SaPC was mixed with either buffer (black), buffer + 200 μM BMOE (purple), 10 mM L -aspartate + 200 μM BMOE (orange), or 0.25 mM acetyl-CoA (green) at 0 sec. Dashed lines represent the fit of the data to Equation 2.

3. Discussion

The carrier domain of PC is known to translocate during catalysis between an intramolecular interaction with the BC domain and an intermolecular interaction with the CT domain on the opposing subunit (Figure 1) (St. Maurice, et al., 2007; Xiang and Tong, 2008; Lasso, et al., 2014; Liu, et al., 2018). Here, we directly observe the positioning of the PC carrier domain, independent of catalytic turnover, using a range of techniques that rely on trapping the carrier domain in an intermolecular conformation, in close proximity to the CT domain. Several models of PC catalysis propose that the carrier domain is governed by an induced conformational change: the carrier domain remains in proximity of the BC domain until a CT domain ligand binds, and is subsequently induced to translocate to the CT domain upon the binding of a CT domain ligand (Easterbrook-

Smith, et al., 1976; Goodall, et al., 1981; Attwood and Wallace, et al., 1986). However, several structures of PC reveal the carrier domain participating in an intermolecular interaction with the CT domain, even in the absence of ligands. These structures suggest that the carrier domain can sample a wide range of conformations, consistent with a conformational selection model where substrates and effectors serve to shift the equilibrium positioning of the carrier domain from one domain to another during catalysis. A conformational selection model is in opposition to previous interpretations, but it is well supported by the direct observations of carrier domain positioning presented in this study. It is particularly noteworthy that, regardless of the presence or identity of the ligands, multiple approaches demonstrate that the carrier domain can be trapped in proximity to the CT domain. This can only be the case if, under all conditions, the carrier domain regularly samples positions proximal to the CT domain, consistent with a conformational selection model. A similar model has recently been proposed to govern conformational dynamics in the nonribosomal polypeptide synthase, gramicidin synthetase I from *Aneurinibacillus migulanus*. Positional changes of the carrier domain in gramicidin synthetase I correlate with the presence of bound ligands, where the carrier domain samples multiple conformations in a dynamic equilibrium (Alfermann, et al., 2017). The carrier domains of polyketide synthases, such as 6-deoxyerythronolide B synthase (DEBS), may also be governed by conformational selection, with the carrier domain positional equilibrium shifted by a turnstile mechanism that ensures synchronization of the assembly line-style reactions (Lowry, et al., 2016).

The observed rates of carrier domain re-equilibration are remarkably consistent across multiple methods of observation (Table 1). The general crosslinking approach,

therefore, provides multiple ways to independently measure rates of carrier domain repositioning, absent of catalytic turnover. It should be noted that the observed rates of repositioning are two orders of magnitude lower than the k_{cat} value and are not a suitable estimate of carrier domain translocation rates during catalytic turnover. Rather, the observed rate constants represent the re-equilibration of the BCCP domain to the exo-binding site within an ensemble population and include the chemical crosslinking steps which are likely to be slow relative to the rate of carrier domain translocation. Nevertheless, the relative rates of re-equilibration clearly indicate that the carrier domain is subject to conformational selection and that ligands alter the equilibrium position of the carrier domain.

Substrates and ligands shift the carrier domain equilibrium as expected. BC domain ligands reduce the rate of intermolecular crosslinking (Figures 2 and 6, Tables 1, 2, and 3) and shift the carrier domain equilibrium away from the CT domain (Figures 4 and 7), consistent with proposals that BC domain ligands shift the carrier domain towards the BC domain (Easterbrook-Smith, et al., 1976; Goodall, et al., 1981; Attwood and Wallace, 1986). These data are consistent with a ground state stabilization of the BC-BCCP domain interaction, resulting in a higher activation energy barrier and slower rate of re-equilibration to the trapped intermolecular interaction with the CT domain. X-ray crystal structures show that the active site lid of the BC domain partially closes when Mg^{2+} and ATP are bound in the active site (Thoden, et al., 2000). When the BCCP domain interacts with the BC domain, the carrier domain is positioned directly against this tightly closed lid of the BC domain (Lietzan, et al., 2011). The lid closure that accompanies ligand binding

produces the binding interface for the carrier domain, stabilizing the BCCP-BC domain conformation, and shifting the BCCP positioning equilibrium toward the BC domain.

Pyruvate, the CT domain substrate, increased the k_{obs} for intermolecular crosslinking (Figures 6 and 7; Tables 1 and 2). These results are consistent with observations that high concentrations of pyruvate inhibit the biotin-dependent ATPase reaction in PC (Zeczycki, et al., 2009). The conformational selection model allows that the carrier domain samples multiple positions and that the carrier domain positional equilibrium shifts to the CT domain as a consequence of biotin-dependent interactions with CT domain substrates (Lietzan, et al., 2013A). Similar interactions are thought to govern carrier protein positioning of SoxYZ with SoxB. In the substrate-unbound state, a mobile loop clashes with the SoxYZ binding site whereas, in the presence of substrate, the loop shifts to favor the SoxYZ interaction with SoxB (Grabarczyk, et al., 2015). These systems offer clear, simple examples of how substrates can locally shift carrier domain positioning through conformational selection, without the need to invoke long-range induced conformational changes to control carrier domain positioning.

Carrier domain positioning in the CT domain active site is proposed to be mediated by biotin (Lietzan, et al., 2013A). The carrier domain was trapped in an intermolecular crosslink, even in the absence of biotin (Figure S3), demonstrating that the carrier domain does not require biotin to adopt an intermolecular position. However, biotinylation strongly influences the carrier domain positioning equilibrium and the sensitivity of the enzyme to ligands. The positional equilibrium shifts dramatically, as observed by a greater than two-fold shift in the amount of uncrosslinked monomer at equilibrium (Figure S3). Furthermore, the unbiotinylated enzyme becomes insensitive to

the BC domain ligands, ADP and phosphonoacetate: in both their presence and absence, the k_{obs} for the unbiotinylated enzyme is equivalent to the rate observed for the biotinylated enzyme in the absence of substrates. Thus, biotin is necessary for the carrier domain to be sensitive to the presence of BC domain substrates and is critical to mediating the binding interactions with both the BC and CT domain active sites.

The allosteric activator, acetyl-CoA, increased the observed fluorescence signal intensity, indicating that acetyl-CoA shifts the carrier domain equilibrium towards the opposing CT domain (Figures 4A and 7). The presence of acetyl-CoA also increased the k_{obs} for inactivation (Figure 6), even when ADP and phosphonoacetate were also present, further suggesting that acetyl-CoA favors an intermolecular positioning for the carrier domain. This agrees with our recent observation that acetyl-CoA uniquely activates an intermolecular catalytic pathway in which the carrier domain translocates to the CT domain on an opposing subunit (Liu, et al., 2018). The current findings suggest that acetyl-CoA activates that translocation pathway by favoring intermolecular carrier domain positioning at the CT domain. Contrary to the effect of acetyl-CoA on carrier domain positioning, L-aspartate had a negligible effect on carrier domain positioning, but it moderately reduced the observed rate of carrier domain intermolecular crosslinking (Figures S6A and S6B). This suggests that at least a portion of the inhibitory effect of L-aspartate derives from reducing the rate of carrier domain translocation, as hypothesized by Sirithanakorn, et al (Sirithanakorn, et al., 2014).

The current study leads to an updated model of conformational selection for carrier domain positioning in PC. The carrier domain exists in an ensemble of conformations, where ligand binding shifts the equilibrium to favor those conformations

that have a higher affinity for the ligand (Boehr, et al., 2009). Prior structural data suggest how these equilibrium shifts can occur. BC domain substrates promote the closing of the B-subdomain lid, generating a favorable binding site for the carrier domain. Similarly in the CT domain, the presence of a CT domain substrate or substrate analogue promotes the formation of a biotin-binding pocket that favors the positioning of biotin in the CT domain active site, shifting carrier domain positioning towards the CT domain (Lietzan, et al., 2013A). Common to both cases, biotin is chiefly responsible for interacting with residues in each active site, mediating the shift in equilibrium positioning of the carrier domain. However, independent of biotin, the carrier domain actively explores what is likely to be a wide variety of conformations. Both biotin and active site ligands promote interactions at the individual domains to shift the conformational equilibrium. Allosteric activation by acetyl-CoA facilitates the release of the carrier domain from the BC domain and promotes the intermolecular positioning of the carrier domain near the CT domain active site. Conformational selection offers a simple and updated model to explain the kinetic behavior of PC in response to substrates and allosteric effectors. Such a model is highly applicable to the positioning and long-range translocation of carrier domains and carrier proteins in a range of other complex multi-modular enzyme systems.

IV. THE CARRIER DOMAIN POSITIONAL EQUILIBRIUM OF *S. AUREUS* PYRUVATE CARBOXYLASE IS GOVERNED BY INTERACTIONS BETWEEN BIOTIN AND ACTIVE SITE RESIDUES

1. Introduction

In chapter III, I demonstrated that the carrier domain positioning of *Sa*PC is governed by conformational selection. Substrates shift the carrier domain positional equilibrium while acetyl-CoA favors an intermolecular positioning of the carrier domain in the presence of substrates. While it is clear from chapter III that substrates, allosteric effectors and biotin alter the equilibrium positioning of the carrier domain, the molecular interactions underlying these positional shifts are not well described.

Carrier domains are used in multi-domain enzymes to shuttle intermediate products between active sites. The molecular interactions that contribute to carrier domain positioning represent an area of intense study in many carrier-domain enzymes. For example, the interaction between the acyl carrier protein (ACP) and the microbial fatty acid synthase pathway enzyme FabA was observed to be regulated by electrostatic interactions between the ACP and the surface of FabA, gating residues at the opening to the active site, and the size of the active site pocket (Finzel, et al., 2015). The conformational equilibrium of the nonribosomal peptide synthase gramicidin synthetase I from *Aneurinibacillus migulanus* has been found to be shifted by product inhibition, with a series of interactions between residues and substrates and intermediate products proposed to be responsible for this shift. (Alfermann, et al., 2017; Branchini, et al., 2011). In the Sox pathway, the interaction of the carrier protein SoxYZ with the enzyme SoxB has been found to be controlled, in part, by the positioning of a surface mobile loop that

exists in different conformations dependent upon the presence of substrate (Grabarczyk, et al., 2015). Studies investigating carrier protein-catalytic domain interactions have detailed numerous mechanisms governing the favorability of these interactions as the presence and identity of ligands change. While the field has begun to elucidate these mechanisms, the descriptions are currently limited to just a few discrete examples, precluding a general description of common mechanism(s) responsible for altering carrier domain positioning. Studies on the interactions between biotin and active-site residues and their contributions to shifting carrier domain positioning in PC will provide fresh examples of how carrier domain positioning is influenced by molecular level interactions.

A number of kinetic and structural studies in PC have sought to unveil the molecular basis for carrier domain positioning. Two x-ray crystal structures of PC offer useful insights into how carrier domain equilibrium positioning may be shifted through interactions with the BC and CT domains. The structure of *R. etli* PC (*Re*PC) co-crystallized with ADP and phosphonoacetate, captured the interaction between the carrier domain and the BC domain (Lietzan, et al., 2011). In this structure, biotin was occluded from the BC domain active site by a salt bridge formed between Arg353 and Glu248. This conserved pair of residues was proposed to act as a molecular gatekeeper, preventing carboxybiotin from returning to the active site where it could undergo abortive decarboxylation (Lietzan, et al., 2011). Similarly, a structure of the isolated CT domain of *Re*PC revealed that a flexible loop in the CT domain active site alters its conformation when pyruvate is bound, providing a stabilizing interaction between the sulfur in the thiophene ring of biotin and the aromatic ring of Tyr628[5]. Another CT domain active site residue, Thr882 in *Re*PC, was shown to play a critical role in shuttling a proton between

the biotin enolate intermediate and pyruvate and was also proposed to play a role in stabilizing the positioning of biotin in the CT domain active site through a hydrogen-bonding interaction with the N-1 of biotin[6]. Kinetic studies on a site-directed mutation of this residue (T882A) were interpreted to suggest that Thr882 is important in carrier domain positioning at the CT domain. Together, conserved residues in both the BC and CT domains are likely to make critical contributions to the positioning of the carrier domain through their interactions with biotin. However, the hypothesized roles of these residues are based on static structures and indirect kinetic studies that do not provide dynamic information on the interplay between ligand, residue, and carrier domain positioning.

In this chapter, I seek to describe the role of three conserved residues that are predicted to interact with biotin to better understand the mechanism of ligand-associated carrier domain positioning changes in pyruvate carboxylase. Site-specific crosslinking is monitored by intrinsic tryptophan fluorescence (ITF) to more precisely determine the effects of ligands and the roles of the "gatekeeper" residues on carrier domain positioning. Tyr621 (equivalent to Tyr628 in *Re*PC) in *S. aureus* PC (*Sa*PC) was shown to have a crucial role in the positioning of the carrier domain, mutation of Glu243 (equivalent to Glu248 in *Re*PC) was observed to shift carrier domain positioning towards the BC domain, and mutation of Thr876 (equivalent to Thr882 in *Re*PC) was also observed to shift carrier domain positioning towards the BC domain while decreasing the effect of pyruvate on carrier domain positioning.

2. Results

2.1 Active Site Mutations Shift Carrier Domain Positioning

As described in chapter III, I have designed and validated a system to trap the carrier domain in the exo-binding site through the introduction of site-specific Cys residues and the maleimide-based homobifunctional crosslinker, BMOE (Figure III-1B). This Q891C/N1102C (QN) mutant was used as a crosslinking-competent background into which additional mutations of active site residues were introduced.

Three residues (Glu243, Thr876 and Tyr621) have been proposed to interact with biotin and contribute to translocation of the carrier domain. Consequently, three mutations were introduced into the Q891C/N1102C (QN) crosslinking-competent background. The proposed role of these residues (E243A, T876A, and Y621) in catalysis is summarized in Table IV-1. The catalytic activities of these mutants are reported in Table IV-2 and are similar to the activities reported in previous studies of these mutations (Lietzan, et al., 2011; Lietzan, et al., 2013).

Table IV-1 Summary of active site residues selected for mutation in PC.

Residue	Location	Proposed Function	Citation
Glu243	BC Domain	One of two "gatekeeper" residues that control biotin access to active site	Lietzan, et al., 2011; Zeczycki, et al., 2011
Tyr621	CT Domain	Stabilize biotin in active site	Lietzan, et al., 2013
Thr876	CT Domain	Proton shuttle during CT domain reaction, H-bond to biotin	Zeczycki, et al., 2011

Table IV-2 Kinetic characterization of Q891/N1102C *Sa*PC and related mutants.

*Sa*PC Mutant	Pyruvate carboxylation k_{cat}, min^{-1}	Oxamate-induced oxaloacetate decarboxylation k_{cat}, min^{-1}	ADP Phosphorylation k_{cat}, min^{-1}
Wild-Type	1440 ± 100	3.9 ± 0.1	0.63 ± 0.01
Q891C/N1102C	440 ± 10	19 ± 1	2.1 ± 0.1
Q891C/N1102C/E243A	2.2 ± 0.1	20 ± 1	3.1 ± 0.1
Q891C/N1102C/Y621A	14 ± 0.2	0.15 ± 0.02	0.47 ± 0.02
Q891C/N1102C/T876A	N/A	N/A	0.62 ± 0.01

The triple mutants were individually mixed with BMOE and were monitored for changes in ITF intensity, to determine the role these residues play in carrier domain positioning. The data were fit to Equation 2, which yields an observed rate constant (k_{obs}) and an observed amplitude for ITF intensity change. In the interpretation of these data, the k_{obs} is considered to be proportional to the kinetic barrier associated with the carrier domain adopting a new conformation. The observed amplitude represents the relative proportion of the carrier domain population that shifts from the initial equilibrium to the crosslinked conformation. As reported in Figure IV-1, both of the CT domain mutations (T876A or Y621A) resulted in an increase in k_{obs}. It was not surprising to observe an increase in k_{obs} considering that Thr876 and Tyr621 are proposed to interact with and stabilize biotin in the CT domain active site (Lietzan, et al., 2013). Perhaps, with these residues mutated, the carrier domain has more freedom to adopt a wider range of conformations and movements that increase the rate of crosslinking to the exo-binding site.

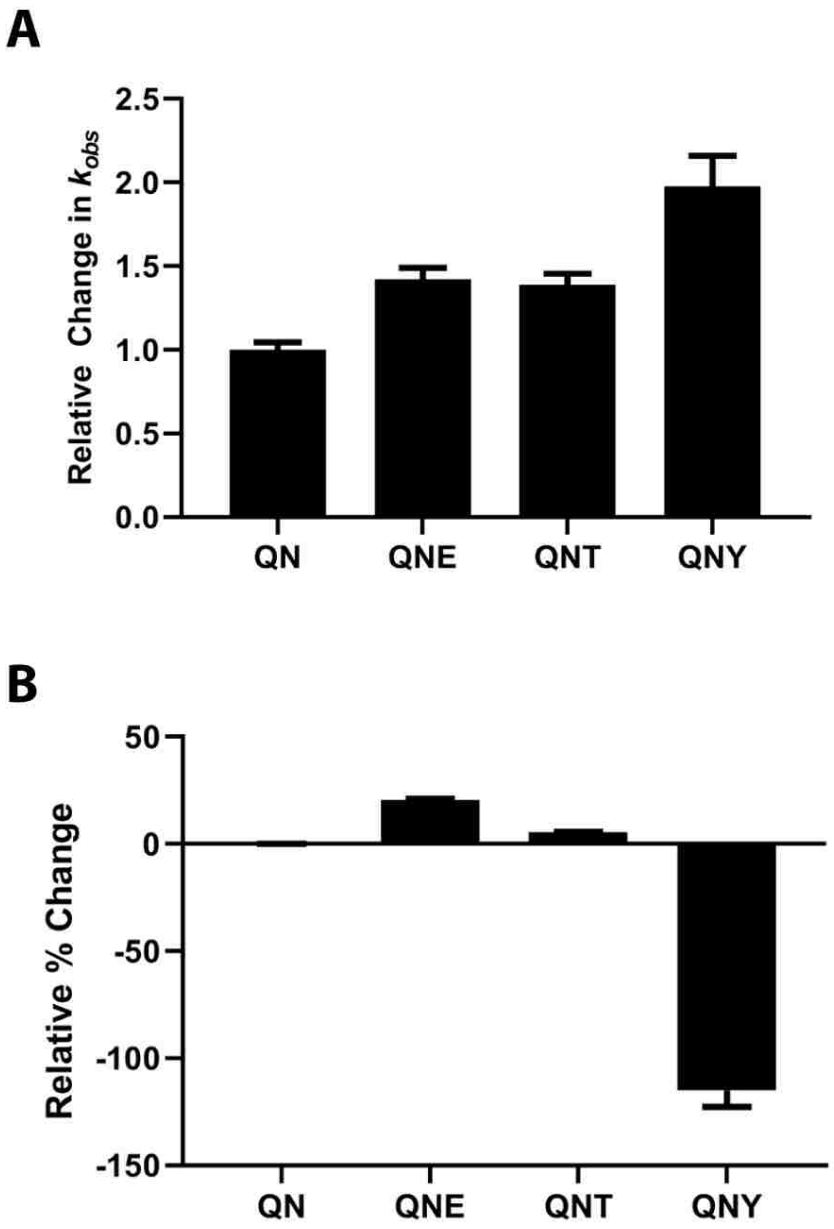

Figure IV-1 Observed rates and amplitudes of ITF change from QN *Sa*PC mutants during crosslinking with BMOE

Q891C/N1102C (QN) *Sa*PC, Q891C/N1102C/E243A (QNE) *Sa*PC, Q891C/N1102C/T876A (QNT) *Sa*PC, and Q891C/N1102C/Y621A (QNY) *Sa*PC were mixed with BMOE at 0 sec. in a stopped-flow instrument with tryptophan excitation at 295 nm and ITF emission measured at 350 nm. A single exponential decay equation was fit to the data. **A.** The relative change in k_{obs} is the k_{obs} obtained for each of the three active-site residue mutants divided by the k_{obs} obtained from the QN background. All measurements were made in triplicate. Error bars represent the standard deviation. **B.** The amplitudes of ITF signal change from the single exponential decay for each of the three active-site residue mutants obtained in A. were divided by the amplitude change obtained for the corresponding crosslinking background to yield a relative % change.

The Y621A mutation produced a drastically different behavior than the other mutations, with a large increase in the magnitude of the ITF signal change observed in the crosslinked Q891C/N1102C/Y621A (QNY) *Sa*PC mutant compared to the QN crosslinking background. It is important to note that crosslinking still occurs in the QNY mutant, as confirmed by the formation of crosslinked dimers of QNY *Sa*PC when analyzed by SDS-PAGE (Figure IV-2A). Interestingly, the ITF signal *decreases* for the QNY mutant in the presence of crosslinker, which is opposite to the behavior observed in all other cases (Figure IV-2B). This dramatic shift in initial equilibrium positioning of the carrier domain, observed by the large change in amplitude, may demonstrate that Tyr621 has an important role in establishing the carrier domain positional equilibrium (Figure IV-1B). In contrast to the QNY mutant, the amplitude of the ITF signal change during crosslinking of the Q891C/N1102C/T876A (QNT) *Sa*PC mutant remained similar to the QN crosslinking background, suggesting that the baseline equilibrium positioning of the carrier domain was not significantly shifted by this mutation.

The observed rate of change in the ITF intensity increased in the Q891C/N1102C/E243A (QNE) *Sa*PC mutant. The overall signal evolution of the ITF signal appeared similar to that of the crosslinking background as shown in Figure IV-2. The amplitude of the ITF signal changes increased in the QNE mutant compared to background, indicating that the carrier domain equilibrium has shifted towards the BC domain in this mutant.

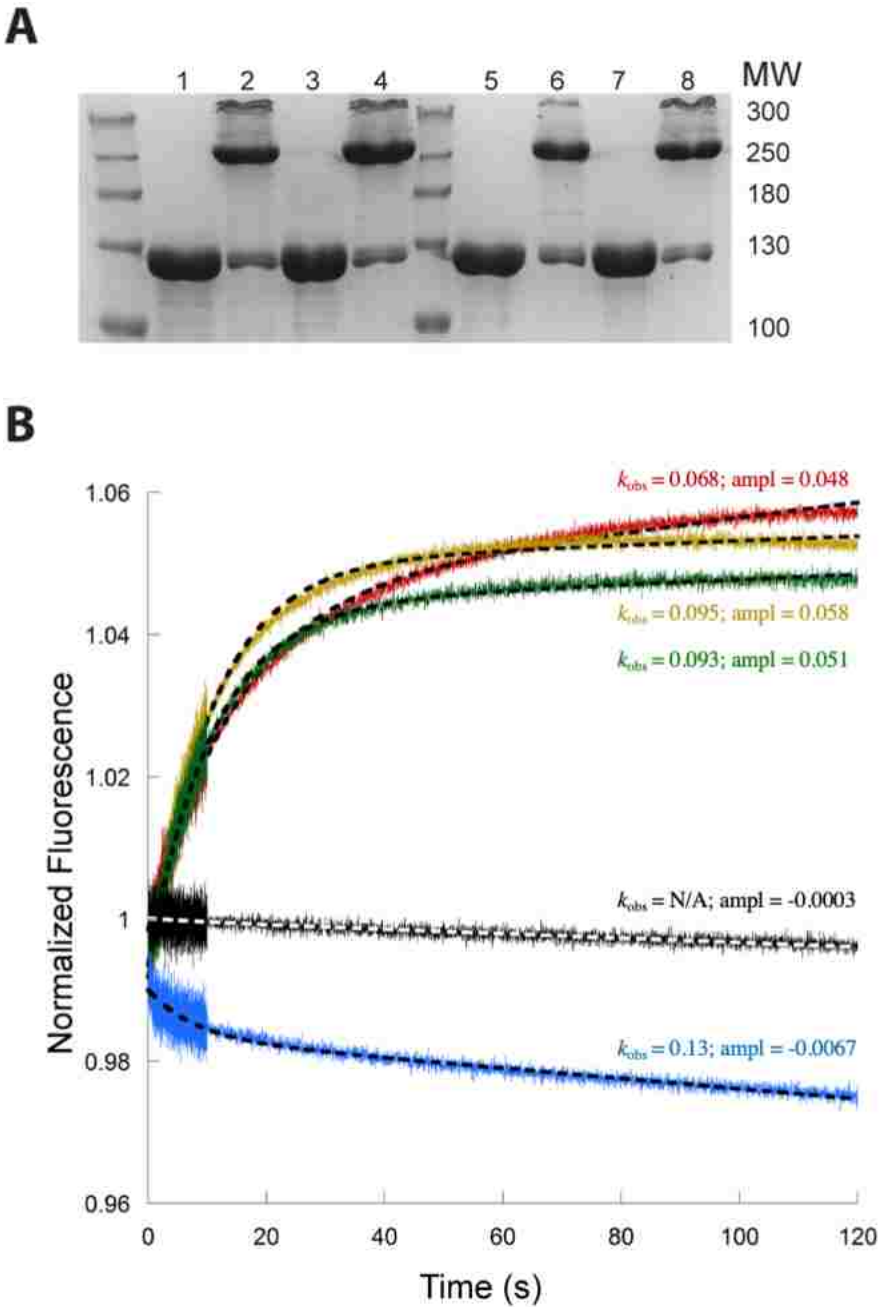

Figure IV-2 QN SaPC mutants crosslinked and ITF intensity changes.
A. *Sa*PC mutants as listed below at 1 mg/mL were reacted with 5% DMSO or 300 μM BMOE for 120 s, then quenched with 13 mM DTT for 15 minutes. 5 μg of *Sa*PC was loaded in each lane. (1) Q891C/N1102C w/ DMSO (2) Q891C/N1102C w/ BMOE (AC); (3) Q891C/N1102C/E243A w/ DMSO; (4) Q891C/N1102C/E243A w/ BMOE; (5) Q891C/N1102C/Y621A w/ DMSO; (6) Q891C/N1102C/Y621A w/ BMOE; (7) Q891C/N1102C/T876A w/ DMSO; (8) Q891C/N1102C/T876A w/ BMOE. The molecular weights for the ladders are shown in kDa. **B**. Q891C/N1102C *Sa*PC (red), Q891C/N1102C/E243A *Sa*PC (gold), Q891C/N1102C/T876A *Sa*PC (green), or Q891C/N1102C/Y621A *Sa*PC (blue) was mixed with a final concentration of 200 μM BMOE at t = 0 and the ITF intensity was recorded for 120 seconds. Tryptophan was excited at 295 nm and ITF emission was recorded at 350 nm.

2.2 Mutation of Glu243 Shifts Carrier Domain Positioning Towards the BC Domain.

Glu243 was proposed to serve as one of two residues that serve as "gatekeepers" to prevent the return of carboxybiotin to the BC domain active site where abortive decarboxylation could occur (Lietzan, et al., 2011). To further investigate the role of Glu243, the response of the QNE system to various substrates and effectors was evaluated in relation to the QN control.

The observed rates of ITF intensity change were quite similar for the QNE mutant relative to the QN background and followed the same trends in the response to ligands (Figure IV-3A). However, the relative amplitude of ITF signal increased when the QNE enzyme was crosslinked in the presence of BC domain ligands compared to the QN background (Figure IV-3B). This is consistent with an overall shift in carrier domain equilibrium positioning towards the BC domain in the QNE mutant, particularly in the presence of BC domain ligands. The E243A mutation seems to have no appreciable effect on the shift in carrier domain positioning in the presence of pyruvate with similar k_{obs} and observed amplitudes of ITF signal change compared to those observed in the crosslinking background (Figure IV-3). In QNE *Sa*PC and in the presence of acetyl-CoA, k_{obs} was ~19% lower than k_{obs} in the absence of acetyl-CoA ($p < .001$), suggesting that this mutation has raised a kinetic barrier to carrier domain repositioning in the presence of acetyl-CoA (Figure IV-3A). The amplitude of observed ITF signal change also increased in the QNE mutant in the presence of acetyl-CoA compared to the QN background, indicating that an equilibrium shift has occurred towards the BC domain in this mutant (Figure IV-3B).

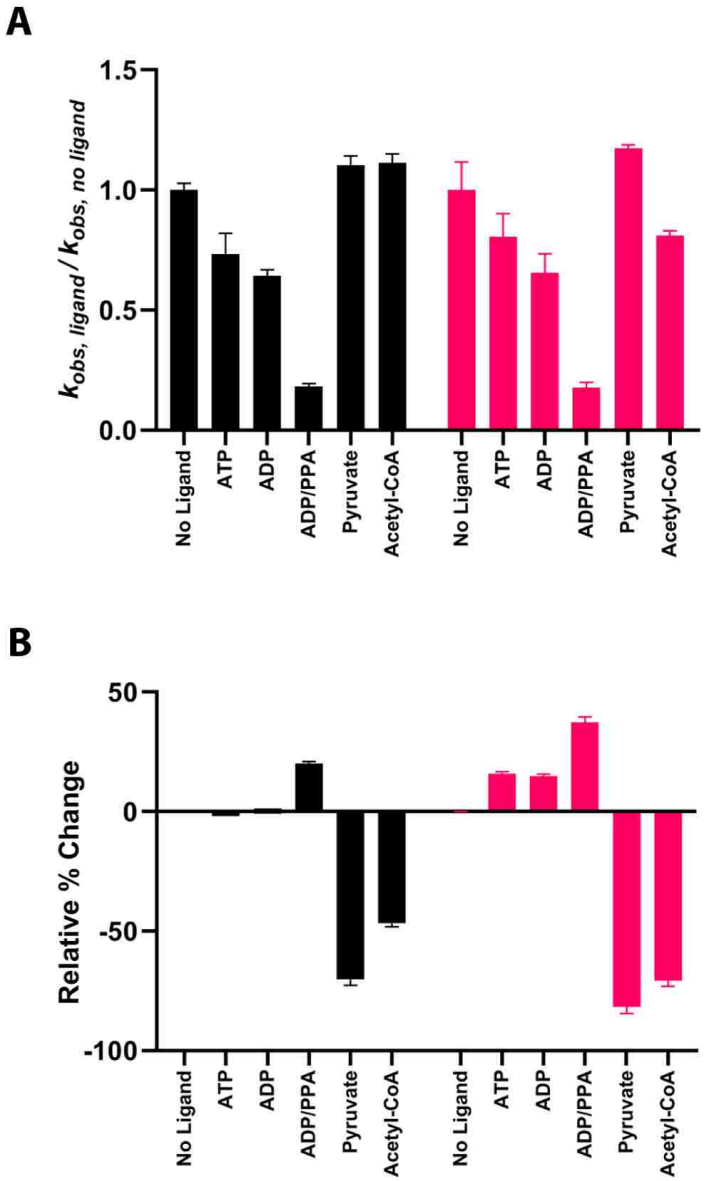

Figure IV-3 Observed rates and amplitudes of ITF change from Q891C/N1102C/E243A SaPC during crosslinking with BMOE in the absence/presence of ligands.
A. Q891C/N1102C SaPC (black) and Q891C/N1102C/E243A SaPC (pink) were incubated for a minimum of 10 minutes with 2.5 mM ATP, 0.25 mM acetyl-CoA, 12 mM sodium pyruvate, 5 mM ADP, or 5 mM phosphonoacetate (PPA) and then mixed with BMOE and an equal concentration of the substrate/effector at 0 sec. in a stopped-flow instrument with tryptophan excitation at 295 nm and ITF emission measured at 350 nm. Equation II-2 was fit to the data and the k_{obs} obtained for each of the three active-site residue mutants compared to the k_{obs} obtained from the corresponding crosslinking background mutant. All measurements were taken in triplicate with the error bars representing the standard deviation in the rate. **B.** The amplitudes of ITF signal change from the single exponential equation for each of the three active-site residue mutants described in panel A were compared to the amplitude obtained for the corresponding crosslinking background.

2.3 Thr876 Mediates Carrier Domain Positioning in Response to Pyruvate

To investigate the role of the CT domain active site threonine (Thr876) in carrier domain positioning, changes in the amplitude and rates of ITF signal changes were measured in the QNT enzyme and compared to the response of the QN background. In the presence of ATP or ADP, the observed rates of ITF intensity change for the QNT mutant were similar to the observed rates in the QN background (Figure IV-4A). However, the amplitude of ITF signal change was larger in the presence of ATP or ADP, suggesting a shift in carrier domain equilibrium towards the BC domain when these ligands are present (Figure IV-4B). The presence of ADP and phosphonoacetate had a major impact on the observed rate of ITF intensity change; the k_{obs} for the QNT mutant was only 2% of k_{obs} measured for the QN background in the presence of ADP and phosphonoacetate (Figure IV-4A). Furthermore, with ADP and phosphonoacetate present, the amplitude of the ITF intensity change was almost 4-fold higher for the QNT mutant relative to the QN background, highlighting a major shift in carrier domain positioning for the T876A *Sa*PC mutant towards the BC domain (Figure IV-4B).

In the presence of pyruvate or acetyl-CoA, the observed rates of ITF intensity change were lower in the QNT mutant compared to the QN background (Figure IV-4A). Pyruvate also had a reduced impact on the amplitude of ITF signal change in the QNT mutant compared to the QN background, suggesting that the effect of pyruvate on carrier domain positioning is diminished in the QNT mutant (Figure IV-4B). In the presence of acetyl-CoA, the amplitude of ITF signal change was similar in the QNT mutant compared to the QN background. Considering that acetyl-CoA decreased the k_{obs} for the QNT mutant compared to the QN background but had a more minimal effect on the amplitude

compared to the QN background, this suggests that a kinetic barrier in the adoption of the crosslinking conformation in the presence of acetyl-CoA has been raised in this mutant (Figure IV-4B).

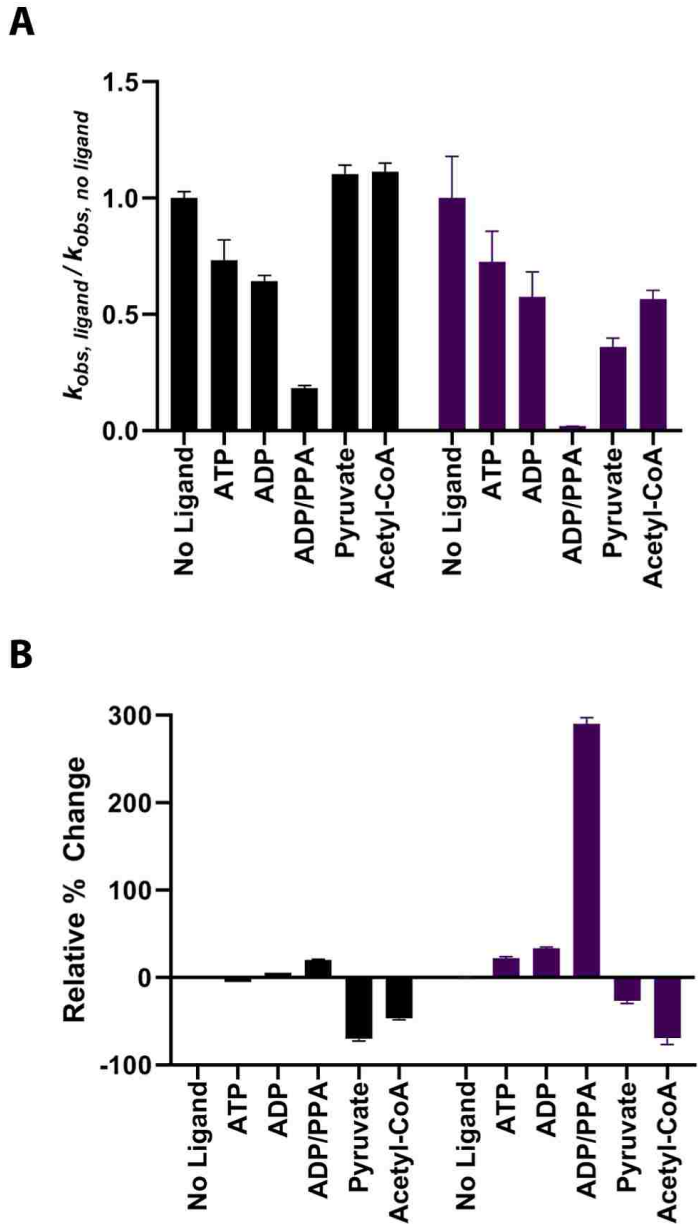

Figure IV-4 Observed rates and amplitudes of ITF change from Q891C/N1102C/T876A SaPC during crosslinking with BMOE in the absence/presence of ligands.
A. Q891C/N1102C SaPC (black) and Q891C/N1102C/T876A SaPC (purple) were incubated for a minimum of 10 minutes with 2.5 mM ATP, 0.25 mM acetyl-CoA, 12 mM sodium pyruvate, 5 mM ADP, or 5 mM phosphonoacetate (PPA) and then mixed with BMOE and an equal concentration of the substrate/effector at 0 sec. in a stopped-flow instrument with tryptophan excitation at 295 nm and ITF emission measured at 350 nm. A single exponential decay equation was fit to the data and the k_{obs} was determined for each of the three active-site residue mutants compared to the k_{obs} obtained from the QN crosslinking background mutant. All measurements were taken in triplicate with the standard deviation in the rate shown as the error bars. **B.** The amplitudes of ITF signal change from Equation II-2 for each of the three active-site residue mutants described in panel A were compared to the amplitude obtained for the corresponding QN crosslinking background.

2.4 CT Domain Tyr621 contributes to the kinetics and thermodynamics of carrier domain positioning.

Tyr621 forms a stabilizing interaction with the thiophene ring of biotin in the CT domain (Lietzan, et al., 2013A). To investigate the contribution of this residue to carrier domain positioning, changes in the amplitude and rates of ITF intensity changes were measured in the QNY mutant relative to the QN background. The overall change in observed ITF signals were quite different than those observed in any other mutant, with the ITF signal decreasing upon introduction of the crosslinker (Figures IV-2). It must be acknowledged that the dramatic change in the observed ITF signal may be the result of a change in this protein that may render this data unable to be interpreted in the same manner used for the other mutations in this study. It is possible that as a result of this mutation, intrinsic fluorescence has changed in a way that is not related to carrier domain positioning. In this section, the QNY mutant data will be interpreted in the same manner under the assumption that carrier domain positioning was linked to changes in Trp fluorescence similar to the other mutants with the understanding that there is a large caveat to this until it can be shown that this assumption is valid. This is further discussed in Chapter VI.

In the presence of BC domain ligands or acetyl-CoA, the measured k_{obs} values for the QNY mutant are relatively unchanged, in stark contrast to observations in the QN background (Figure IV-5A). The magnitude of the measured amplitudes decreased in the presence of BC domain ligands in the QNY mutant, indicating that the equilibrium position of the carrier domain had shifted away from the BC domain (Figure IV-5B). This result may support previous observations that alterations to one active site

can have an effect on a separate active site, suggesting communication between the BC and CT domains (Westerhold, et al., 2016; Lietzan, et al., 2014).

However, in the presence of pyruvate, there was an increase in the measured k_{obs} (Figure IV-5A), combined with a large increase in the magnitude of the amplitude change for the QNY *Sa*PC, which is opposite to what was observed for the QN background (Figure IV-5B). The observation that the presence of pyruvate still has an effect on carrier domain positioning, despite this mutation, suggests that Y621A is not the sole residue responsible for mediating the effect of pyruvate on carrier domain positioning. The effect of acetyl-CoA on the measured ITF amplitude changes also diminished (Figure IV-5B), suggesting that Tyr621 mediates the effect of acetyl-CoA on carrier domain positioning.

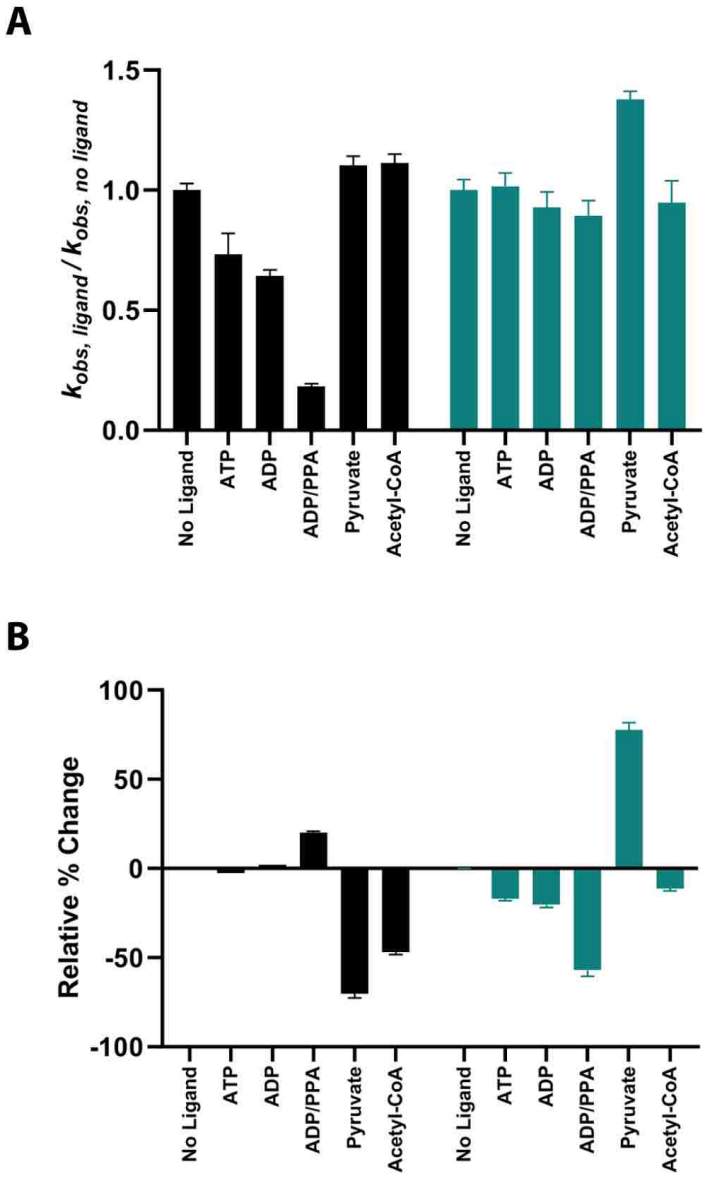

Figure IV-5 Observed rates and amplitudes of ITF change from Q891C/N1102C/Y621A SaPC during crosslinking with BMOE in the absence/presence of ligands.
A. Q891C/N1102C SaPC (black) and Q891C/N1102C/Y621A SaPC (green) were incubated for a minimum of 10 minutes with 2.5 mM ATP, 0.25 mM acetyl-CoA, 12 mM sodium pyruvate, 5 mM ADP, or 5 mM phosphonoacetate (PPA) and then mixed with BMOE and an equal concentration of the substrate/effector at 0 sec. in a stopped-flow instrument with tryptophan excitation at 295 nm and ITF emission measured at 350 nm. Equation II-2 was fit to the data and the k_{obs} obtained for each of the three active-site residue mutants compared to the k_{obs} obtained from the corresponding crosslinking background mutant. All measurements were taken in triplicate with the error bars representing the standard deviation in the rate. **B.** The amplitudes of ITF signal change from the single exponential equation for each of the three active-site residue mutants described in panel A were compared to the amplitude obtained for the corresponding crosslinking background.

3. Discussion

Regulation of carrier domain positioning is crucial for the coordination of multi-step reactions in multi-domain enzymes and for the protection of reaction intermediates. However, the molecular mechanism linking the presence of ligand and an observed shift in carrier domain positioning or translocation pathway remains unclear (Lowry, et al., 2016; Liu, et al., 2018) or unconfirmed (Alfermann, et al., 2017). The studies presented here sought to directly observe carrier domain positioning in order to provide insights into molecular level contributions from key active site residues to carrier domain positioning.

Glu243 Acts to Shift Carrier Domain Positioning Away from BC Domain. In the absence of substrates, the E243A *Sa*PC mutant shows an increase in the ITF signal amplitude when crosslinked with BMOE in the QN crosslinking background (QNE) (Figure IV-1B). This suggests that loss of the Glu243 "gatekeeper" residue shifts the carrier domain position towards the BC domain. This is consistent with observations by Lietzan, et al. that the salt bridge interaction between Glu243 and Arg346 (analogous to *Re*PC Arg353) serves to control carboxybiotin access to the active site (Lietzan, et al., 2011; Zeczycki, et al., 2011A). The loss of this gatekeeping residue resulted in a greater observed amplitude of ITF signal change, indicating that the carrier domain equilibrium had shifted towards the BC domain as a result of this mutation, as might be expected with greater biotin access to the active site.

The relative increase in the ITF signal amplitude for QNE in the presence of BC domain ligands further supports the idea that Glu243 functions to regulate biotin access to the BC domain active site (Figure IV-3B). Thus, mutations of these gatekeeper

residues allow greater biotin access to the BC domain active site. It is, therefore, unsurprising that the current data with the QNE mutant is consistent with a shift in the carrier domain positioning towards the BC domain when the Glu243 gatekeeper residue is mutated to an alanine. With the gate-closing mechanism disrupted, biotin would have greater access to the BC domain active site in the presence of BC domain reaction products, such as ADP, further stabilizing the BCCP-BC domain interaction. However, there is likely more than one mechanism to regulate carrier domain interactions with the BC domain given observations that ADP or ADP/PPA shift carrier domain positioning towards the BC domain in the QN background. This is likely to include the formation of the BC domain / carrier domain interface by the B-subdomain lid closure in the presence of BC domain ligands (Menefee and Zeczycki, 2014). Thus, even if ADP is bound and the gatekeeper residue system is blocking biotin access to the active site, the carrier domain may still have a favorable interface to remain docked at the BC domain active site.

Tyr621 has a critical role in carrier domain positioning. Tyr621 was proposed to stabilize the positioning of biotin in the CT domain active site (Lietzan, et al., 2013A). The Y621A *Sa*PC mutant displayed a dramatically different ITF signal behavior than any other *Sa*PC variant. This could be the result of either a large shift in initial carrier domain equilibrium positioning or a failure of the carrier domain to adopt the final crosslinking conformation. However, as shown in Figure IV-2A, this mutant still adopts the intermolecular crosslinking conformation, with crosslinked dimers formed when the QNY mutant was reacted with BMOE. This indicates that initial carrier domain positioning equilibrium was strongly shifted as a result of this mutation, which led to the

dramatic difference in ITF signal change behavior as the carrier domain was crosslinked to the final intermolecular conformation. In the absence of ligands, the observed rate constants for ITF signal change were also increased two-fold in the QNY mutant compared to the QN background (Figure IV-5A) suggesting that a kinetic barrier to the carrier domain repositioning has been reduced. This could result from the carrier domain being less anchored at the CT domain due to the disruption of the proposed biotin-tyrosine interaction and, therefore, the carrier domain is freed to adopt a variety of conformations.

The accompanying large change in amplitude upon crosslinking the QNY mutant compared to the QN background suggests a relatively large thermodynamic change in the BCCP-CT domain interaction, which resulted in a shift in carrier domain positioning (Figure IV-1B). This supports the hypothesis proposed by Lietzan, et al. that sulfur-pi interaction between the sulfur in the thiophene ring of biotin and the aromatic ring of Tyr621 contributes to the positioning of biotin in the CT domain active site[5]. In the Y621A mutation (QNY) this stabilizing interaction is lost, reestablishing a new initial equilibrium for the carrier domain position, as evidenced by the general reversal in behavior. An increase in the observed amplitude upon crosslinking is interpreted as a shift in the initial carrier domain positional equilibrium towards the BC domain. Thus, the decrease in amplitude observed in Figure IV-1B indicates an equilibrium shift *away* from the BC domain, perhaps towards the exo-binding site.

As introduced in Section I.2.3, Tyr621 links pyruvate binding in the active site to biotin binding. Curiously, the response of the carrier domain to the presence of pyruvate was not abolished in this mutant. In fact, it was observed that the magnitude of the

amplitude during crosslinking decreased in the presence of pyruvate (Figure IV-5B), indicating that more than one residue may be responsible for interacting with both pyruvate and biotin. The Sox B and Sox YZ interaction behaves in a similar manner, with a substrate stabilizing a particular active-site conformation that itself favors interaction of the Sox B enzyme with the Sox YZ carrier domain (Grabarczyk, et al., 2015).

The observed amplitude change in the presence of acetyl-CoA, however, was dramatically reduced in this mutant (Figure IV-5B). Acetyl-CoA favors the symmetrical conformation of PC which includes the carrier domain being positioned intermolecularly (Lasso, et al., 2014; Sirithanakorn, et al., 2016). These results suggest that while acetyl-CoA may have an effect at the N-terminal portion of the carrier domain, where its binding site is located, the stabilization of biotin by Tyr621 in the CT domain active site is necessary for stable adoption of the carrier domain conformation favored by acetyl-CoA. Without Tyr621, biotin and the flexible carrier domain have lost the anchoring site for biotin, destabilizing the intermolecular carrier conformation.

Thr876 contributes to shifts in carrier domain positioning. Thr876 acts to shuttle a proton between the biotin enolate and pyruvate during pyruvate carboxylation and it is within hydrogen-bonding distance to the N-1 position of biotin (Zeczycki, et al., 2009). As such, it may play a role in shifting carrier domain positioning. The T876A mutant displayed the smallest ITF amplitude changes in the absence of ligands compared to the QN crosslinking background (Figure IV-1B). Unexpectedly, the presence of pyruvate also led to a smaller amplitude of ITF signal change in this mutant (Figure IV-4) compared to the QN background, suggesting that this mutation reduced the impact of pyruvate on carrier domain repositioning. This result could have two different

explanations. First, the biotin-stabilizing hydrogen bonding network that normally forms in the presence of pyruvate has been disrupted. Second, the alanine introduced at this position has an unfavorable interaction with pyruvate, leading to conformational changes that disfavor the positioning of biotin in the active site.

The presence of BC domain ligands led to an increase in the observed ITF amplitude change for the QNT mutant, including a dramatic increase observed in the presence of ADP and phosphonoacetate (Figure IV-4B). This coincided with a dramatic reduction in the observed rate constant with ADP and phosphonoacetate (Figure IV-4A), further suggesting that the carrier domain favors an interaction with the BC domain in this mutant. This supports the observation by Zeczycki, et al. that mutation of Thr882 in *Re*PC (equivalent to Thr876 in *Sa*PC) led to an increased rate of ADP phosphorylation in the BC domain, which was further accelerated in the presence of free biotin (Zeczycki, et al., 2009). The authors of that study proposed that the Thr882 mutation shifted carrier domain positioning towards the BC domain, where the increased local concentration of biotin in the active site contributed to accelerating the rate of ADP phosphorylation. The data presented here also indicates that mutation of Thr876 shifts carrier domain positioning towards the BC domain.

In summary, direct observations of carrier domain positioning in *Sa*PC demonstrate that carrier domain positioning is shifted by interactions between biotin and specific conserved active-site residues. These residues control the access of biotin to the active site, which leads to shifts in carrier domain positioning. While multi-domain enzymes are diverse, the directionality of these reactions and the mechanism by which carrier domain translocation is controlled is becoming clearer as a result of studies like

these. In the related biotin-dependent enzyme, acetyl-CoA carboxylase from *Saccharomyces cerevisiae,* it has been shown that the conformational flexibility of the enzyme is controlled by the binding of a regulatory loop to an allosteric site that restricts conformational flexibility and disfavors a catalytically-relevant high-energy conformation (Hunkeler, et al., 2016). The binding of acetyl-CoA in pyruvate carboxylase may have a similar role, confining the flexible carrier domain to promote an intermolecular, catalytically-relevant conformation at the CT domain active site that is stabilized through the biotin-Tyr621 interaction in *Sa*PC. The results described in this chapter clarify how carrier domain positioning, governed by conformational selection, can be shifted by ligand binding events in *Sa*PC. These findings may be useful in explaining how carrier domain translocation can be controlled at the molecular level by similar interactions in many other complex multi-domain enzyme systems.

V. THE EFFECTS OF LIGANDS AND ACTIVE SITE MUTATIONS ON CARRIER DOMAIN TRANSLOCATION IN *S. AUREUS* PYRUVATE CARBOXYLASE

1. Introduction

Chapters III and IV summarized the effect of ligands on carrier domain positioning and clarified the relationship between active site residues and carrier domain positioning. The carrier domain is governed by conformational selection, where ligand binding serves to shift the carrier domain positioning equilibrium. The QN crosslinking system was based on a structure where biotin occupies the exo-binding site and not the CT domain active site. In an effort to discern between carrier domain interactions at the active site and carrier domain interactions at the exo-binding site, a new system was created: D907C/Q1118C (DQ) *Sa*PC (Figure V-1A).

Many studies were performed in the DQ system, which showed quite different behavior relative to the QN system described in the previous chapters. The studies in the DQ system described in this chapter were initially interpreted to inform on the differences between the exo-binding site-carrier domain conformation as compared to the CT domain active site-carrier domain conformation. However, in a series of experiments run only weeks prior to the submission of this dissertation (as described in the Results section), it was revealed that the DQ mutant behaves identically to a single Q1118C *Sa*PC mutant. Thus, all of the data collected in the DQ system, in fact, represents a BCCP-BCCP crosslink rather than a BCCP-CT crosslink. While the BCCP dimer is not expected to be a catalytically relevant conformation, it does represent a novel state in which the carrier domain is trapped in the process of translocating between active sites. Given the late breaking nature of this result, it was not possible to regenerate all of the

mutations, originally generated in the DQ background, in the single Q1118C background. This chapter will demonstrate that the DQ mutant and the Q1118C single mutant are indistinguishable in their behavior and will then investigate the impact of ligands and mutations in the DQ double mutant system. All results with the DQ system will be interpreted as being due exclusively to the Q1118C-Q1118C crosslink.

2. Results

2.1 Characterization of the D907C/Q1118C *Sa*PC Crosslinking System

A second conformation, observed in X-ray crystal structures of *Sa*PC, was used to direct the design of a crosslink trap in which the carrier domain was bound in the catalytically competent conformation, with biotin extending into the CT domain active site (Figure V-1B). This was designed to facilitate the detection and comparison of two different conformational states for the BCCP domain. To trap this second conformation, Asp907 on the CT domain and Gln1118 on the BCCP domain were mutated to cysteines to generate the double mutant D907C/Q1118C *Sa*PC (DQ) based on the X-ray crystal structure of *Sa*PC (PDB ID: 3BG5) (Xiang and Tong, 2008).

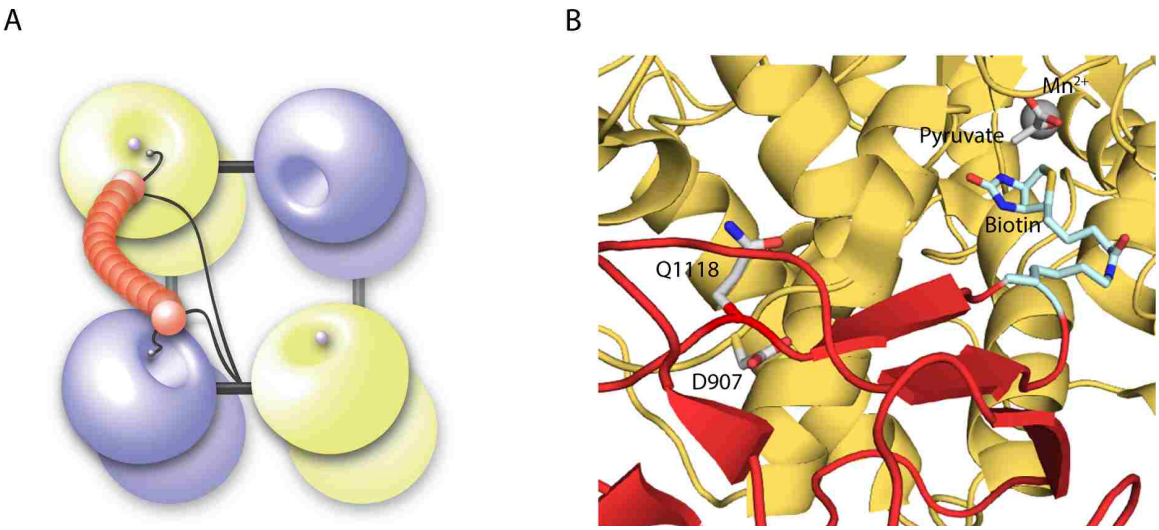

Figure V-1 *Sa*PC carrier domain motions and conformations.
A. A schematic of the PC tetrameric structure and intermolecular carrier domain translocation. BC domains are colored in blue, CT domains in yellow, and the BCCP carrier domain in red. A hypothetical intermolecular translocation pathway is traced for a single carrier domain from the BC domain of its own subunit to the active site in the CT domain of a neighboring subunit. **B.** The *Sa*PC X-ray crystal structure (PDB ID: 3BG5) showing the BCCP domain of one subunit (red) interacting at the active site of the CT domain on the opposing subunit (yellow). The Mn^{2+} ion, colored as a grey sphere, and pyruvate are shown in the CT domain active site. Asp907 on the CT domain and Gln1118 on the BCCP domain were both mutated to cysteine to enable maleimide-based crosslinking to trap the BCCP domain in an intermolecular conformation.

SDS-PAGE analysis of crosslinking in the DQ double-mutant compared with the Q1118C single-mutant, however, revealed that the crosslinking levels for both mutants were very similar (Figure V-2A). To confirm this, Q1118C *Sa*PC was analyzed for ITF intensity changes during crosslinking and compared to D907C/Q1118C *Sa*PC. The ITF signals obtained from crosslinking both of these mutants are virtually identical (Figure V-2B). Thus, the D907C/Q1118C system is equivalent to Q1118C alone and represents a BCCP-BCCP dimerization and not the BCCP-CT interaction. This interaction could not have been predicted from the X-ray crystal structure of a BCCP dimer from *E. coli* acetyl-CoA carboxylase (PDB ID: 1BDO), which shows that the BCCP domain dimer that forms in the crystal lattice positions these residues on opposite sides of the dimer

(Figure V-2). While this system does not capture the desired BCCP-CT domain interaction, it is interesting that Q1118C can crosslink only when both of the BCCP domains are in motion, away from either active site. Consequently, this system can be used to report on how ligands and mutations impact the translocation of the BCCP domain, even if the final position captured in these crosslinks is not catalytically relevant. All of the DQ *Sa*PC data was collected prior to making this observation. The late-breaking nature of this result prevents the re-collection of this data in the Q1118C *Sa*PC system alone. For the remainder of this chapter, the data in the DQ system will be analyzed on the assumption that the carrier domain is being trapped in a BCCP-BCCP crosslink during translocation.

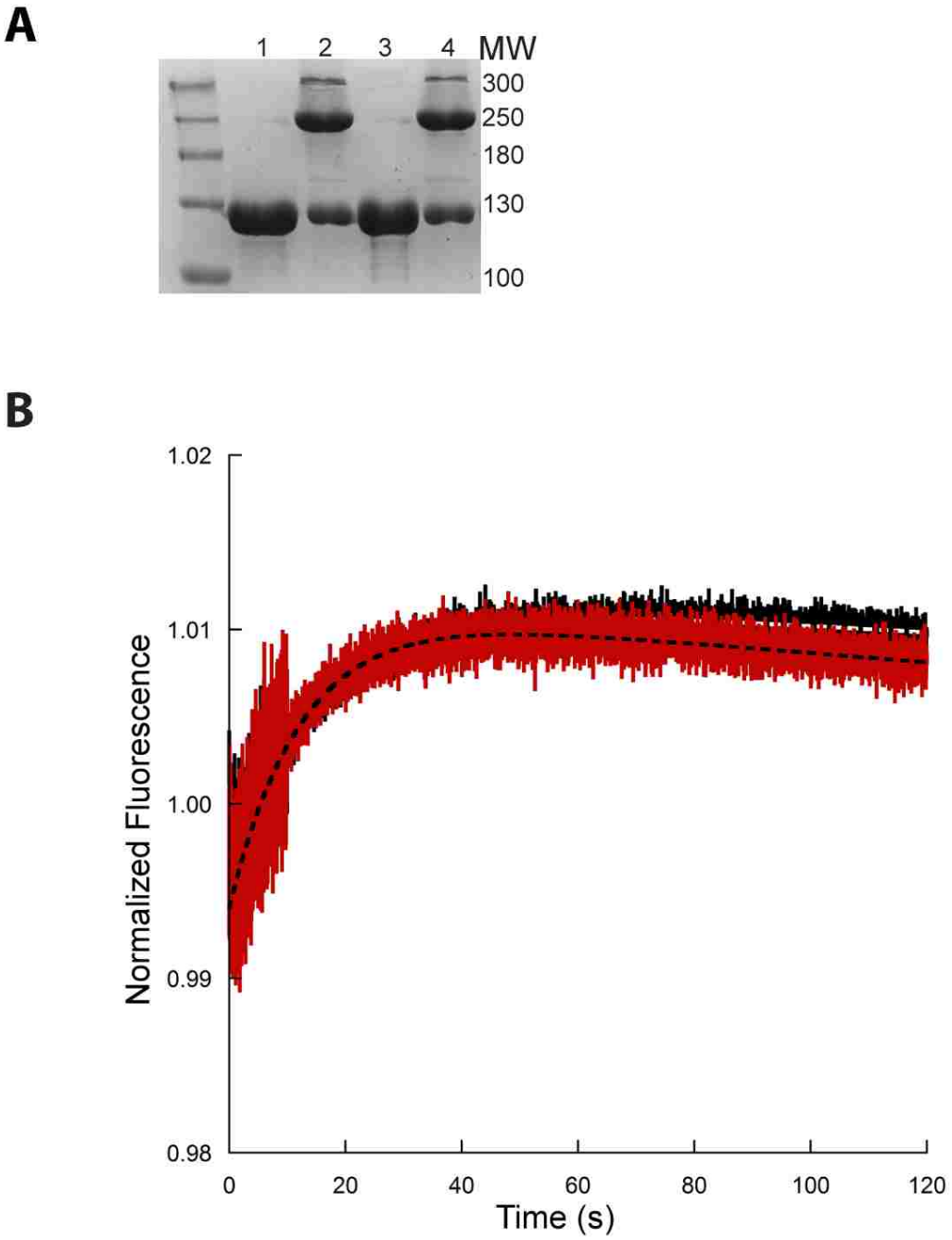

Figure V-2 D907C/Q1118C *Sa*PC mutants crosslinked.
A. *Sa*PC mutants as listed below at 1 mg/mL were reacted with 5% DMSO or 300 μM BMOE for 120 s, then quenched with 13 mM DTT for 15 minutes. 5 μg was loaded in each lane. (1) D907C/Q1118C w/ DMSO; (2) D907C/Q1118C w/ BMOE; (3) Q1118C w/ DMSO; (4) Q1118C w/ BMOE. The molecular weights for the ladders on the left and right are shown in kDa. **B.** *Sa*PC mutants mixed with 200 μM BMOE and ITF intensity changes measured. D907C/Q1118C *Sa*PC (grey/black) or Q1118C *Sa*PC (red) were mixed with a final concentration of 200 μM BMOE at t = 0 and the ITF intensity was recorded for 120 seconds. Tryptophan was excited at 295 nm and ITF emission was recorded at 350 nm.

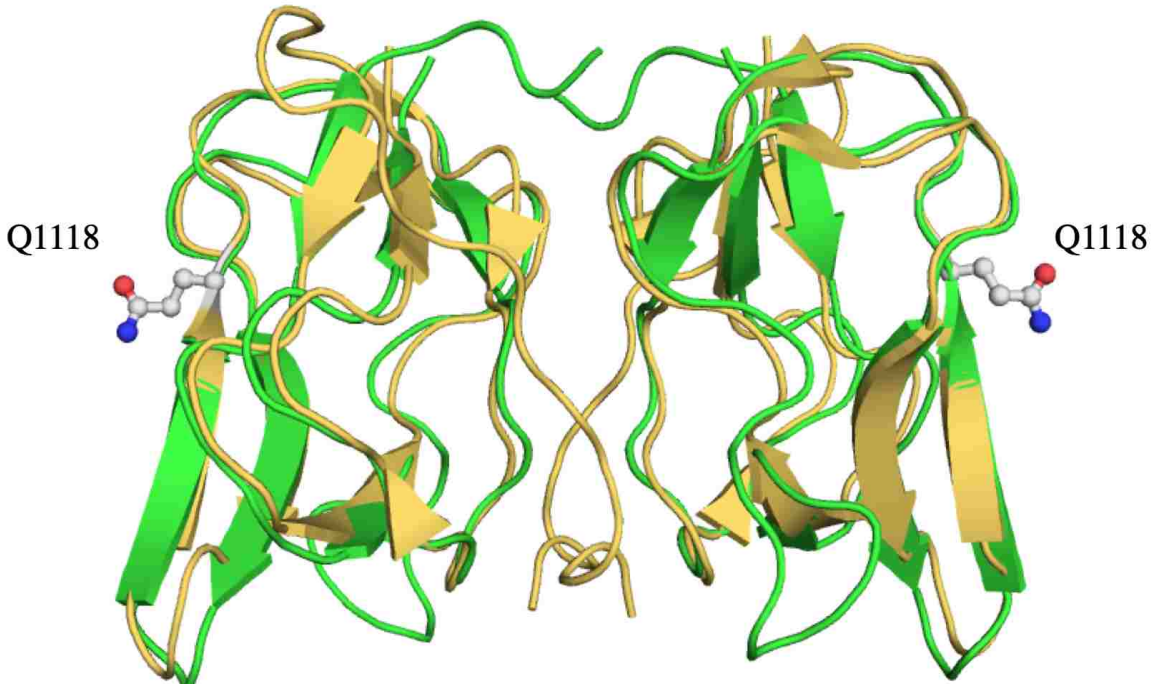

Figure V-3 Acetyl-CoA Carboxylase BCCP Domain Dimer Comparison
The BCCP dimer of acetyl-CoA carboxylase from *E. coli* (yellow; PDB ID: 1BDO) is shown overlayed with the *S. aureus* PC BCCP domain (green; PDB ID: 3BG5) The *S. aureus* PC BCCP domain is overlayed over each subunit of the acetyl-CoA carboxylase dimer. Shown in sticks are Gln1118 (Gln1150 in *H. sapiens* numbering).

The DQ *Sa*PC mutants were subjected to the same experimental setup as in Chapter III. Rates of ITF signal change were determined by fitting the data to a single exponential decay equation. As shown in Figure V-4 and summarized in Table V-1, the presence of acetyl-CoA increased k_{obs} 2.5-fold compared to the rate observed in the absence of ligands, a remarkably more pronounced response to acetyl-CoA compared to the QN crosslinking background. The ITF signal observed when acetyl-CoA was mixed with DQ *Sa*PC appears virtually identical to the ITF signal observed when DQ *Sa*PC was mixed with BMOE (Figure V-4B), suggesting that acetyl-CoA on its own promotes a conformation very similar to the BCCP-BCCP crosslinked conformation trapped by BMOE. Similar to what was observed in QN *Sa*PC, the rate of ITF signal change during crosslinking increased when acetyl CoA was combined with ATP, as compared to the

sample incubated with ATP alone (Figure V-4A). However, the addition of acetyl-CoA to ATP resulted in a much more pronounced increase in the rate for the DQ crosslinking system (2.5-fold faster; 150% increase over ATP alone) compared to the QN crosslinking system (~20% increase over ATP alone). These relative rates are summarized in Tables III-4 for the QN system and V-1 for the DQ system.

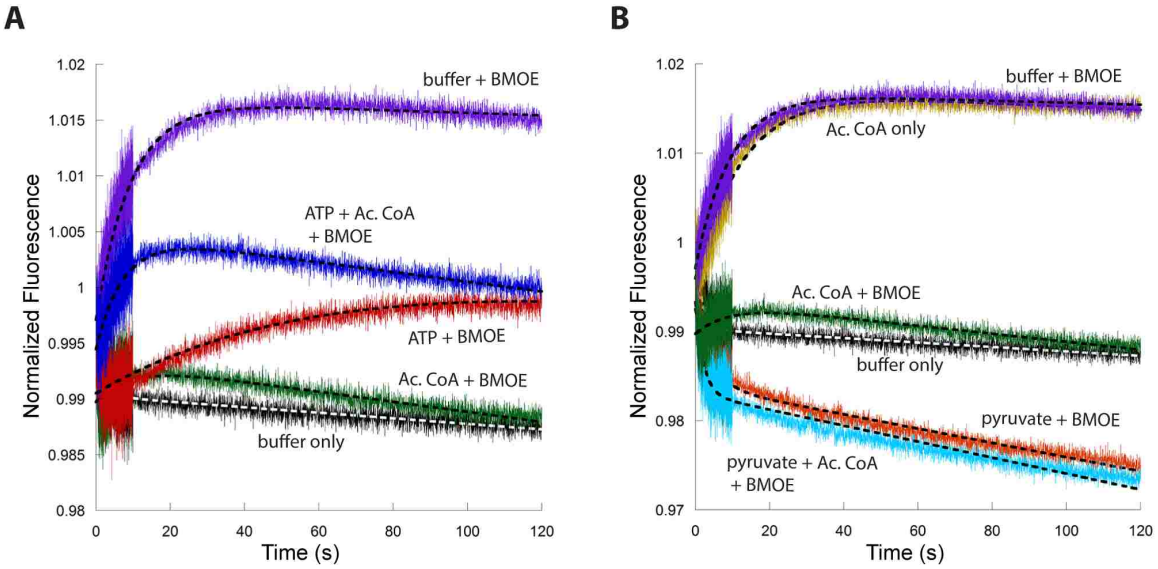

Figure V-4 D907C/Q1118C SaPC crosslinked in the presence of ligands and monitored for change in ITF intensity.

A final concentration of 0.175 mg/mL D907C/Q1118C (DQ) SaPC was mixed with either buffer or various substrates at final concentrations listed in the Methods section, with 200 μM BMOE present at 0 s in a stopped-flow instrument with tryptophan excitation at 295 nm and emission measured at 350 nm. **A.** DQ SaPC was mixed with either buffer (black), buffer + BMOE (purple), ATP + BMOE (orange), acetyl-CoA and BMOE (green), or ATP + acetyl-CoA + BMOE (blue). **B.** DQ SaPC was mixed with either buffer (black), buffer+BMOE (purple), acetyl-CoA + BMOE (green), pyruvate + BMOE (orange), or acetyl-CoA + pyruvate +BMOE (blue), or acetyl-CoA only (gold). Dashed lines represent the fit of the data to Equation 2.

Table V-1 The effect of ligands on the observed rates of ITF intensity change.

substrate (+ BMOE)	D907C/Q1118C SaPC k_{obs} (s^{-1})	k_{obs} / (k_{obs} [No Substrate])
None	[1.3 ± 0.3] x 10^{-1}	-
ATP	[0.7 ± 0.3] x 10^{-1}	0.54
Acetyl-CoA + ATP	[1.8 ± 0.3] x 10^{-1}	1.4
Acetyl-CoA	[3.3 ± 0.7] x 10^{-1}	2.5
Pyruvate	[2.6 ± 0.3] x 10^{-1}	2.0
Pyruvate + Acetyl-CoA	[4.9 ± 0.1] x 10^{-1}	3.8
None*	[1.9 ± 0.2] x 10^{-1}	-
L-aspartate*	[1.3 ± 0.3] x 10^{-1}	0.70

* Assay performed independently from above data. (n = 3; errors represent standard deviations)

The addition of pyruvate, the CT domain substrate, had a similar impact on the observed rates of ITF intensity change for the DQ system as it did in the QN system (Figure V-4B, Table V-1). Again, however, the effect was magnified in the DQ system: while the observed rate increased only slightly with the addition of pyruvate in the QN background (Table III-4), the observed rate increased two-fold in the DQ background. Finally, in the DQ background, the combination of acetyl CoA and pyruvate resulted in a nearly four-fold increase in the k_{obs} compared to the k_{obs} recorded in the absence of ligands and a two-fold increase compared to pyruvate alone (Figure V-4B). This nearly four-fold increase in k_{obs} in the presence of acetyl-CoA and pyruvate is similar to the observed increase in k_{obs} in the QN system indicating that a kinetic barrier to translocation (DQ) and intermolecular positioning (QN) was reduced in the presence of these ligands.

2.2 Active Site Mutations Contribute to Carrier Domain Positioning

This D907C/Q1118C (DQ) mutant was used as a crosslinking background in which to further introduce mutations of active site residues that are proposed to interact with biotin and influence the translocation of the carrier domain: Glu243, Thr876, and Tyr621 (Lietzan, et al., 2011; Lietzan, et al., 2013) were each mutated to alanine in the DQ crosslinking background. These mutations are the same as those introduced in the QN crosslinking background and described in Chapter IV. The catalytic activities of these mutants are shown in Table V-2 (Lietzan, et al., 2011; Lietzan, et al., 2013). All of the mutants also form similar degrees of intermolecular crosslinks, (Figure V-5), prompting the investigation of these mutants with the more sensitive ITF approach.

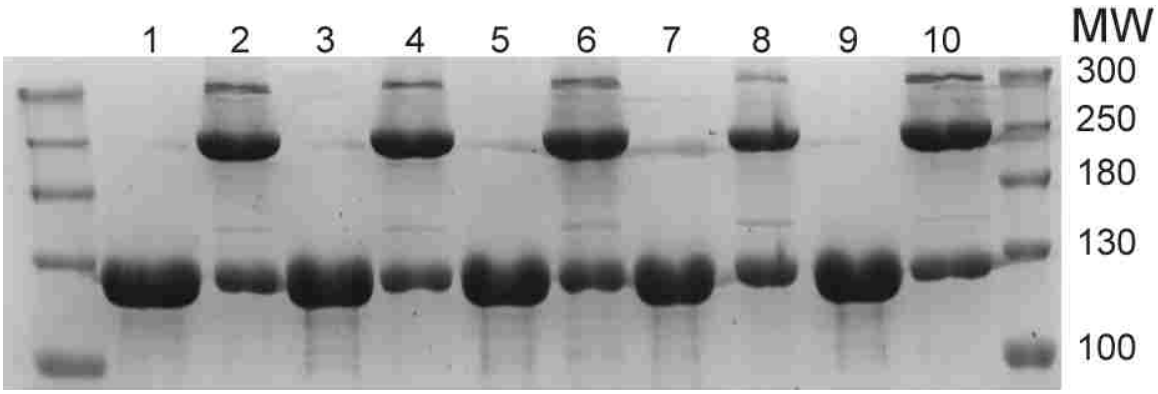

Figure V-5 D907C/Q1118C *Sa*PC mutants crosslinked.
A..*Sa*PC mutants as listed below at 1 mg/mL were reacted with 5% DMSO or 300 μM BMOE for 120 s, then quenched with 13 mM DTT for 15 minutes. 5 μg was loaded in each lane. (1) D907C/Q1118C w/ DMSO; (2) D907C/Q1118C w/ BMOE; (3) Q1118C w/ DMSO; (4) Q1118C w/ BMOE; (5) D907C/Q1118C/E243A w/ DMSO; (6) D907C/Q1118C/E243A w/ BMOE; (7) D907C/Q1118C/Y621A w/ DMSO; (8) D907C/Q1118C/Y621A w/ BMOE; (9) D907C/Q1118C/T876A w/ DMSO; (10) D907C/Q1118C/T876A w/ BMOE. The molecular weights for the ladders on the left and right are shown in kDa.

Table V-2 Kinetic characterization of D907C/Q1118C *Sa*PC and related mutants

*Sa*PC Mutant	Pyruvate carboxylation k_{cat}, min^{-1}
Wild-Type	1440 ± 100
D907C/Q1118C	740 ± 10
D907C/Q1118C/E243A	3.3 ± 0.2
D907C/Q1118C/Y621A	8.8 ± 0.2
D907C/Q1118C/T876A	N/A

Each of the three mutants were individually mixed with 200 μM BMOE and the changes in ITF intensity were recorded to gain an initial determination of the role played by these residues in carrier domain translocation. Representative ITF signal changes upon introduction of the BMOE crosslinker are shown in Figure V-6.

Overall, increases in k_{obs} in the DQ crosslinking background with either the Y621A or T876A mutation suggest that these mutations reduce kinetic barriers to carrier domain translocation (Figure V-7A). The amplitude of the ITF signal change during crosslinking of the DQT mutant remained similar to the DQ crosslinking background, suggesting that baseline equilibrium positioning of the carrier domain wasn't shifted by this mutation. The DQY mutant displayed a large shift in amplitude compared to the DQ crosslinking background (Figure V-7B), similar to what was observed in the QN crosslinking system.

The amplitude of the ITF signal change increased slightly in the DQE mutant compared to the DQ crosslinking background, suggesting that carrier domain equilibrium has shifted towards the BC domain in this mutant (Figure V-7B), in agreement with the conclusions from the QN system in Chapter IV. The rate of ITF signal change during

crosslinking decreased in DQE *Sa*PC compared to the DQ crosslinking background, indicating that carrier domain translocation has become more kinetically unfavorable as a result of this mutation (Figure V-7A).

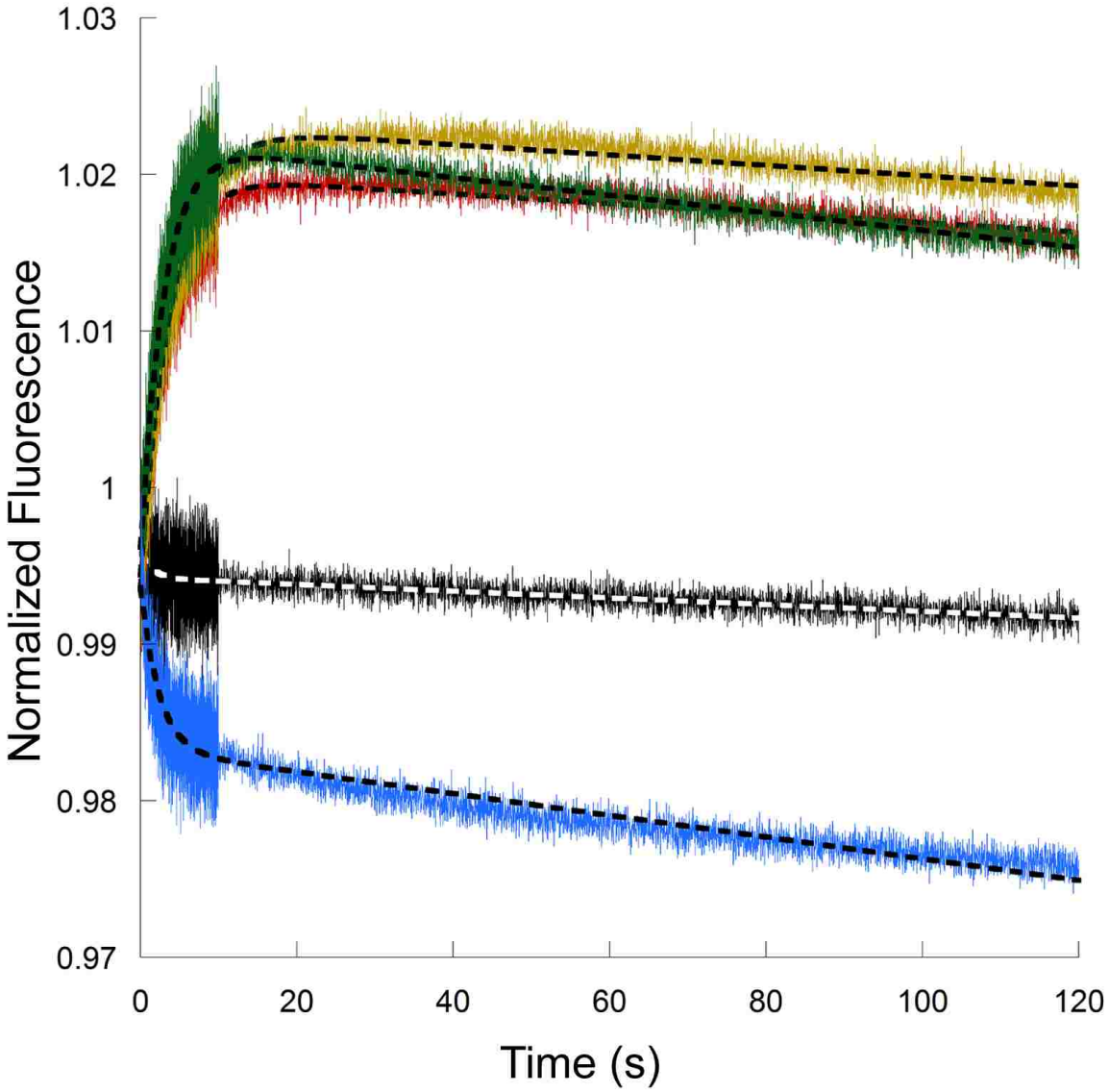

Figure V-6 DQ SaPC Mutants ITF intensity changes during crosslinking.
D907C/Q1118C *Sa*PC (red), D907C/Q1118C/E243A *Sa*PC (gold), D907C/Q1118C/T876A *Sa*PC (green), or D907C/Q1118C/Y621A *Sa*PC (blue) was mixed with a final concentration of 200 μM BMOE at t = 0 and the ITF intensity was recorded for 120 seconds. Tryptophan was excited at 295 nm and ITF emission was recorded at 350 nm.

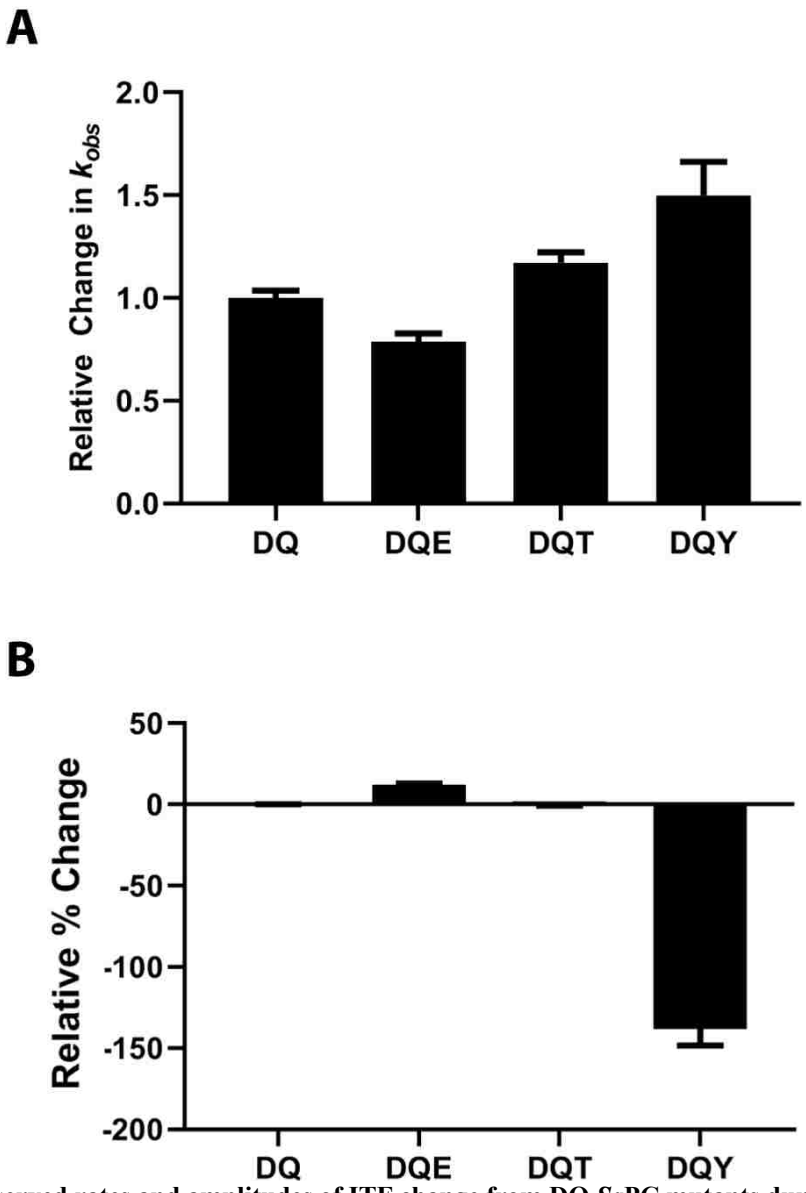

Figure V-7 Observed rates and amplitudes of ITF change from DQ *Sa*PC mutants during crosslinking with BMOE

D907C/Q1118C (DQ) *Sa*PC, D907C/Q1118C/E243A (DQE) *Sa*PC, D907C/Q1118C/T876A (DQT) *Sa*PC, and D907C/Q1118C/Y621A (DQY) *Sa*PC were mixed with BMOE at 0 sec. in a stopped-flow instrument with tryptophan excitation at 295 nm and ITF emission measured at 350 nm. A single exponential decay equation was fit to the data. A. The relative change in k_{obs} is the k_{obs} obtained for each of the three active-site residue mutants divided by the k_{obs} obtained from the QN background. All measurements were made in triplicate. Error bars represent the standard deviation. B. The amplitudes of ITF signal change from Equation II-2 for each of the three active-site residue mutants obtained in panel A were divided by the amplitude change obtained for the corresponding crosslinking background to yield a relative % change.

2.3 Mutation of Glu243 Shifts Carrier Domain Positioning Towards BC Domain.

The observed rates of crosslinking of the DQE mutant were attenuated in the presence of BC domain ligands compared to the DQ crosslinking background (Figure V-8A). This is matched by a smaller increase in amplitude of ITF signal change for the DQE mutant compared to the DQ background (Figure V-8B). In this mutant, biotin has increased access to the active site. As a result of this, the carrier domain may have already adopted the positional equilibrium favored by these substrates, which would lessen the effect of the substrate on carrier domain positioning.

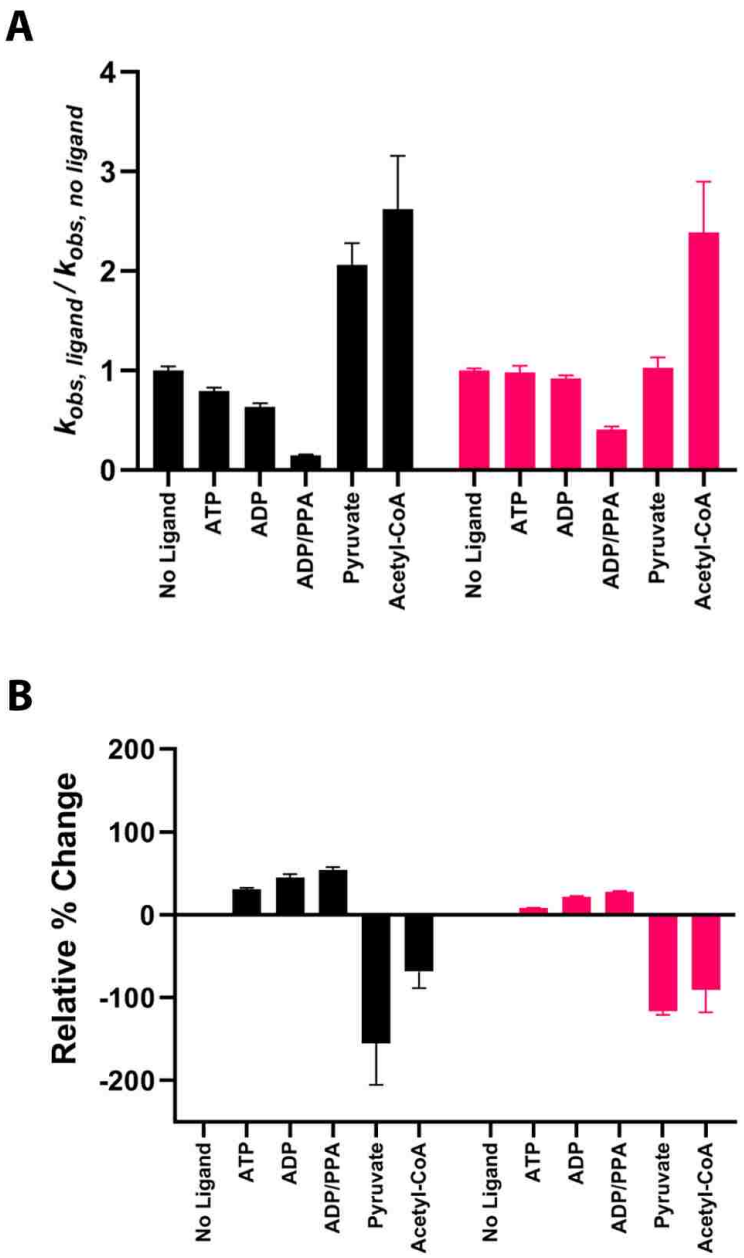

Figure V-8: Observed rates and amplitudes of ITF change from D907C/Q1118C/E243A SaPC during crosslinking with BMOE in the absence/presence of ligands.
A. D907C/Q1118C SaPC (black) and D907C/Q1118C/E243A SaPC (pink) were incubated for a minimum of 10 minutes with 2.5 mM ATP, 0.25 mM acetyl-CoA, 12 mM sodium pyruvate, 5 mM ADP, or 5 mM phosphonoacetate (PPA) and then mixed with BMOE and an equal concentration of the substrate/effector at 0 sec. in a stopped-flow instrument with tryptophan excitation at 295 nm and ITF emission measured at 350 nm. Equation II-2 was fit to the data and the k_{obs} obtained for each of the three active-site residue mutants compared to the k_{obs} obtained from the corresponding crosslinking background mutant. All measurements were taken in triplicate with the error bars representing the standard deviation in the rate. **B.** The amplitudes of ITF signal change from the single exponential equation for each of the three active-site residue mutants described in panel A were compared to the amplitude obtained for the corresponding crosslinking background.

2.4 Thr876 Mediates Translocation of the Carrier Domain in Response to Pyruvate

The observed rates of ITF intensity change in DQT *Sa*PC were similar to those in the DQ background in the presence of BC domain ligands (Figure V-9A). The amplitudes of ITF signal change (Figure V-9B) in the presence of these ligands were also similar to background, in stark contrast to the observations in QNT *Sa*PC, especially in the presence of ADP and phosphonoacetate. While the large drop in k_{obs} in DQT in the presence of ADP and phosphonoacetate is similar to that observed in QNT, the difference in how the amplitudes vary is astounding. The lack of difference in observed amplitudes in DQT compared to the DQ background indicates that the thermodynamics of translocating have not changed as a result of this mutation in the presence of ADP and phosphonoacetate. Rather, the large increase in amplitude observed in QNT compared to QN in the presence of these ligands indicates a large equilibrium positioning shift towards the BC domain.

The observed amplitudes in DQT were similar to those of the DQ background in the presence of pyruvate (Figure V-9B). However, the observed rate dramatically decreased in the presence of pyruvate in the DQT *Sa*PC mutant compared to the DQ background (Figure V-9A). Combined with a similar effect observed in the QNT *Sa*PC mutant, these observations strongly suggest that Thr876 mediates the effect of pyruvate on carrier domain translocation (DQT) and positioning (QNT). In the presence of pyruvate with this mutation, there is a larger kinetic barrier to overcome to translocate or adopt positioning in the exo-binding site. Finally, the observed rate of ITF intensity change in DQT *Sa*PC in the presence of acetyl-CoA increased approximately 4-fold compared to in the absence of acetyl-CoA suggesting that a kinetic barrier to the translocation of the carrier domain has been reduced by the mutation of this active site

threonine (Figure V-9A). A larger change in the amplitude of ITF signal change in the presence of acetyl-CoA compared to the DQ crosslinking background in the presence of acetyl-CoA indicates that carrier domain translocation may be more thermodynamically favorable as a result of this mutation in the presence of acetyl-CoA.

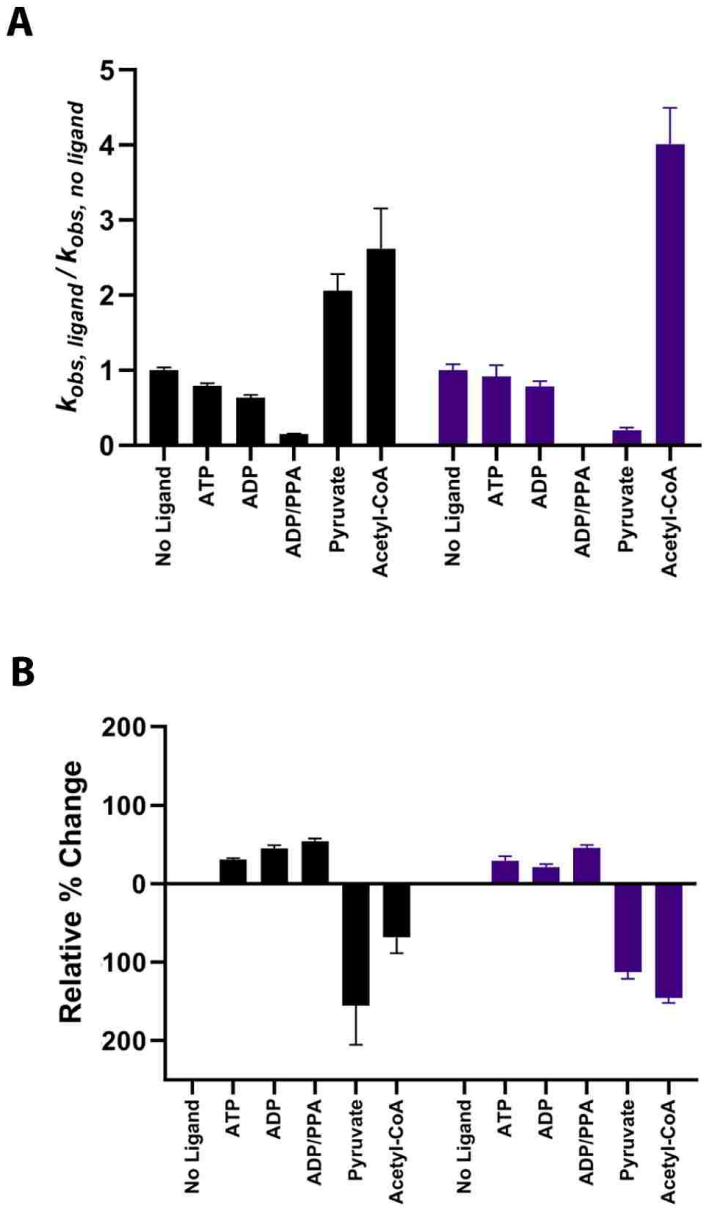

Figure V-9: Observed rates and amplitudes of ITF change from D907C/Q1118C/T876A SaPC during crosslinking with BMOE in the absence/presence of ligands.
A. D907C/Q1118C SaPC (black) and D907C/Q1118C/T876A SaPC (purple) were incubated for a minimum of 10 minutes with 2.5 mM ATP, 0.25 mM acetyl-CoA, 12 mM sodium pyruvate, 5 mM ADP, or 5 mM phosphonoacetate (PPA) and then mixed with BMOE and an equal concentration of the substrate/effector at 0 sec. in a stopped-flow instrument with tryptophan excitation at 295 nm and ITF emission measured at 350 nm. Equation II-2 was fit to the data and the k_{obs} obtained for each of the three active-site residue mutants compared to the k_{obs} obtained from the corresponding crosslinking background mutant. All measurements were taken in triplicate with the error bars representing the standard deviation in the rate. **B.** The amplitudes of ITF signal change from the single exponential equation for each of the three active-site residue mutants described in panel A were compared to the amplitude obtained for the corresponding crosslinking background.

2.5 CT Domain Tyr621 Has A Crucial Role in Mediating Carrier Domain Positional Response to Pyruvate and Acetyl-CoA

As described in Chapter IV and Chapter VI, this data may not be able to be interpreted in the same manner as the other mutants given the dramatic difference in ITF signals observed. The observed rate of ITF intensity change varied similarly in the DQY mutant as in the QNY mutant, with only small decreases in k_{obs} in the presence of BC domain ligands (Figure V-10A), further evidence that alterations to one domain, such as the Y621A CT domain mutation, may affect the behavior of the other active site, as discussed in Chapter IV. While acetyl-CoA dramatically increased k_{obs} in the DQ crosslinking background, it had virtually no effect in DQY *Sa*PC (Figure V-10A). The effect of acetyl-CoA on the amplitude of the ITF signal changes is also diminished (Figure V-10B). Combined with the observations from QNY *Sa*PC, this strongly suggests that Tyr621 is necessary for acetyl-CoA to affect carrier domain positioning (QNY) and translocation (DQY). The effect of pyruvate on observed rates of ITF intensity change was also reduced in this mutant, but not completely abolished (Figure V-10A). Similar to QNY *Sa*PC, a large increase in the magnitude of the amplitude change was observed in DQY *Sa*PC when crosslinked with pyruvate, as well, indicating that both carrier domain positioning (QNY) and translocation (DQY) in this mutant still responds to the presence of pyruvate (Figure V-10B).

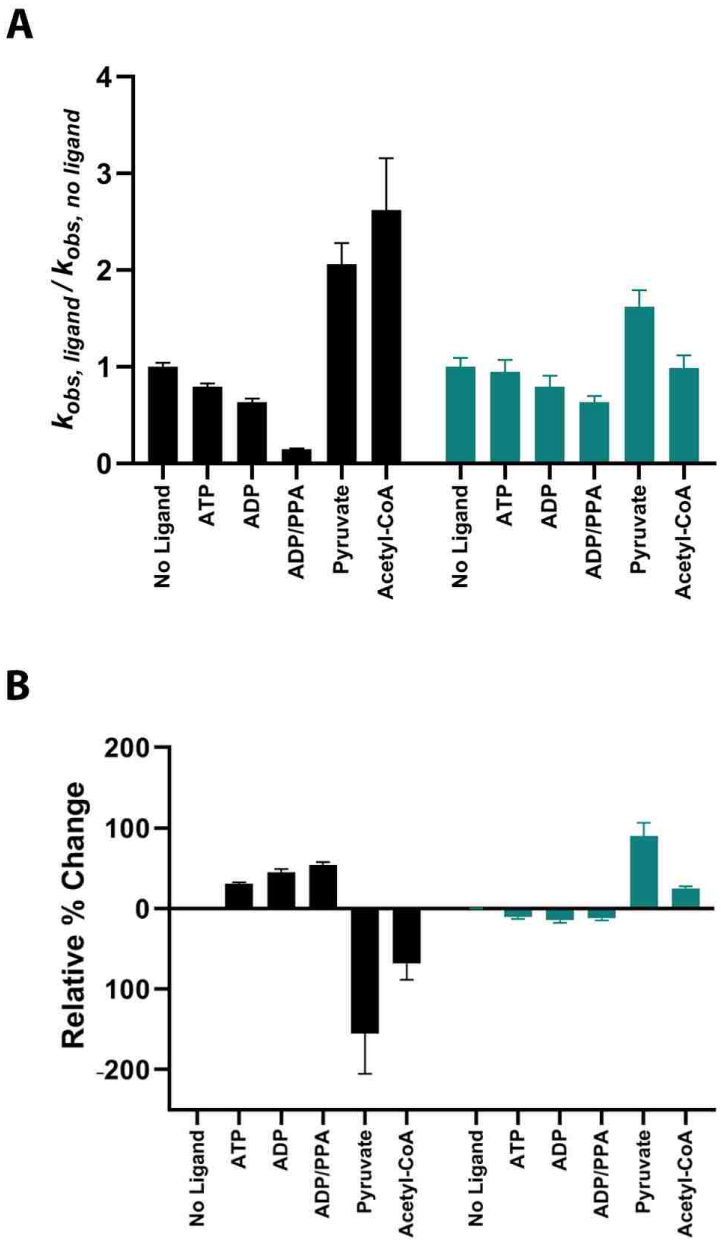

Figure V-10: Observed rates and amplitudes of ITF change from D907C/Q1118C/Y621A *Sa*PC during crosslinking with BMOE in the absence/presence of ligands.
A. D907C/Q1118C SaPC (black) and D907C/Q1118C/Y621A SaPC (green) were incubated for a minimum of 10 minutes with 2.5 mM ATP, 0.25 mM acetyl-CoA, 12 mM sodium pyruvate, 5 mM ADP, or 5 mM phosphonoacetate (PPA) and then mixed with BMOE and an equal concentration of the substrate/effector at 0 sec. in a stopped-flow instrument with tryptophan excitation at 295 nm and ITF emission measured at 350 nm. Equation II-2 was fit to the data and the k_{obs} obtained for each of the three active-site residue mutants compared to the k_{obs} obtained from the corresponding crosslinking background mutant. All measurements were taken in triplicate with the error bars representing the standard deviation in the rate. **B.** The amplitudes of ITF signal change from the single exponential equation for each of the three active-site residue mutants described in panel A were compared to the amplitude obtained for the corresponding crosslinking background.

3. Discussion

In the current study, the crosslinking system, D907C/Q1118C *Sa*PC, was designed to trap the carrier domain in a conformation with biotin projecting into the CT domain active site. An important control experiment was overlooked in the initial evaluation of this system and the Q1118C mutation was not assessed until *after* all the data had been collected on the DQ system. Due to the observation that the single Q1118C mutation readily crosslinked two BCCP domains through a Q1118C-Q1118C crosslink, the trapped conformation captured in the DQ system actually represents the carrier domain in a state of translocation, outside of either active site. However, due to the absence of single mutant controls for these experiments, the data is being interpreted as it is, but there is added uncertainty to the validity of these interpretations. For instance, some amount of D907C-Q1118C crosslinking may result in the presence of some or all of these mutations or in the presence of ligands, which would substantially weaken these interpretations.

The presence of acetyl-CoA resulted in a 2.5-fold increase in observed ITF signal change rates when crosslinking compared to the rate observed in the absence of ligands, in stark contrast to the negligible effect of acetyl-CoA on observed rates in the QN crosslinking background (Table V-1, Figure V-4). A moderate downward amplitude change was also observed in the presence of acetyl-CoA, which is interpreted to suggest a shift in carrier domain positioning away from the BC domain in favor of translocation. This data suggests that the presence of acetyl-CoA favors the release of the carrier domain from the BC domain for translocation. In order to crosslink the carrier domain in this system, the carrier domain must be in motion. Since acetyl-CoA increases the k_{obs}

2.5-fold compared to its absence, translocation of the carrier domain between sites is increasing. The presence of pyruvate led to a two-fold increase of k_{obs} while the combination of pyruvate and acetyl-CoA during crosslinking in DQ *Sa*PC produced a nearly four-fold increase in k_{obs} compared to k_{obs} in the absence of ligands or a two-fold increase compared to k_{obs} in just the presence of pyruvate (Table V-1, Figure V-4), suggesting a large drop in the kinetic barrier for translocation between sites. This result is consistent with observations of a 2-fold activation of *Sa*PC catalytic activity by acetyl-CoA (Yu, et al., 2009).

The amplitude of ITF signal changes during crosslinking in the presence of BC domain ligands was observed to be smaller in DQE *Sa*PC than in the DQ *Sa*PC crosslinking background (Figure V-8B), suggesting that the mutation shifts the carrier domain positioning equilibrium towards the BC domain. Combined with the reduced observed rate of crosslinking in the absence of substrates and the reduced effect of BC domain substrates on k_{obs}, these results are consistent with the proposal that Glu243 is part of a gatekeeper system to control the access of biotin to the BC domain active site. The E243A mutation in *Sa*PC resulted in a larger kinetic barrier for carrier domain translocation. This greater kinetic barrier is a consequence of stabilizing the BCCP-BC domain interaction in the ground state. This is illustrated in Figure V-11.

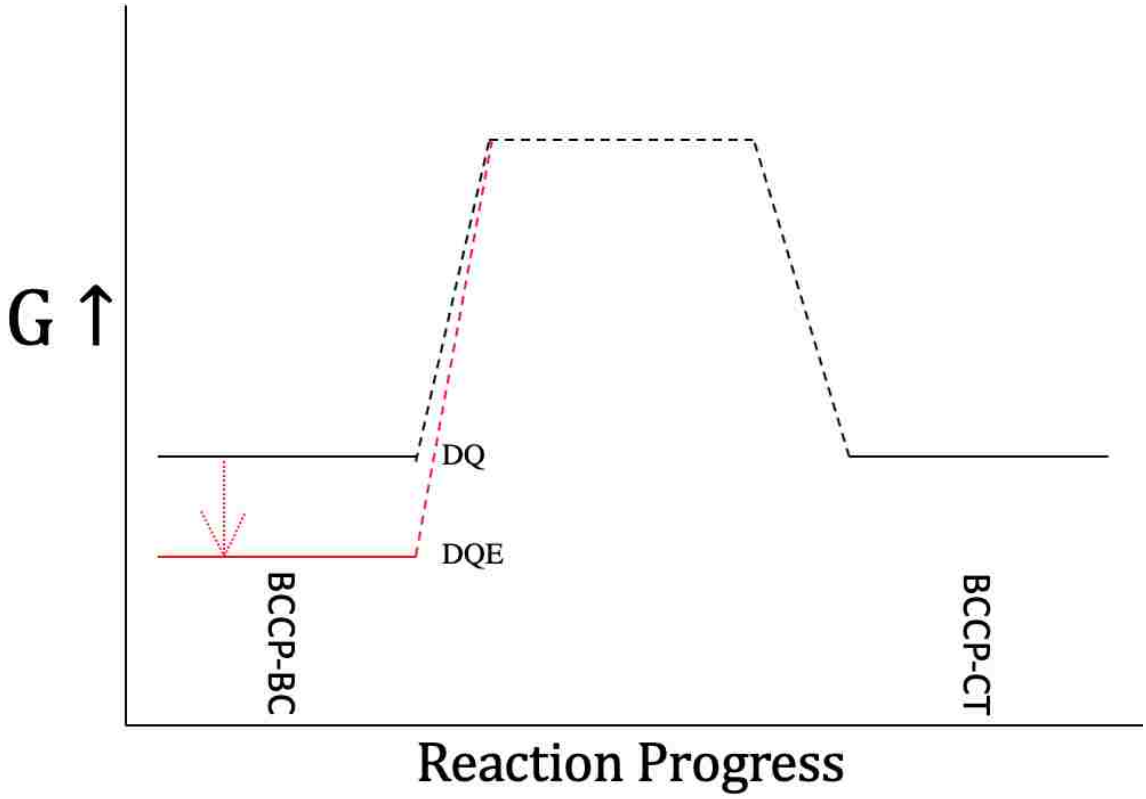

Figure V-11: Free energy diagram for DQE *Sa*PC
A potential energy landscape is shown for the DQE *Sa*PC mutant. The Gibbs free energy (G) is plotted against the translocation progress of BCCP between the BC and CT domains. The kinetic barrier is represented by a dashed black line. The wild-type reaction is represented in black while the mutation is represented in red.

Observed ITF signal change rates during crosslinking were increased in the DQY *Sa*PC mutant by 50% compared to the observed rates in the DQ background (Figure V-8A), suggesting that the carrier domain was less anchored in the CT domain and freer to translocate and adopt a variety of conformations. Just as in the QNY system, a large increase in amplitude was observed in DQY *Sa*PC, indicating a shift in carrier domain positioning towards the BC domain (Figure V-10B) as illustrated in Figure V-12. This is consistent with the proposal that Tyr621 stabilizes carrier domain positioning in the CT domain in the presence of pyruvate (Lietzan, et al., 2013). The loss of this stabilizing

interaction in the CT domain of this mutant, results in a shift in carrier domain positioning towards the BC domain.

The effect of acetyl-CoA in the DQY *Sa*PC mutant was nearly abolished with no significant difference in the k_{obs} between the DQY *Sa*PC and the DQ crosslinking background (Figure V-10A). Similarly, the observed amplitude in the presence of acetyl-CoA was also reduced in this mutant (Figure V-10B). These results indicate that the biotin-binding pocket in the CT domain active site plays an important role in mediating the effect of acetyl-CoA on carrier domain translocation. While acetyl-CoA binds near the flexible linker to the carrier domain, the flexible carrier arm is ultimately stabilized by interactions with biotin, such as those at the cleft of the exo-binding site. For example, the interaction between Tyr621 and biotin stabilizes the carrier domain in an intermolecular position. Acetyl-CoA has been shown to favor that conformation. In the absence of this Tyr621-biotin interaction, the carrier domain is granted greater translocational freedom.

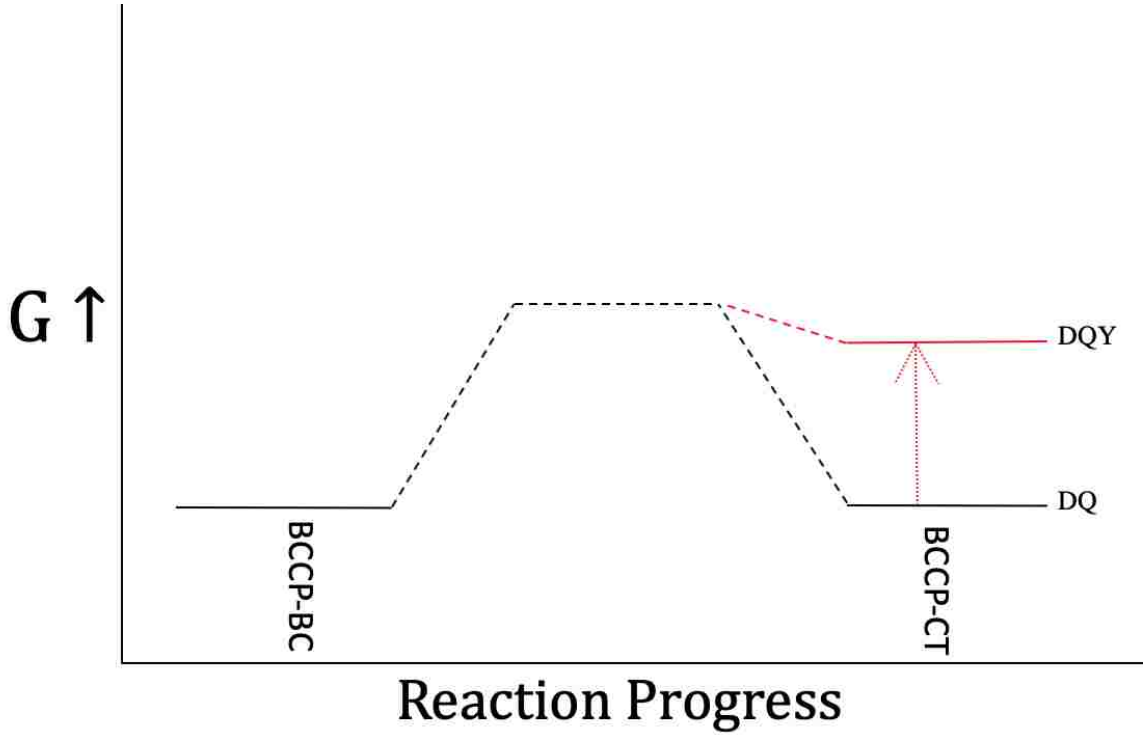

Figure V-12: Free energy diagram for DQY *Sa*PC
A potential energy landscape is shown for the DQY *Sa*PC mutant. The Gibbs free energy (G) is plotted against the translocation progress of BCCP between the BC and CT domains. The kinetic barrier is represented by a dashed black line. The wild-type reaction is represented in black while the mutation is represented in red.

The T876A mutant displayed the smallest amplitude changes in the absence of ligands compared to DQ crosslinking background (Figure V-7B). A remarkably decreased k_{obs} in the presence of pyruvate was observed in DQT *Sa*PC with a rate ~20% of that observed in the DQ background (Figure V-9A). The decreased observed rates of ITF intensity change in the presence of pyruvate for this mutant support the hypothesis by Zeczycki, et al. that biotin positioning is stabilized in the CT domain active site by the T876A mutant in the presence of pyruvate (Zeczycki, et al., 2009). With the DQ *Sa*PC system capturing the translocation of the carrier domain, a decreased k_{obs} indicates that the combination of this active site mutation and the presence of pyruvate has increased a kinetic barrier to carrier domain translocation.

The observed amplitude in the DQT mutant did not significantly change compared to the DQ crosslinking background in the presence of BC domain ligands, suggesting that mutation to the CT domain Thr876 did not alter the ground state free energies in the presence of ATP or ADP (Figure V-9B). However, there was a dramatic reduction in k_{obs} for the DQT *Sa*PC in the presence of ADP and phosphonoacetate, compared to the DQ crosslinking background (Figure V-9A), indicating that the carrier domain is favored to remain interacting with the BC domain in these mutants as a consequence of a larger kinetic barrier. These observations are consistent with the observation by Zeczycki, et al. that mutation of Thr882 in *Re*PC (the analogous residue to Thr876 in *Sa*PC) increased the rate of ADP phosphorylation in the BC domain (Zeczycki, et al., 2009). The authors proposed that carrier domain positioning was shifted towards the BC domain as a result of this mutation, increasing the presence of biotin in the active site and accelerating the rate of ADP phosphorylation. The DQT data presented in this chapter suggest that the thermodynamics of translocation largely weren't affected by this mutation, with the exception of pyruvate, as discussed. Rather, carrier domain translocation has become more unfavorable due to an increase in the energy barrier for translocation in the presence of ADP and phosphonoacetate, hinting at a complex change in the energy landscape in this mutation. This special case is illustrated in Figure V-13 where both the lowering of a kinetic barrier by the mutation and the thermodynamic change proposed by the addition of ADP and phosphonoacetate is shown. The reduced Gibbs free energy of the BCCP-BC domain interaction in the presence of ADP and phosphonoacetate results in both a shift in equilibrium positioning and a larger kinetic barrier to translocation relative to the absence of ligands.

In this chapter, I have presented data from a novel study investigating the kinetic and thermodynamic effects of active site mutations in PC on carrier domain translocation by directly observing the capture of the carrier domain "in flight". These results have further illustrated the important role each active site residue plays in shifting carrier domain positioning and how carrier domain positioning can be controlled within the conformational selection model.

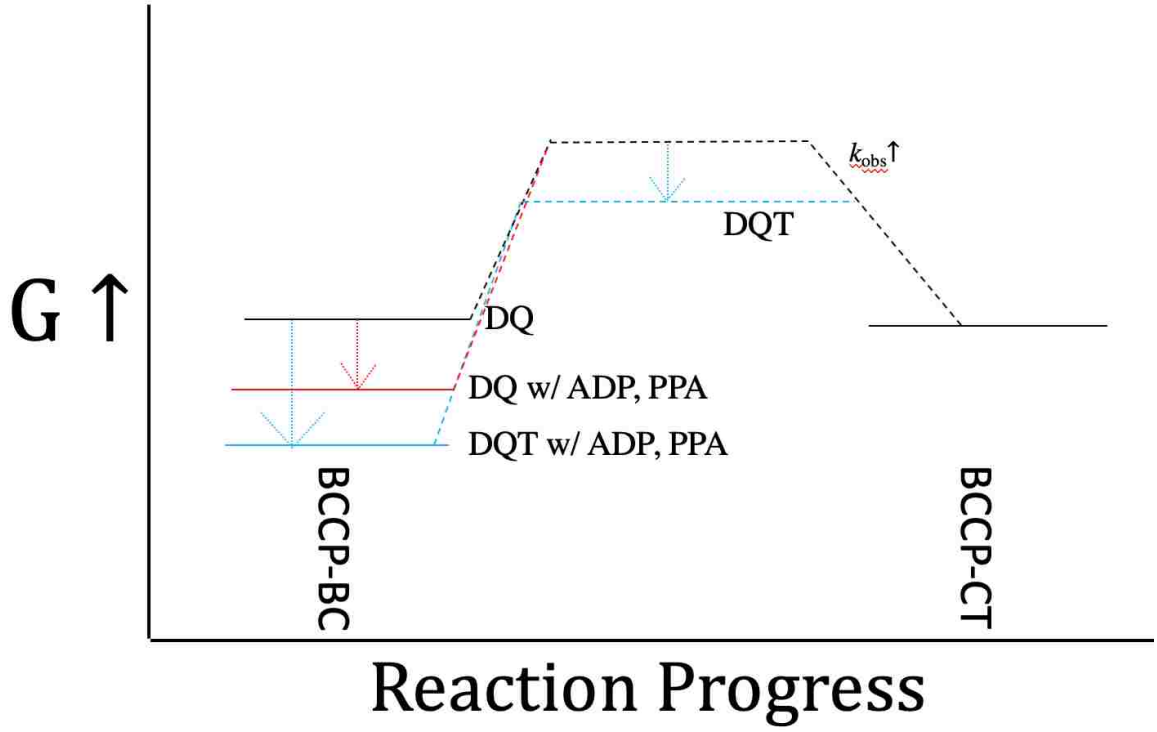

Figure V-13: Energy landscape diagram for DQT *Sa*PC
A potential energy landscape is shown for the DQE *Sa*PC mutant. The Gibbs free energy (G) is plotted against the translocation progress of BCCP between the BC and CT domains. The kinetic barrier is represented by a dashed black line. The wild-type reaction is represented in black while the mutation is represented in blue. The effect of the presence of ADP and phosphonoacetate (PPA) in the mutant on this landscape is shown in red while in the DQT mutant it is shown in blue.

VI. CONCLUSIONS

1. Mechanism Governing Carrier Domain Translocation in *S. aureus* Pyruvate Carboxylase

In this section, the conformational selection model will be utilized to explain the translocation of carrier domain in *S. aureus* pyruvate carboxylase. The application of this model will attempt to integrate all of the results from the current study to generate a comprehensive view of how carrier domain translocation is controlled. The contribution of each domain to the regulation of carrier domain positioning will be discussed. A model will be proposed for how acetyl-CoA may influence carrier domain positioning that attempts to account for a wide-range of observations. Finally, the findings discussed here will be compared to several multi-domain enzymes.

Conformational selection governs carrier domain positioning. As introduced in Chapter I, the induced conformational change model would predict that the carrier domain in PC remains in one conformation in the absence of a ligand (Easterbrook-Smith, et al., 1976; Goodall, et al., 1981; Attwood and Wallace, 1986). Alternatively, the conformational selection model predicts that the carrier domain exists in an ensemble of conformations regardless of ligand present. The results presented in Chapter III all support the conformational selection model as the mechanism governing carrier domain positioning. The carrier domain was observed to position itself intermolecularly or get trapped in the state of translocation between sites irrespective of the presence or identity of ligands. Under no circumstances was the carrier domain unable to be trapped in either "state", consistent with the conformational selection model. It is important to note that an assumption has been made that the QN crosslinking system can distinguish between the

BCCP-exo binding site and BCCP-CT domain conformations. An X-ray crystal structure of crosslinked PC or a comparison between the QN system and a system that traps the carrier domain while interacting with the CT domain active site would provide evidence for this, as no evidence currently exists. However, the distance between the Q891C and N1102, which crosslink in the exo-binding site conformation, are ~22 Å apart when the carrier domain is positioned with biotin in the CT domain active site (PDB ID: 3BG5). This is a much greater distance than the 8 Å BMOE crosslinker used throughout these experiments, which supports the ability of this system to distinguish the two conformations.

BC domain ligands shift carrier domain positioning towards the BC domain as observed by the increased observed amplitudes of ITF signal change when crosslinking the carrier domain during translocation or in the exo-binding site conformation in the presence of BC domain ligands compared to in the absence of ligands. Observed rates of ITF signal change (k_{obs}) decreased when the carrier domain was crosslinked in either system in the presence of BC domain ligands, indicating that a kinetic barrier increased for the translocation of the carrier domain and for the positioning of the carrier domain away from the BC domain in the exo-binding site (Tables V-1, III-4). The observed amplitudes also increased during crosslinking in the QN or DQ system in the presence of BC domain ligands, indicating a shift in carrier domain positioning towards the BC domain (Figures V-7B, IV-3B). The results presented here are also consistent with observations in 1965 when Scrutton and Utter observed that BC domain substrates protected PC from avidin deactivation (Scrutton and Utter, 1965). Avidin binds to the carrier domain-tethered biotin, preventing it from contributing to catalysis. When biotin

is positioned in the BC domain active site, such as when BC domain ligands are present, biotin would be unavailable to react with avidin, leading to a reduction in deactivation by avidin binding.

Pyruvate, the CT domain substrate, has the opposite effect, as expected, shifting carrier domain positioning towards an intermolecular position. However, there is some subtlety to this behavior. The creation of the two different crosslinking constructs has allowed a finer determination to be made of what carrier domain state is favored in the presence of pyruvate. The conformation in which the carrier domain is translocating between active sites, trapped by D907C/Q1118C SaPC, is kinetically favored, with a 2-fold increase in k_{obs} when crosslinking in the presence of pyruvate. In contrast, the presence of pyruvate only yields a 1.1-fold increase in k_{obs} when crosslinking the carrier domain in the exo-binding site conformation (Tables III-4, V-1). However, the observed amplitudes do not differ much between crosslinking the carrier domain with biotin positioned in the exo-binding site or in the translocation state. Pyruvate has been shown to bind/unbind approximately twice per catalytic cycle, diffusing relatively easily into and out of the active site (Warren G.B. and Tipton K.F., 1974, Cheung Y.F. and Walsh C., 1976, Zeczycki, T.N., et al., 2011). When pyruvate dissociates, the biotin-binding pocket that Lietzan, et al. observed would no longer be stabilized, making the BCCP-CT interaction less favorable (Lietzan, et al., 2013). Therefore, the carrier domain would be more likely to leave the CT domain after which BCCP-biotin would be free to translocate and could become temporarily stabilized in the nearby exo-binding site, providing an explanation for the similar amplitude changes observed in ITF signal changes when crosslinking to either conformation. These observations also suggest that the role of the

exo-binding site may be to stabilize the carrier domain close to the CT domain, effectively increasing the local concentration of carboxybiotin.

My findings in favor of the conformational selection model are not inconsistent with early kinetic observations in PC (Easterbrook-Smith, et al., 1976, Goodall, et al., 1981, Attwood and Wallace, 1986) in which the authors followed the decarboxylation of biotin and observed that the rate of biotin decarboxylation increased in the presence of CT domain ligands. These results were interpreted to suggest that CT domain ligands induce carrier domain translocation towards the CT domain. Rather, the carrier domain positioning, which exists in an equilibrium, was shifted to favor the CT domain in the presence of CT domain ligands. The CT domain promotes the decarboxylation of biotin, so an increased presence of carboxybiotin in the CT domain naturally leads to an increased rate of decarboxylation. Conversely, without a CT domain ligand present, the carrier domain may still attain this conformation, but biotin would not be stabilized as the active site tyrosine would not be properly positioned to stabilize biotin in the active site. Thus, rates of carboxybiotin decarboxylation in the absence of a CT domain ligand would be low.

Physiological Relevance. The induced conformational change model might seem to be the more efficient model for governing carrier domain positioning in PC or other enzymes since the carrier domain would only translocate to the next active site when the relevant substrate is bound and the active site ready to accept the intermediate product from the first active site. However, the K_M value for many enzymes, the ligand concentration at which half of the binding sites have ligand bound, is often close to the physiological concentration of the respective substrate (Waelbroeck, 2007; Berg, et al.,

2002). If the assumption that all active sites must have substrate bound for an induced conformational change to take place is valid, this model would lead to a less productive enzyme when substrate concentrations are near or below K_M. In this situation, substrate could be bound without carrier domain translocation or reaction completion. However, the conformational selection model would allow for comparatively more productivity in these conditions. In a case where substrate concentrations are around the K_M value, approximately half of the active sites would have substrate bound. Thus, those active sites would favor interactions with the carrier domain, leading to the formation of product. Comparatively, if the same enzyme were governed by the induced conformational change model, very little product would be formed since it would be rarer to have all active sites bound with substrate to induce carrier domain translocation. Overall, when substrate values are near or below K_M, I believe that the conformational selection would be favored for organismal fitness.

Conversely, if the assumption that all active sites must have substrate bound for an induced conformational change to take place is not valid, there would not be such a clear distinction between these models and organismal fitness. For example, if half of the active sites were required to be bound with substrate for an induced conformational change to take place, this model would perform similarly to the conformational selection model when substrate concentrations are at K_M, since by the definition of K_M, approximately half of the active sites would have substrate bound. The complexity of this topic is highlighted by studies that have investigated proteins that can utilize both models, dependent upon ligand concentration. Dihydrofolate reductase (DHFR) was observed to operate via conformational selection at low ligand concentrations and via an

induced fit mechanism at high ligand concentrations. At intermediate concentrations, both mechanisms were observed to be in use (Hammes, et al., 2009; Grieves and Zhou, 2014). Thus, enzymes may have evolved more than one mechanism to ensure the efficient coupling of reactions over a range of substrate concentrations.

BC domain interactions with the carrier domain. The interface between the carrier domain and BC domain is composed of the B-subdomain lid, a solvent-exposed loop belonging to the C-subdomain, and the carrier domain (Lietzan, et al., 2011). Only two pairs of residues directly interact while the majority of contact between these domains are non-specific, burying ~1200 $Å^2$. Given the lack of direct or conserved interactions, it's reasonable to expect that changes in the positioning of the B-subdomain lid would alter the docking favorability of the carrier domain to the BC domain. B-subdomain lid conformations have been observed to shift to more closed conformations in the presence of BC domain ligands in several crystal structures (Kondo S., et al., 2004, Thoden JB, et al., 2000, Chou CL, et al., 2009, Chou CY and Tong L., 2011, Lietzan, et al., 2011). The presence of tethered biotin was observed to lead to tighter lid closure than the presence of free biotin (Lietzan, et al., 2011). This relationship between the presence of BC domain ligands and the composition of the BCCP-BC domain interface may be the primary mechanism in the BC domain to govern carrier domain positioning.

The second BC domain mechanism that may play a role in shifting carrier domain positioning was observed by Lietzan, et al. in 2011 in an X-ray crystal structure of T882A *Re*PC that was co-crystallized with MgADP and phosphonoacetate (Lietzan, et al. 2011). In this structure, the carrier domain was docked at the BC domain, which was the first high-resolution structure to capture this, but carboxybiotin was positioned outside of

the active site. A pair of residues that were located between the active site and the entry site for carboxybiotin, Arg353 and Glu248, were oriented such that a salt bridge formed between them, stabilizing the positioning of Arg353 which was proposed to preclude carboxybiotin access. The authors proposed that this interaction may prevent abortive decarboxylation, serving as a mechanism to control carboxybiotin positioning. This interaction between these residues and biotin had not since been studied to determine the effect on carrier domain positioning.

As discussed in chapter IV and V, mutation of Glu243 in *Sa*PC, the homolog of Glu248 in *Re*PC, resulted in a shift in carrier domain positioning towards the BC domain, consistent with proposals that this residue may preclude carboxybiotin access to the BC domain active site. Presumably, a more favorable interaction between the BC and BCCP domains occurs with increased carboxybiotin access to the BC domain active site. When crosslinking to the exo-binding site conformation, the presence of BC domain substrates led to an increase in the observed amplitudes of ITF signal change in the E243A *Sa*PC mutant, indicating a greater shift in carrier domain positioning towards the BC domain as a result of this mutation (Figure IV-3B). However, when capturing the translocating carrier domain, the opposite results were observed, potentially indicating an increased amount of carrier domain translocation (Figure V-8B). Rates of ITF signal change remained unchanged in this mutant when crosslinking to the exo-binding site in the presence of BC domain ligands (Figure IV-3A). However, the decrease in k_{obs} was attenuated when crosslinking in the DQE mutant with BC domain ligands present compared to the decrease in k_{obs} in the DQ background (Figure V-8A). While it might seem that this indicates that this mutation has lowered a kinetic barrier to the

translocation of the carrier domain in the presence of BC domain ligands, recall that in the absence of any ligands, the k_{obs} for this mutant was decreased compared to the DQ background (Figure V-6). This indicates that the BC domain substrates have less of an effect in this mutant because a kinetic barrier to carrier domain translocation has increased as a consequence of the mutation itself. Conversely, the rate of crosslinking translocating carrier domains in DQE was attenuated and indistinguishable from the crosslinking background in the presence of pyruvate. This indicates that a kinetic barrier has increased for the translocation of the carrier domain in the presence of pyruvate, consistent with the effect observed in the presence of BC domain ligands.

CT domain interactions with the carrier domain. When the carrier domain is positioned at the CT domain, there are several pairs of residues that engage in hydrogen-bonding and many hydrophobic interactions occur, as well (Xiang S. and Tong L., 2008). However, no alterations to the binding interface have been reported in the presence/absence of ligands. Rather, small conformational changes occur in the active site in the presence of a CT domain ligand, such as pyruvate (Lietzan, et al., 2013). The carboxyl moiety of pyruvate was shown to form a salt bridge with the guanidinium group of Arg621 (*Re*PC numbering), which promoted the movement of an active site loop. This loop movement ultimately resulted in a reorientation of Tyr628 (Tyr621 in *Sa*PC) to rotate towards the CT domain active site. Based on an overlay with *H. sapiens* PC, biotin was proposed to position itself over this tyrosine in a stable interaction between the sulfur of the thiophene ring of biotin and the aromatic ring of tyrosine. The rotation of tyrosine towards the active site in the presence of pyruvate has been proposed to stabilize biotin in the CT domain active site.

The findings that I presented in chapters IV and V have shown the important role of this residue in the positioning of the carrier domain with the CT domain. The BCCP-CT domain interaction likely became less thermodynamically favorable in the presence of pyruvate in the DQY mutant. This was observed as a large increase in k_{obs} when trapping the translocating carrier domain in the DQY mutant without any ligands present, indicating that a kinetic barrier has decreased for the translocation of the carrier domain (Figure V-7A). Similarly, a large change in the observed amplitude when trapping the translocating carrier domain was observed in this mutant, indicating a large shift in carrier domain equilibrium away from the BC domain, potentially towards the translocation state and/or an intermolecular interaction (Figure V-7B). A large shift in amplitude was also observed in the QNY mutant when crosslinking in the absence of ligands, supporting the proposal that the carrier domain equilibrium has shifted towards the exo-binding site (Figure IV-5B). It is clear that the kinetic and thermodynamic landscape for carrier domain interaction with the CT domain has been dramatically altered, presumably with the CT domain active site becoming more unfavorable for the positioning of biotin and the carrier domain in this mutant.

Only minimal decreases in k_{obs} were observed when crosslinking in the QNY or DQY mutants in the presence of BC domain ligands (Figures IV-5A, V-10A). This was a strange result in that a CT domain mutation altered the effect of BC domain ligands on carrier domain positioning at the exo-binding site. This result may support previous observations that mutations or ligand binding in one active site can have an effect on a distant active site. This effect was recently observed in *Sa*PC and *Re*PC, respectively, with results interpreted to suggest communication between the BC and CT domains

(Westerhold, et al., 2016; Lietzan, et al., 2014). However, no specific mechanism for this has been proposed or observed to date. Given that the symmetric/asymmetric conformation of PC is linked to carrier domain positioning (St. Maurice, et al., 2007; Yu, et al., 2009; Lasso, et al., 2014), this communication could be the result of shifts in the carrier domain positional equilibrium caused by ligand binding or mutations that influence the overall symmetric state of PC. If this were true, for example, the mutation of Tyr621 would be predicted to disrupt acetyl-CoA binding. Since Tyr621 presumably shifts the carrier domain equilibrium away from the CT domain, the asymmetric form of PC would be more favorable. This form of PC has two binding sites for acetyl-CoA, while the disfavored symmetric form has four binding sites (Lasso, et al., 2014). Thus, this mutation may ultimately have an effect on the cooperativity and observed Hill coefficients of acetyl-CoA binding.

Pyruvate was observed to still have an effect on k_{obs} and amplitudes in the Y621A mutants. The effect of pyruvate on carrier domain positioning may be reduced when crosslinking in the DQY mutant compared to the QNY mutant, but there is still a relatively large change in the amplitude of observed ITF signal change compared to in the absence of pyruvate, indicating there is likely another interaction that occurs between pyruvate binding and biotin (Figures IV-5B, V-10B). Interestingly, a difference exists in the response to pyruvate between the QNY and DQY mutants. In the QNY mutant, pyruvate increases the k_{obs} compared to the QN background in the presence of pyruvate (Figure IV-5A). Conversely, in the DQY mutant, this increase in k_{obs} is attenuated (Figure V-10A). Taken together, this suggests a reduced kinetic barrier for the positioning of the carrier domain in the exo-binding site in the presence of pyruvate while pyruvate has a

reduced effect on lowering the kinetic barrier for carrier domain translocation. In the QNY system, the destabilization of the carrier domain in the CT domain by the loss of the biotin-Tyr621 interaction can explain this observation. A reduced interaction energy increases the off rate for the BCCP domain in the CT domain, thereby increasing the likelihood of positioning at the exo-binding site. Similarly, without the Tyr621 residue to "communicate" the presence of pyruvate to biotin and stabilize biotin in the CT domain, the effect of pyruvate on translocation will be weakened, as observed, with the carrier domain likely remaining stabilized in other low energy wells, such as the exo-binding site or BC domain.

The second residue CT domain active site residue that biotin was proposed to interact with is Thr876 in *Sa*PC numbering (Thr882 in *Re*PC). The N-1 position of biotin is proposed to hydrogen-bond with this residue when biotin is positioned in the active site (Zeczycki, et al, 2009). In the presence of ADP and phosphonoacetate, I observed that a kinetic barrier has dramatically increased for the translocation of the carrier domain and for the positioning of the carrier domain in the exo-binding site (Figures IV-4A, V-9A). The carrier domain positioning was also observed to shift towards the BC domain with a much larger amplitude in the presence of ADP and phosphonoacetate in QNT *Sa*PC compared to the QN background, whereas the amplitude is virtually unchanged when crosslinking the translocating carrier domains (Figure V-9B). This large equilibrium shift suggests Thr876 may have a role stabilizing biotin in the CT domain active site, where this residue is located.

The observed behavior of the T876A mutants is also dramatically altered in the presence of pyruvate. Whether crosslinking the carrier domain to the exo-binding site or

crosslinking translocating carrier domains in the presence of pyruvate, a kinetic barrier has increased, with slower rates of ITF signal change observed compared to the crosslinking backgrounds (Figures IV-4A, V-9A). This observation strongly supports the proposal by Zeczycki, et al. that because the T876A mutant cannot complete the proton-transfer step, the reaction cannot be completed and biotin would remain in the CT domain active site (Zeczycki, et al., 2009). If the carrier domain were "trapped" in the CT domain, translocation would become more unfavorable, as well as positioning in the exo-binding site.

A comparable observation to the QNY/DQY systems was made in the presence of pyruvate in the QNT/DQT systems in that the effect of pyruvate was attenuated but not abolished. This residue may be the other residue predicted above to mediate the effect of pyruvate on carrier domain positioning and translocation. The CT domain active site has a network of hydrogen bonds between pyruvate and biotin. Disruption of that by mutation of this residue may explain these observations. An experiment observing the effects of pyruvate on k_{obs} and amplitudes in double mutant crosslinking systems in which both Tyr621 and Thr876 are mutated would allow further clarification of the roles of these residues in mediating the effect of pyruvate on carrier domain positioning.

Role of acetyl-CoA in carrier domain positioning. A multitude of kinetic and structural studies have been performed to determine how acetyl-CoA activates PC. Kinetic studies have determined that acetyl-CoA stimulates the BC domain reaction (Attwood and Graneri, 1992; Branson, et al., 2002; Legge, Branson, and Attwood, 1996; Phillips, et al., 1992; Jitrapakdee, et al., 2010) and not the CT domain reaction (Attwood and Wallace, 1986). However, the exact mechanism by which this acceleration occurs is

not known. It has been proposed that acetyl-CoA may promote Mg^{2+} binding (Attwood and Graneri, 1992) or substrate binding in the BC domain (Legge, Branson and Attwood, 1996). The structure of *Re*PC with acetyl-CoA bound did not show any significant conformational change in the BC domain ligand binding sites, suggesting that the activation effects of acetyl-CoA extend beyond the BC domain active site (St. Maurice, et al., 2007) (Lietzan, et al., 2011).

Acetyl-CoA has also been shown to have a role in coupling the two half-reactions, with the coupling efficiency being increased in the presence of acetyl-CoA. Because the translocation of the carrier domain is what physically couples these reactions, it was proposed that the translocation of the carrier domain was regulated by acetyl-CoA (Zeczycki, et al., 2011B). Pyruvate and MgATP were also shown to be thermodynamically linked in the presence of acetyl-CoA (Westerhold, et al., 2017). In the same study, ATP cleavage was observed to be promoted by pyruvate binding in the CT domain, which was suggested to show communication between the two active sites, possibly connected by carrier domain translocation. Westerhold, et al. also showed that activation entropy decreased in *Sa*PC in the presence of acetyl-CoA, which the authors suggested meant that carrier domain movement was restricted in the presence of acetyl-CoA (Westerhold, et al., 2017). While investigating carrier domain translocation pathways, Liu, et al. (Liu, et al., 2018) showed that acetyl-CoA stimulates catalytic activity for the translocation pathway between the intramolecular BC domain and intermolecular CT domain, which is consistent with the observation by Westerhold, et al. that activation entropy is decreased by acetyl-CoA. Finally, in studies investigating the roles of allosteric binding site residues in *Re*PC, it was proposed that acetyl-CoA favored

the symmetric conformation of PC which is associated with the carrier domain positioned across the face of the tetramer (Choosangtong, et al., 2015; Sirithanakorn, et al., 2016).

I have observed that acetyl-CoA, when mixed with *Sa*PC, promotes a carrier domain conformation very similar, if not identical, to that captured by crosslinking translocating carrier domains (Figure V-4). A kinetic barrier for the translocation of the carrier domain and for the intermolecular positioning of the carrier domain was lowered when acetyl-CoA is added to either ATP or pyruvate (Figures IV-1, V-4). Further, a decrease in the amplitude of the ITF signal when crosslinking to the exo-binding site conformation was observed in the presence of acetyl-CoA, indicating an equilibrium positioning shift of the carrier domain towards an intermolecular interaction (Figure IV-3). A similar decrease in amplitude was observed when crosslinking translocating carrier domains, suggesting that it has become more thermodynamically favorable to translocate between active sites (Figure V-8). Further, I have observed that mutation of Tyr621 virtually abolished the effect of acetyl-CoA on carrier domain positioning and translocation (Figures IV-5, V-10. While acetyl-CoA may promote positioning of the carrier domain at or near the CT domain, without a way to stabilize the C-terminal side of the flexible carrier domain in a specific conformation, such as when Tyr621 is mutated, the effect of acetyl-CoA on carrier domain positioning was lost (Figures IV-5, V-10).

Based on these observations, I conclude that acetyl-CoA favors the release of the carrier domain from the BC domain and stabilizes its positioning at or near the opposing CT domain. The release of the carrier domain from the BC domain would allow the opening of the B-subdomain lid, aiding the release of products and binding of Mg^{2+} and nucleotides (Menefee and Zeczycki, 2014). Acetyl-CoA has been observed to decrease

the affinity of chicken liver PC for nucleotides (Geeves, et al., 1995). This is consistent with the B-subdomain lid attaining a more open conformation due to a shift in carrier domain positioning away from the BC domain, allowing easier diffusion of ligands in and out of the active site. Further, as introduced in Section I.2.2.2, the B-subdomain lid must close for proper positioning of the P-loop, which aids in substrate binding. If the B-subdomain lid is in a more open conformation, the P-loop would most likely be poorly positioned to aid substrate binding, which could increase the dissociation constant. However, the overall effect of acetyl-CoA on BC domain reaction steps is complex. For instance, ATP-cleavage was determined to be the rate-limiting step in the acetyl-CoA sensitive sheep and chicken liver PC enzymes (Goodall, et al., 1981; Attwood and Wallace, 1986). Acetyl-CoA was also shown to increase the productive cleavage of ATP in chicken liver PC (Legge, et al., 1996). Overall, differences exist between PCs from different species in which step is rate-limiting, which could be a result of changes in the locus of activation by acetyl-CoA (Adina-Zada, et al., 2012).

Overall, while it may seem contradictory to have evidence that acetyl-CoA enhances BC domain catalysis and evidence that acetyl-CoA favors the release of the carrier domain and translocation away from the BC domain, findings from a recent cryo-EM study of *Sa*PC help to unite these observations (Lasso, et al., 2014). In this study, distinct populations of *Sa*PC were observed in either the asymmetric conformation or the symmetric conformation. In the asymmetric conformation, with the carrier domain interacting with the BC domain, two binding sites for acetyl-CoA exist. Conversely, in the symmetric conformation, four acetyl-CoA binding sites exist. Thus, irrespective of the positioning of the carrier domain, acetyl-CoA could be present and enhancing BC

domain catalysis. As acetyl-CoA concentrations increase, the symmetric conformation would be favored, shifting carrier domain positioning towards an intermolecular interaction. By promoting a specific or more limited set of conformations near the CT domain, acetyl-CoA would be favoring the translocation pathway between the intramolecular BC domain and intermolecular CT domain, as Liu, et al. observed (Liu, et al., 2018). The constraint of favorable carrier domain conformations by acetyl-CoA would also have the effect of reducing activation entropy, as the carrier domain's conformational flexibility would be reduced, as Westerhold, et al. observed (Westerhold, et al., 2017).

Role of biotin in carrier domain positioning. While many studies suggest that biotin plays a key role in the positioning of the carrier domain and coupling of the half-reactions, it has been difficult to study the role of biotin in carrier domain positioning since the loss of biotin abolishes much of the catalytic activity of PC (Zeczycki, et al. 2009; Lietzan, et al., 2014; Menefee and Zeczycki, 2014). As my studies are independent of catalytic activity and I can directly observe carrier domain positioning, the systems presented here enable me to study the role of biotin in carrier domain positioning. The loss of biotin was observed to greatly diminish carrier domain sensitivity to BC domain substrates (Figure III-8). Unfortunately, ITF signals are dependent on the presence of biotin, making more detailed observations impossible at the current time (Figure III-6C). However, given the importance of the previously discussed residues that interact with biotin to affect carrier domain positioning, I propose that biotin leads the interaction between the carrier domain and the active sites/exo-binding site when establishing an equilibrium or when an equilibrium shift occurs due to the presence of a ligand. An

inability to stabilize a conformation due to a mutation of one of these residues, such as Tyr621, results in dramatically altered carrier domain behavior.

However, biotin and the interactions with active site residues are not the sole participant in shifting carrier domain positioning. In the unbiotinylated *Sa*PC mutant, the presence of ADP and phosphonoacetate still had some effect on carrier domain behavior with the observed rate of crosslinking decreasing in the presence of the ligands (Figure III-8). I believe that this result can be explained by the interface that is formed between the carrier domain and the BC domain. With ligands bound, the B-subdomain lid of the BC domain should be in a closed conformation, forming the final binding interface for carrier domain docking (Menefee and Zeczycki, 2014). While biotin may not be present to interact with the "gatekeeper" residue or enter the active site, the carrier domain would encounter a favorable binding interface that would stabilize carrier domain positioning and lead to a shift in equilibrium positioning.

Shifting energy landscapes in Q891C/N1102C/E243A *Sa*PC mutant. The QNE mutants was observed to have a higher k_{obs} and an increased amplitude compared to the QN *Sa*PC background (Figure IV-1). The presence of ADP and phosphonoacetate during crosslinking resulted in little change in k_{obs} in the QNE mutant but an increase in observed amplitude compared to in the absence of ligands in QNE *Sa*PC (Figure IV-3). This can be visualized in the energy landscape diagram shown in Figure VI-1. The traditional interpretation is shown in Figure VI-1A with the E243A mutation lowering the free energy of interaction in the BC domain, presumably due to greater biotin access of the BC domain active site. This lower free energy would result in the observed increase in amplitude during crosslinking in this mutant due to a shift in carrier domain

positioning towards the BC domain (Figure IV-1B). A reduction in the kinetic barrier to adoption of the BCCP-CT interaction is also shown to take the increased k_{obs} into account. The presence of ADP and phosphonoacetate is also shown to further reduce the free energy of the BCCP-BC interaction as well, matching the increased amplitudes observed (Figure IV-3B).

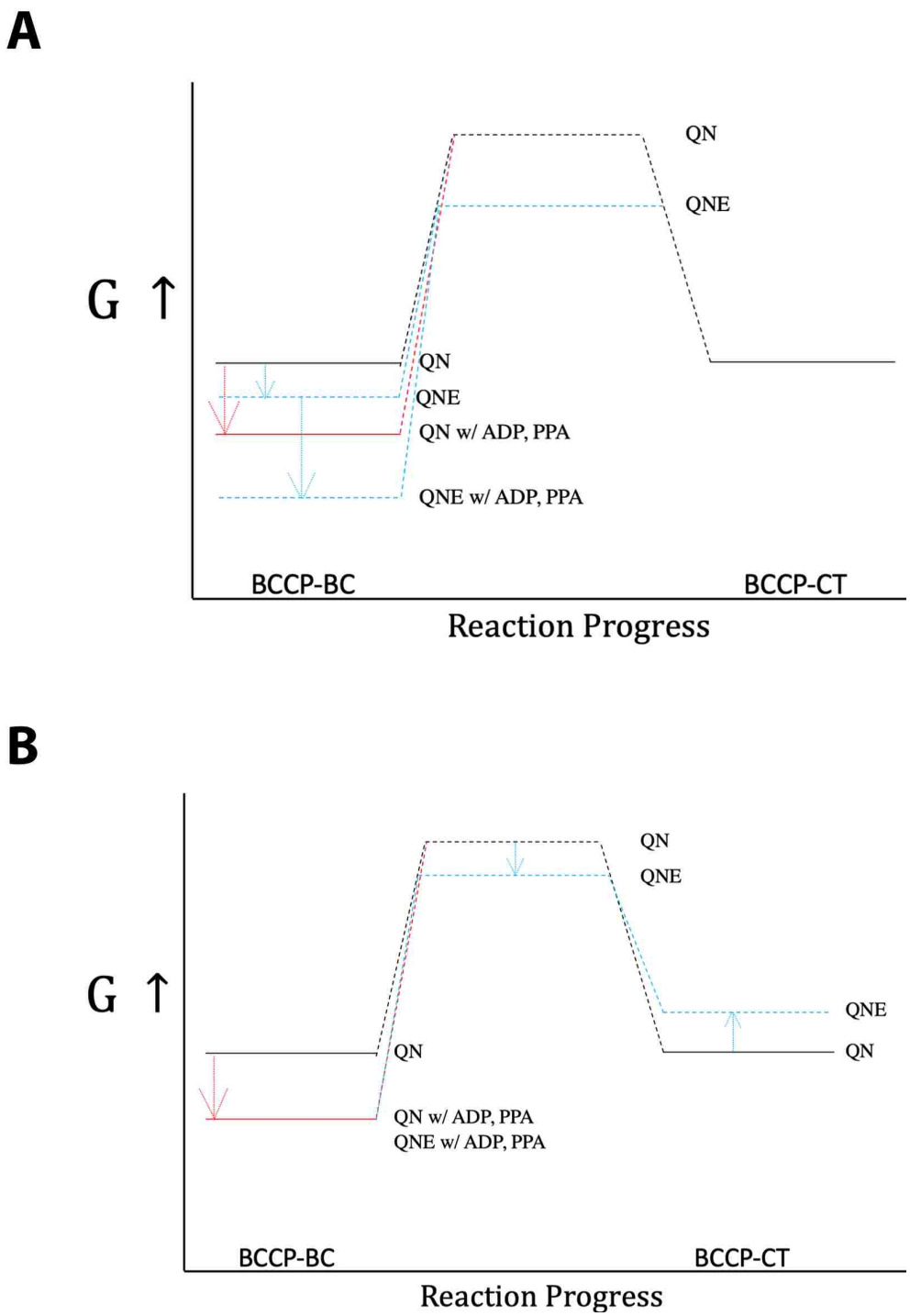

Figure VI-1: Energy landscape diagram for QNE *Sa*PC
A potential energy landscape is shown for the QNE *Sa*PC mutant. The Gibbs free energy (G) is plotted against the translocation progress of BCCP between the BC and CT domains. The kinetic barrier is represented by a dashed black line. The wild-type reaction is represented in black while the mutation is represented in blue. The effect of the presence of ADP and phosphonoacetate (PPA) in the QN mutant on this landscape is shown in red while in the QNE mutant it is shown in blue. **A.** The traditional interpretation is shown with the BC domain mutation affecting the BCCP-BC interaction. **B.** An alternate interpretation is shown.

However, an alternate interpretation is possible with the E243A mutation resulting in an increase in the free energy of the BCCP-CT interaction (Figure VI-1B). This increase in the free energy would result in a destabilization of the BCCP-CT interaction, shifting carrier domain positioning towards the BC domain. This would also have the effect of increasing the observed amplitude during crosslinking in this mutant (Figure IV-1B). A reduction in the kinetic barrier to adoption of the BCCP-CT interaction, similar to that in the traditional interpretation, is also shown to take the increased k_{obs} into account (Figure IV-1A). In this alternate interpretation, the presence of ADP and phosphonoacetate have a similar reduction in the free energy of interaction for the BCCP-BC, resulting in the increased amplitudes observed. Due to the increased shift in carrier domain positioning due to the QNE mutation, the observed amplitude in the presence of ADP and phosphonoacetate would be larger.

Shifting energy landscapes in Q891C/N1102C/T876A *Sa*PC mutant. The QNT mutant was observed to have a higher k_{obs} but a negligible amplitude change compared to the QN *Sa*PC background (Figure IV-1). The presence of ADP and phosphonoacetate during crosslinking resulted in a large decrease in k_{obs} in the QNT mutant compared to in the QN mutant. A large increase in observed amplitude compared to the observed amplitude in the absence of ligands in QNT *Sa*PC or compared to the QN mutant in the presence of ADP and phosphonoacetate (Figure IV-4). This can be visualized in the energy landscape diagram shown in Figure VI-2. The traditional interpretation is shown in Figure VI-2A with the T876A mutation having little effect on the free energy of interaction in the BC domain, resulting in negligible change in amplitude during crosslinking in this mutant due to little or no shift in carrier domain positioning towards

the BC domain (Figure IV-4B). A reduction in the kinetic barrier to adoption of the BCCP-CT interaction, the primary observed effect of this mutation in the absence of ligands, is also shown to account for the increased k_{obs} in QNT *Sa*PC (Figure IV-1A). The presence of ADP and phosphonoacetate is also shown to dramatically reduce the free energy of the BCCP-BC interaction as well, matching the large increase of amplitude change observed (Figure IV-4B). This drop in the free energy of interaction also results in a much larger kinetic barrier to the adoption of the BCCP-CT interaction, matching the observed drop in k_{obs} in QNT *Sa*PC in the presence of ADP and phosphonoacetate (Figure IV-4A)

An alternate interpretation is possible with the T876A mutation resulting in an increase in the free energy of the BCCP-CT interaction in the presence of ADP and phosphonoacetate (Figure VI-2B). This would have the similar effect of shifting carrier domain positioning towards the BC domain in the presence of these ligands, resulting in a larger observed amplitude change during crosslinking. An increase in the kinetic barrier to adoption of the BCCP-CT interaction in the presence of ADP and phosphonoacetate is also shown. This would result in the decreased k_{obs} observed in QNT *Sa*PC in the presence of ADP and phosphonoacetate (Figure IV-4A). A reduction in the kinetic barrier to adoption of the BCCP-CT interaction is still necessary, as shown in Figure VI-2B, in the absence of ligands to account for the increased k_{obs} in QNT *Sa*PC (Figure IV-1).

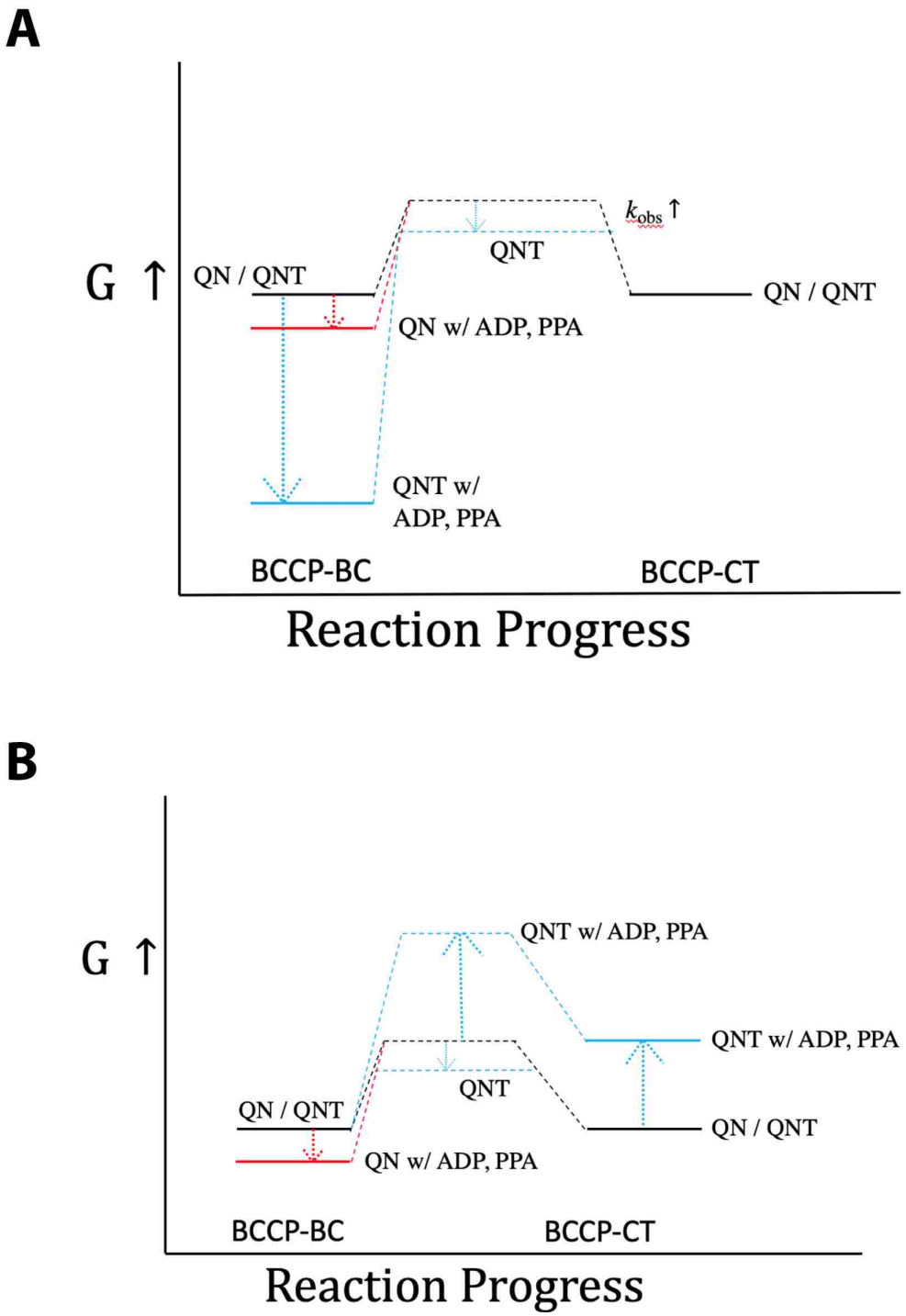

Figure VI-2: Energy landscape diagram for QNT *Sa*PC
A potential energy landscape is shown for the QNT *Sa*PC mutant. The Gibbs free energy (G) is plotted against the translocation progress of BCCP between the BC and CT domains. The kinetic barrier is represented by a dashed black line. The wild-type reaction is represented in black while the QNT mutation is represented in blue. The effect of the presence of ADP and phosphonoacetate (PPA) in the QN mutant on this landscape is shown in red while in the QNT mutant it is shown in blue. **A.** The traditional interpretation is shown with the mutation affecting the kinetic barrier in the absence of ligand. **B.** An alternate interpretation is shown.

Shifting energy landscapes in Q891C/N1102C/Y621A *Sa*PC mutant. An acknowledgement of the complexity of this system needs to be made in light of the odd ITF signal behavior in this mutant. The data may be unable to be interpreted in the same manner as the other mutants, given the starkly different ITF signal observed. The alteration in ITF signal could be due to a different set of interactions between biotin and tryptophans in QNY *Sa*PC due to the Y621A mutation. The mutation may have caused a change in observed fluorescence that was not due to an alteration in carrier domain positional equilibrium. Another possibility for the difference in observed signal could be due to an alteration in the orientation of biotin in this mutant. This could occur if we consider that Y621 not only positions biotin in a specific location in the CT domain active site, but most likely orients it in a specific plane for optimal interaction between the aromatic ring of Y621 and the thiophene ring of biotin. This orientation of biotin may influence interactions with tryptophans either inside the CT domain active site or Trp808, located near the exo-binding site. However, if the interactions between biotin and tryptophans in QNY *Sa*PC remain similar and changes in the observed fluorescence signal were due to changes in carrier domain positioning, the data will be interpreted in the following paragraphs in a similar manner to the other *Sa*PC mutations.

To interpret this data in a similar manner as the other mutations, a subtle distinction needs to be made between the CT domain active site and exo-binding site. Whereas the T876A mutation did not have a significant impact on carrier domain positioning in the absence of ligands, the Y621A mutation was observed to, with a large decrease in amplitude change compared to the QN *Sa*PC background (Figure IV-1). Generally, an increase in amplitude has been interpreted as a shift towards the BC

domain while a decrease in amplitude has been interpreted as a shift towards an intermolecular interaction for crosslinking. More precisely, the conformation trapped due to crosslinking was chosen to be the conformation in which biotin is positioned in the exo-binding site. Thus, I propose that the mutation of Y621A resulted in a large shift in carrier domain positioning away from the CT domain active site. This shift would lead to a higher population of carrier domains occupying to exo-binding site conformation, among potential other conformations, including BCCP-BC interactions. The increased population of the exo-binding site would lead to a higher initial ITF signal intensity. When the crosslinker was introduced, a much smaller magnitude of the amplitude was observed, consistent with a smaller shift in carrier domain equilibrium due to the large initial re-equilibration due to the mutation (Figure IV-2B). The equilibrium may be such that ITF is at or close to a maximum possible value and the introduction of the crosslinker pulls the carrier domain equilibrium away from that maximum, resulting in a decrease in ITF signal intensity during crosslinking (Figure IV-2B).

The QNY mutant was observed to have a higher k_{obs} and a decreased amplitude compared to the QN *Sa*PC background (Figure IV-1).The presence of ADP and phosphonoacetate during crosslinking resulted in a small decrease in k_{obs} in the QNY mutant and a decrease in observed amplitude compared to the QNY mutant in the absence of ligands (Figure IV-3). However, it should be noted that this decrease in observed amplitude actually results in a larger ITF signal intensity, due to the fact that the signal is starting out with a negative amplitude. These concepts can be visualized in the energy landscape diagram shown in Figures VI-5A,B. Figure VI-5A depicts the increase in the free energy of the BCCP-CT interaction as a result of the Y621 mutation, which

results in a carrier domain positioning shift towards the exo-binding site and a reduction in the kinetic barrier for this equilibrium shift.

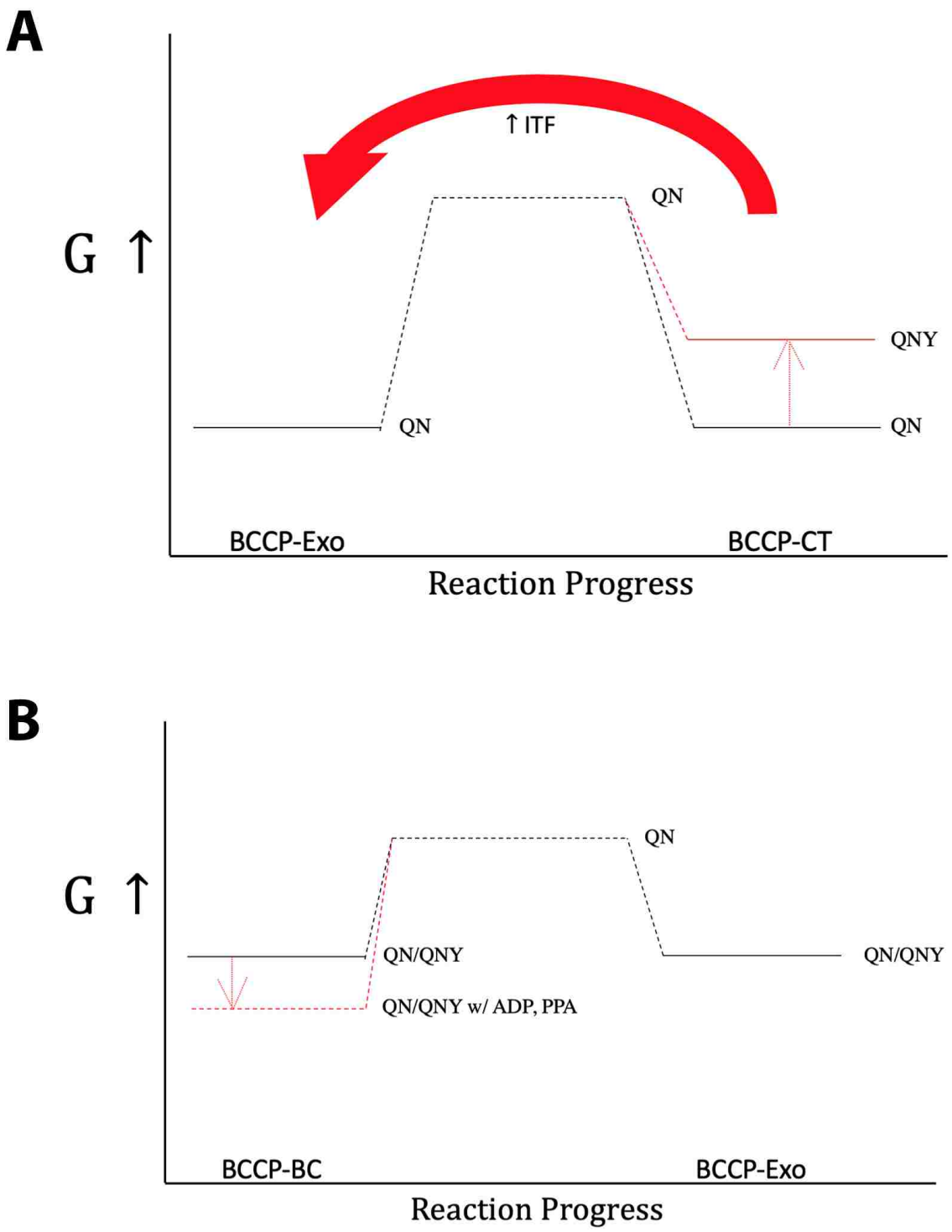

Figure VI-3: Energy landscape diagram for QNY *Sa*PC
A potential energy landscape is shown for the QNY *Sa*PC mutant. The Gibbs free energy (G) is plotted against the translocation progress of BCCP between the BC and CT domains. The kinetic barrier is represented by a dashed black line. The wild-type reaction is represented in black while the mutation is represented in red. **A.** The BCCP-Exo and BCCP-CT interactions are shown. **B.** The BCCP-BC and BCCP-Exo interactions are shown. The effect of the presence of ADP and phosphonoacetate (PPA) in the QN mutant on this landscape is shown in red.

Figure VI-3B illustrates the energy landscape between the BCCP-BC and BCCP-Exo interactions. The addition of ADP and phosphonoacetate results in a reduction in the free energy of the BCCP-BC interaction. This would result in a shift in carrier domain positioning towards the BC domain, increasing the fluorescence intensity observed in QNY *Sa*PC compared to that in the absence of ligands in the QNY *Sa*PC mutant. A smaller change in k_{obs} in the presence of these ligands compared to QN background could result from a simpler translocation pathway. The kinetic barrier to crosslinking in the exo-binding site may be decreased due to the proposed instability of positioning at the CT domain active site. If the carrier domain does not interact with the CT domain active site while translocating from the BC domain to the exo-binding site, there is one less kinetic barrier to overcome to adopt the final crosslinking conformation.

An alternate interpretation of the energy landscape is possible with the Y621A mutation resulting in an increase in the BCCP-BC interaction free energy. As observed, this would lower the kinetic barrier for the adoption of an intermolecular conformation, resulting in a higher k_{obs} in the Y621A mutant (Figure IV-1A). This would also shift carrier domain positioning towards the CT domain and/or exo-binding site, resulting in a decrease in observed amplitude when crosslinking in the absence of ligands (Figure IV-1B). The presence of ADP and phosphonoacetate results in a small decrease in the free energy of the BCCP-BC interaction as illustrated in Figure VI-4 and observed by an increase in absolute ITF signal in Figure IV-5B.

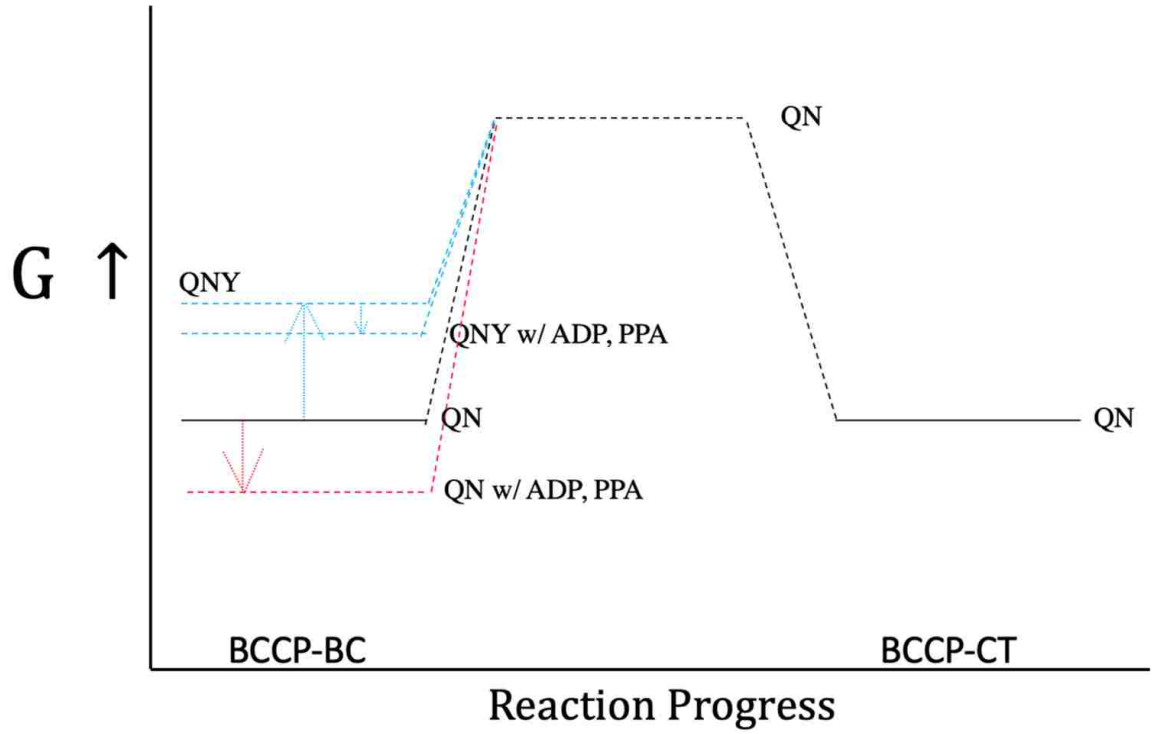

Figure VI-4: Alternate energy landscape diagram for QNY *Sa*PC
A potential alternate energy landscape is shown for the QNY *Sa*PC mutant. The Gibbs free energy (G) is plotted against the translocation progress of BCCP between the BC and CT domains. The kinetic barrier is represented by a dashed black line. The wild-type reaction is represented in black while the mutation is represented in blue. The effect of the presence of ADP and phosphonoacetate (PPA) in the QN mutant on this landscape is shown in red while in the QNY mutant it is shown in blue.

Experimentally testing these energy landscape models. The experiments conducted in this study inform on the relative difference in free energies between the interactions. Thus, the limitation in this approach is that absolute energies of the interactions are unable to be measured. Further, the relative height of the kinetic barrier moving from the BC domain to the CT domain is measured but the height of the kinetic barrier moving towards the BC domain isn't measured by this system. These limitations are due to the conformation crosslinked, with the carrier domain positioned in the vicinity of the CT domain. Carrier domains traveling from a position away from the CT domain, such as those interacting with the BC domain must overcome the kinetic barrier to

interact with the CT domain. In order to measure the relative height of the kinetic barrier on the right side of these depictions, a system must be designed that crosslinks the carrier domain when interacting with the BC domain. ITF experiments and analysis similar to that presented in Chapters IV and V would be performed to obtain a thermodynamic and kinetic analysis of the effect of mutations and the presence of ligands on the carrier domain energy landscape. I predict that the ITF signal intensity would decrease in many cases when crosslinking to the BC domain, since carrier domain positioning would be drawn away from the tryptophans in the vicinity of the CT domain.

To further explore the relationship between the observed tryptophan fluorescence signal as it relates to carrier domain positioning in Y621A *Sa*PC, solution FRET could be utilized as a way to sidestep any change in interactions between biotin and the CT domain tryptophans compared to the QN background that may cause the signal to be untrustworthy. With a FRET-compatible fluorophore introduced onto the carrier domain and a matching FRET-compatible fluorophore placed in the CT domain, whether through maleimide-based reactions or using non-natural amino acids and click chemistry, an analysis of carrier domain positioning should be possible. Instead of receiving a high tryptophan fluorescence signal upon crosslinking of the carrier domain or a shift in positioning towards the CT domain, a higher FRET signal should be observed. A similar analysis to that presented in these studies should be possible to reveal the effect of this mutation on carrier domain positioning.

To distinguish whether a change in the free energy of interaction is occurring in the BC or CT domain, dynamic light scattering could be used to measure thermodynamic parameters of interacting proteins (Hanlon, et al., 2010). This technique has been used in

other systems to study protein-protein interactions. However, given that the PC tetramer stays intact during the translocation process and that this technique is generally used more to study entire proteins during association and dissociation, a different technique may be better suited to study this phenomenon. A technique that may be able to more directly investigate these free energies of domain interactions is isothermal calorimetry. This technique can measure the entropic and enthalpic contributions to the affinity between two proteins and is likely the most applicable technique for directly investigating alterations in the affinity between the carrier domain and BC or CT domains (Valazquez-Campoy, et al., 2015). A number of controls must be investigated given the multitude of interactions that exist in PC. For example, the protein with the carrier domain truncated would serve as an important control to be able to account for any measured energy changes due to ligand binding and small active-site conformational changes from the free energy change of a carrier domain associating and dissociating with another domain. Finally, microscale thermophoresis may offer an alternative technique to measure these thermodynamic parameters. This technique follows changes in either intrinsic fluorescence or signal changes due to the interaction of fluorophores across a range of temperatures to allow the deduction of a number of thermodynamic quantities that would ultimately allow the measurement of changes in Gibbs free energies of interacting proteins (Jerabek-Willemsen, et al., 2014).

2. Extending the Model to Other Multi-Domain Enzymes

The carrier domain of *S. aureus* PC was observed here to be governed by conformational selection with the equilibrium positioning shifted by the presence/absence

of ligands that alter interactions between BCCP-biotin and active-site residues. These findings are consistent with the conformational flexibility observed in *S. cerevisiae* acetyl-CoA carboxylase (Hunkeler, et al., 2016). While carrier domain conformational changes haven't been investigated in acetyl-CoA carboxylase to date, a large, non-catalytic central domain (CD) has been shown to exhibit great conformational flexibility that allows two distant BC domains to come together and dimerize, forming a catalytically-active conformation. A regulatory loop controls these conformational dynamics, when phosphorylated, restricting the conformational flexibility in the CD and preventing the BC domain dimerization necessary for catalysis. This is similar to the role of acetyl-CoA in PC, where it has been observed to limit conformational flexibility of the carrier domain (Westerhold, et al., 2017; Liu, et al., 2018). In the case of acetyl-CoA, however, this confinement of conformational dynamics results in more efficient catalysis, not the inability to form a catalytically-relevant conformation as is the case with phosphorylation of the regulatory loop in acetyl-CoA carboxylase. Given the lack of studies on carrier domain positioning in acetyl-CoA carboxylase, it seems reasonable to expect its positioning to be governed by conformational selection, similar to PC. One potential mechanism to favor/disfavor carrier domain positioning was recently discovered. As introduced in Section I.3.1, a loop that sterically blocks carrier domain binding is shifted out of the way when the BC domain dimerizes (Wei and Tong, 2015). Future crystal structures with the carrier domain interacting with either active site would aid in further determining how the positioning of the carrier domain of acetyl-CoA carboxylase is regulated.

The assembly line polyketide synthase, 6-deoxyerythronolide B synthase (DEBS), is a composition of three polypeptides that in total contain six homologous, homodimeric modules that catalyze the production of the macrocyclic core of erythromycin. As described in the Introduction, this multi-domain enzyme uses an acyl-carrier protein to shuttle the growing polyketide chain from the intramodular ketosynthase (KS) domain to the downstream KS domain. A recent study has investigated how vectorial synthesis may be coordinated to maintain proper reaction directionality during chain elongation (Lowry, et al., 2016). A novel turnstile mechanism was discovered that prevents the KS domain from premature acylation until the previous elongation and modification reactions product have been removed from the intramolecular ACP domain. This model appears consistent with conformational selection as well, with catalytic steps energetically coupled without relying on a complex induced conformational change mechanism. This energetic coupling of reaction steps is also similar to an observation made in *Sa*PC in which the two half-reactions are thermodynamically coupled in the presence of the allosteric activator, acetyl-CoA (Westerhold, et al., 2017). Both of these mechanisms rely on regulation of translocation of the carrier domain to efficiently couple the multi-step reactions. In the case of PC, acetyl-CoA was observed to favor translocation of the carrier domain (Figure V-8) with the effects of mutation to several active-site residues on carrier domain translocation discussed above.

The bacterial sulfur oxidation pathway enzyme SoxB interacts with the carrier protein SoxYZ, which carries Sox pathway intermediates. A recent study investigated the interaction between these two proteins to better understand how carrier proteins transport intermediates between enzymes in the Sox pathway (Grabarczyk, et al., 2015). It was

observed that the carrier protein has 2 major points of interaction with the SoxB enzyme. One point of contact is in the active site tunnel with multiple points of hydrogen bonding between the carrier protein and SoxB. More tangential to my research is the formation of a second point of contact outside of the active size. A mobile loop on the surface of SoxB was observed to be stabilized when substrate-bound SoxYZ bound with SoxB. In the substrate-free form, this mobile loop occupies a different conformation that clashes with SoxYZ binding, favoring the release of SoxYZ after the reaction has completed. This mechanism is similar to the CT domain mechanism of stabilizing biotin in the active-site of PC in that when substrate is bound in the CT domain, Tyr621 adopts a conformation favorable for carrier domain positioning at the CT domain active site.

Finally, gramicidin synthase I, a non-ribosomal peptide synthase, was recently investigated to study the control of interactions between the catalytic and carrier domains (Alfermann, et al., 2017). It was observed that this flexible enzyme exists in an equilibrium of at least two conformations, with product inhibition, and in general the presence of ligands, shifting the conformational equilibrium. A series of interactions between active site residues, carrier domain residues and prosthetic groups, and ligands were proposed to be responsible for these equilibrium shifts. These findings are consistent with the work presented here regarding how the positioning of the carrier domain of pyruvate carboxylase is governed. The authors have come to a very similar conclusion in that the enzyme exists in a conformational equilibrium that is shifted by the presence of ligands.

In summary, our understanding of how carrier domain positioning is regulated has progressed dramatically in recent years. Mechanisms have been discovered in several

enzyme systems that have revealed various types of interactions between carrier domains and catalytic domains, pushing forward our understanding of the underlying biophysical nature of how carrier domain translocation is governed for efficient catalysis. The studies that I have performed in PC offer further evidence of conformational selection governing carrier domain positioning and translocation while offering to further extend our understanding of how interactions between active site residues and the prosthetic group of carrier domains can shift equilibrium positioning.

VII. FUTURE DIRECTIONS

To explore trapping the carrier domain during translocation in a cleaner system, the single mutant Q1118C needs to be investigated in the same manner as presented here. A double mutant that would trap the carrier domain in the conformation in which biotin extends into the active site, which was the goal of the D907C/Q1118C *Sa*PC mutant, should also be generated and investigated. These two systems would allow a higher confidence of interpretation of not only the data regarding carrier domain translocation in Chapter V, but also offer a comparison to the data presented in Chapter III and IV. For instance, if carrier domain positioning if observed to have shifted towards the BC domain, is it shifting away from every other state/conformation equally? Trapping the carrier domain in more states would allow this more thorough explanation of carrier domain dynamics. Throughout this current work, the positioning of the carrier domain at the BC domain has been presumed when carrier domain positioning is shifted away from the intermolecular CT domain in the presence of BC domain ligands. While this is a reasonable assumption, this study would be further supported by the ability to trap the carrier domain at the BC domain to more completely assess shifts in carrier domain positioning. Similar to the crosslinking system introduced in this study, a pair of cysteines would need to be introduced that would come within crosslinking range (<8 Å) when the carrier domain is docked at the BC domain for the generation of this new crosslinking system.

As Liu, et al. demonstrated, the carrier domain can interact with both the intramolecular and intermolecular BC domains (Liu, et al., 2018). This presents a problem in that assaying crosslinking by SDS-PAGE would only report on intermolecular

crosslinking and be blind to intramolecular crosslinking. Thus, inactivation kinetics, which measures the inactivation of the enzyme due to carrier domain crosslinking in either form, would be more appropriate to use when assessing the total amount of crosslinking. Alternatively, a co-expression of two different mutants would allow a fuller assessment of only intermolecular crosslinking. One mutant would have a cysteine introduced onto the BC domain while the other mutant would have a cysteine introduced onto the carrier domain. This population would form a hybrid tetramer *in vivo* during co-expression (Liu, et al., 2018). Thus, the carrier domain on one polypeptide chain would only be able to form crosslinks with the BC domain cysteine on a separate polypeptide chain, trapping the intermolecular interaction. For either the system assessing both intramolecular and intermolecular crosslinking or just intermolecular crosslinking, the techniques described in this study would be applied to assess kinetic and thermodynamic changes to carrier domain positioning as a result of mutations or the presence of ligands.

The use of solution FRET, as used to investigate conformational shifts in an NRPS as described in the introduction, could be implemented in *Sa*PC to study shifts in carrier domain positioning due to mutations or the presence of ligands without the need for crosslinking (Alfermann, et al., 2017). FRET-compatible fluorophores could be covalently attached to the carrier domain and either the BC domain or CT domain for an introductory set of studies. These fluorophores could be bound through the introduction of cysteines in the desired locations for maleimide-based linking or through the use of non-natural amino acids in the desired location and click chemistry-based fluorophore linking. Given that 5 cysteines exist naturally in *Sa*PC, the use of non-natural amino acids

for fluorophore labeling would most likely yield the greatest chance of success as undesired background labeling of the enzyme should be limited.

A crystal structure of Q891C/N1102C *Sa*PC with the carrier domain crosslinked would allow an analysis of the positioning of biotin in relation to the tryptophans located in the CT domain. The attainment of such a crystal structure would be a possible next step in determining the origin of changes in the observed tryptophan fluorescence signals with the goal of better understanding the exact positioning of the carrier domain in relation to the observed signal. Alternatively, these tryptophans could be individually conservatively mutated to phenylalanines or histidines to determine their contributions to the observed fluorescence signal. However, 2 of the 4 remaining tryptophans to be studied are strictly conserved, which suggests that their mutation could result in an unstable protein. The tryptophan mutated as part of the studies described in Chapter III is also strictly conserved with mutation of that tryptophan resulted in an unstable protein. In summary, I believe the obtainment of a crystal structure of crosslinked *Sa*PC would be the logical next step for the determination of the origin of the tryptophan fluorescence signal.

Finally, carrier domain movement could be investigated to determine the effects of ligands, including acetyl-CoA and L-aspartate, on carrier domain movement rates. For example, in chapter III, L-aspartate wasn't observed to alter carrier domain positioning but exhibited an effect on the kinetic barrier to translocation. Perhaps the movement rate of the carrier domain is slowed by L-aspartate, resulting in a reduction in catalytic rate. Carrier domain movement could be determined either through single-molecule FRET studies, fluorescence anisotropy, or RFQ-DEER (rapid freeze quench-double electron-

electron resonance). While our lab does not currently have direct experience with these techniques, they would represent a new frontier of research for not only the lab, but studies of carrier domain motion in carrier domain enzyme systems. Initial studies of carrier domain movement have been investigated with fluorescence anisotropy in collaboration with Dr. Evgueni Kovriguine. However, it was determined that either a much higher percentage of fluorophore labeling of *Sa*PC was required or a much higher concentration of protein was necessary, as the obtained fluorescence signals were inconclusive. Thus, for many of the research pathways described here, an optimization of the specific labeling of PC with various fluorophores is necessary to expand our investigations of carrier domain positioning and movement.

BIBLIOGRAPHY

Adina-Zada A, Jitrapakdee S, Attwood PV. (2019) “Characterization of the kinetics and activation thermodynamics of intra- and inter-organism hybrid tetramers of pyruvate carboxylase.” *Arch Biochem Biophys.* 665:87-95.

Alfermann, J., Sun, X., Mayerthaler, F., Morrell, T. E., Dehling, E., Volkmann, G., Komatsuzaki, T., Yang, H., and Mootz, H. D. (2017) “FRET monitoring of a nonribosomal peptide synthetase.” *Nat. Chem. Biol.* 13, 1009-1015

Athappilly FK, Hendrickson WA. **(**1995**) “**Structure of the biotinyl domain of acetyl-coenzyme A carboxylase determined by MAD phasing. *Structure* 3:1407–19

Attwood PV, Geeves MA. (2002) “Changes in catalytic activity and association state of pyruvate carboxylase which are dependent on enzyme concentration.” *Arch Biochem Biophys.* 401(1):63-72.

Attwood PV, Graneri BD. (1992) “Bicarbonate-dependent ATP cleavage catalysed by pyruvate carboxylase in the absence of pyruvate.” *Biochem J.* 287 (Pt 3):1011-7.

Attwood PV, Mayer F, Wallace JC. (1986) “Avidin as a probe of the conformational changes induced in pyruvate carboxylase by acetyl-CoA and pyruvate.” *FEBS Lett.* 203(2):191-6.

Attwood, P. V. (1995) "The structure and the mechanism of action of pyruvate carboxylase." *The international journal of biochemistry & cell biology* 27 (3):231-249.

Attwood, P. V., and J. C. Wallace. (1986) "The carboxybiotin complex of chicken liver pyruvate carboxylase. A kinetic analysis of the effects of acetyl-CoA, Mg2+ ions and temperature on its stability and on its reaction with 2-oxobutyrate." *The Biochemical journal* 235 (2):359-364.

Attwood, P. V., J. H. Coates, and J. C. Wallace. (1984) "Interaction of formycin A-5'-triphosphate with pyruvate carboxylase." *FEBS letters* 175 (1):45-50.

Attwood, P. V., W. Johannssen, A. Chapman-Smith, and J. C. Wallace. (1993) "The existence of multiple tetrameric conformers of chicken liver pyruvate carboxylase

and their roles in dilution inactivation." *The Biochemical journal* 290 (Pt 2) (Pt 2):583-590.

Belshaw, P.J., Walsh, C.T. & Stachelhaus, T. (1999) "Aminoacyl-CoAs as probes of condensation domain selectivity in nonribosomal peptide synthesis." *Science* 284, 486–489

Bennett Jr., WS, Steitz, TA. (1978) "Glucose-induced conformational change in yeast hexokinase." *Proc Natl Acad Sci USA*. 75(10): 4848–4852.

Berg JM, Tymoczko JL, Stryer L. Biochemistry. 5th edition. New York: W H Freeman; 2002. Section 8.4, The Michaelis-Menten Model Accounts for the Kinetic Properties of Many Enzymes. Available from: https://www.ncbi.nlm.nih.gov/books/NBK22430/

Bertrand D, Devillers-Thiéry A, Revah F, Galzi JL, Hussy N, Mulle C, Bertrand S, Ballivet M, Changeux J-P: (1992) "Unconventional pharmacology of a neuronal nicotinic receptor mutated in the channel domain." *Proc Natl Acad Sci U S A* 89:1261-5.

Boehr, D. D., Nussinov, R., and Wright, P. E. (2009) "The role of dynamic conformational ensembles in biomolecular recognition." *Nat Chem Biol* 5, 789-796

Broussard, T. C., Pakhomova, S., Neau, D. B., Bonnot, R., & Waldrop, G. L. (2015) "Structural analysis of substrate, reaction intermediate, and product binding in Haemophilus influenzae biotin carboxylase." *The Biochemist* 54, 3860–3870.

Cazzulo, J. J., and Stoppani, A. O. (1968) "The regulation of yeast pyruvate carboxylase by acetyl-coenzyme A and L-aspartate." *Arch. Biochem. Biophys.* 127, 563-567

Changeux J-P, Rubin MM. (1968) "Allosteric interactions in aspartate transcarbamylase. III. Interpretations of experimental data in terms of the model of Monod, Wyman, and Changeux. *Biochemistry*. 7:553-61.

Changeux JP, Gerhart JC, Schachman HK. (1968) "Allosteric interactions in aspartate transcarbamylase. I. Binding of specific ligands to the native enzyme and its isolated subunits." *Biochemistry* 7:531-8.

Choe HW, Park JH, Kim YJ, Ernst OP. (2011) “Transmembrane signaling by GPCRs: insight from rhodopsin and opsin structures.” *Neuropharmacology* 60:52-7.

Chou, C. Y., L. P. Yu, and L. Tong. (2009) "Crystal structure of biotin carboxylase in complex with substrates and implications for its catalytic mechanism." *The Journal of biological chemistry* 284 (17):11690-11697. doi: 10.1074/jbc.M805783200

Colquhoun D, Sakmann B. (1985) “Fast events in single-channel currents activated by acetylcholine and its analogues at the frog muscle end-plate.” *J Physiol* 369:501-57.

Conti E, Stachelhaus T, Marahiel MA, Brick P. (1997) “Structural basis for the activation of phenylalanine in the non-ribosomal biosynthesis of gramicidin S.” *EMBO J.* 16(14):4174-83.

Corbett, P.T.; Tong, L.H.; Sanders, J.K.; Otto, S. (2005) “Diastereoselective amplification of an induced-fit receptor from a dynamic combinatorial library.” *J. Am. Chem. Soc.* 127, 8902–8903.

Cronan, J. E., Jr., & Waldrop, G. L. (2002) “Multi-subunit acetyl-CoA carboxylases.” *Progress in Lipid Research*. 41, 407–435.

Diamandis EP, Christopoulos TK. (1991) “The biotin-(strept)avidin system: principles and applications in biotechnology.” *Clin Chem.* 37(5):625-36.

Dimroth P, Hilbi H. (1997) “Enzymic and genetic basis for bacterial growth on malonate.” *Mol Microbiol.* 25(1):3-10.

Duval M, DeRose RT, Job C. Faucher D, Douce R, Job D. **(**1994**) “**The major biotinyl protein from Pisum sativum seeds covalently binds biotin at a novel site.**”** *Plant Mol. Biol.* 26:265–73

Easterbrook-Smith, S. B., Hudson, P. J., Goss, N. H., Keech, D. B., and Wallace, J. C. (1976) “Pyruvate carboxylase: mechanism on the second partial reaction.” *Arch. Biochem. Biophys.* 176, 709-720

Finzel K, Nguyen C, Jackson DR, Gupta A, Tsai SC, Burkart MD. (2015) “Probing the Substrate Specificity and Protein-Protein Interactions of the E. coli Fatty Acid Dehydratase, FabA.” *Chem Biol.* 22(11):1453-1460.

Fischer, E. (1894) “Einfluβ der Konfiguration auf die Wirkung der Enzyme” *Ber. Ges. Dtsch. Chem.*, 27, p. 2985

Geeves MA, Branson JP, Attwood PV. (1995) “Kinetics of nucleotide binding to pyruvate carboxylase.” *Biochemistry.* 34(37):11846-54.

Gerich, J., Woerle, H.J., Meyer, C., Stumvoll, M. 2001. “Renal Gluconeogenesis.” *Diabetes Care*. 24: 382-391.

Goodall, G. J., Baldwin, G. S., Wallace, J. C., and Keech, D. B. (1981) “Factors that influence the translocation of the N-carboxybiotin moiety between the two sub-sites of pyruvate carboxylase.” *Biochem. J*. 199, 603-609

Grabarczyk, D. B., Chappell, P. E., Johnson, S., Stelzl, L. S., Lea, S. M., and Berks, B. (2015) “Structural basis for specificity and promiscuity in a carrier protein/enzyme system from the sulfur cycle.” *Proc. Natl. Acad. Sci.* U.S.A. 112, E7166-E7175.

Greives N, Zhou HX. (2014) “Both protein dynamics and ligand concentration can shift the binding mechanism between conformational selection and induced fit.” Proc Natl Acad Sci USA. 111(28):10197-202.

Gulick AM. (2009) “Conformational dynamics in the Acyl-CoA synthetases, adenylation domains of non-ribosomal peptide synthetases, and firefly luciferase.” *ACS Chem Biol.* 4(10):811-27.

Hammes GG, Chang YC, Oas TG. (2009) “Conformational selection or induced fit: a flux description of reaction mechanism.” *Proc Natl Acad Sci USA*. 106 (33):13737-41.

Han, J, Liu, YQ. (2010) “Reduction of islet pyruvate carboxylase activity might be related to the development of type 2 diabetes mellitus in Agouti-K mice.” *J Endocrinol.* 204(2):143-52

Hanlon AD, Larkin MI, Reddick RM. (2010) “Free-solution, label-free protein-protein interactions characterized by dynamic light scattering.” *Biophys J*. 98 (2): 297-304.

Hunkeler, M., Stuttfeld, E., Hagmann, A., Imseng, S., & Maier, T. (2016). “The dynamic organization of fungal acetyl-CoA carboxylase.” *Nature Communications* 7, 11196.

Jackson MB. (1984) “Spontaneous openings of the acetylcholine receptor channel.” *Proc Natl Acad Sci U S A* 81:3901-4.

Jerabek-Willemsen, M., André, T., Wanner, R., Roth, H.M., Duhr, S., Baaske, P., Breitsprecher, D. (2014). “Microscale thermophoresis: interaction analysis and beyond.” Jour. Of Molec. Struc. 1077: 101-113.

Jiang J, Baiesc FL, Hiromasa Y, Yu X, Hui WH, Dai X, Roche TE, Zhou ZH. (2018) “Atomic Structure of the E2 Inner Core of Human Pyruvate Dehydrogenase Complex.” *Biochemistry.* 57(16):2325-2334.

Jitrapakdee, S., Adina-Zada, A., Besant, P. G., Surinya, K. H., Cleland, W. W., Wallace, J. C., and Attwood, P. V. (2007) “Differential regulation of the yeast isozymes of pyruvate carboxylase and the locus of action of acetyl CoA.” *Int. J. Biochem. Cell Biol.* 39, 1211-1223

Jitrapakdee, S., M. E. Walker, and J. C. Wallace. (1999) "Functional expression, purification, and characterization of recombinant human pyruvate carboxylase." *Biochemical and biophysical research communications* 266 (2):512-517. doi: 10.1006/bbrc.1999.1846.

Jitrapakdee, S., M. St Maurice, I. Rayment, W. W. Cleland, J. C. Wallace, and P. V. Attwood. (2008) "Structure, mechanism and regulation of pyruvate carboxylase." *The Biochemical Journal* 413 (3):369-387. doi: 10.1042/BJ20080709.

Kato, M, Wynn, RM, Chuang, JL, Brautigam, CA, Custorio, M, Chuang, DT. (2006) “A synchronized substrate-gating mechanism revealed by cubic-core structure of the bovine branched chain α-ketoacid dehydrogenase complex.” *EMBO J.* 25(24): 5983–5994.

Keech DB, Utter MF. (1963) “Pyruvate carboxylase II. Properties.” *J Biol Chem.* 238:2609-14.

Khew-Goodall YS, Johannssen W, Attwood PV, Wallace JC, Keech DB. (1991) “Studies on dilution inactivation of sheep liver pyruvate carboxylase.” *Arch Biochem Biophys.* 284(1):98-105.

Khosla, C., Herschlag, D., Cane, D. E., and Walsh, C. T. (2014) “Assembly Line Polyketide Synthases: Mechanistic Insights and Unsolved Problems.” *Biochemistry* 53, 2875-2883

Kondo S, Nakajima Y, Sugio S, Yong-Biao J, Sueda S, Kondo H. (2004) “Structure of the biotin carboxylase subunit of pyruvate carboxylase from Aquifex aeolicus at 2.2 A resolution.” *Acta Crystallogr D Biol Crystallogr.* 486-92.

Koshland, D. E., Jr. (1959) “Enzyme flexibility and enzyme action.” *J Cell Comp Physiol* 54, 245-258

Koshland, D. E., Jr., Nemethy, G., and Filmer, D. (1966) “Comparison of experimental binding data and theoretical models in proteins containing subunits.” *Biochemistry* 5(1), 365-385

Kull, FJ, Endow SA. (2013) “Force generation by kinesin and myosin cytoskeletal motor proteins.” *J Cell Sci.* 126(1): 9–19.

Lasso G, Yu LP, Gil D, Xiang S, Tong L, Valle M. (2010) “Cryo-EM analysis reveals new insights into the mechanism of action of pyruvate carboxylase.” *Structure.* 18(10):1300-10.

Lasso, G., Yu, L. P., Gil, D., Lazaro, M., Tong, L., and Valle, M. (2014) “Functional conformations for pyruvate carboxylase during catalysis explored by cryoelectron microscopy.” *Structure* 22, 911-922

Legge, G. B., J. P. Branson, and P. V. Attwood. (1996) "Effects of acetyl CoA on the pre-steady-state kinetics of the biotin carboxylation reaction of pyruvate carboxylase." *Biochemistry* 35:3849-3856.

Lietzan, A. D., and M. St Maurice. (2013A) "A substrate-induced biotin binding pocket in the carboxyltransferase domain of pyruvate carboxylase." *The Journal of Biological Chemistry* 288 (27):19915-19925. doi: 10.1074/jbc.M113.477828; 10.1074/jbc.M113.477828.

Lietzan, A. D., and M. St Maurice. (2013B) "Insights into the carboxyltransferase reaction of pyruvate carboxylase from the structures of bound product and intermediate analogs." *Biochemical and biophysical research communications* 441 (2):377-382. doi: 10.1016/j.bbrc.2013.10.066 [doi].

Lietzan, A. D., and St. Maurice, M. (2014) “Functionally diverse biotin-dependent enzymes with oxaloacetate decarboxylase activity.” *Arch. Biochem. Biophys.* 544, 75-86

Lietzan, A. D., Menefee, A. L., Zeczycki, T. N., Kumar, S., Attwood, P. V., Wallace, J. C., Cleland, W. W., and St Maurice, M. (2011) “Interaction between the biotin carboxyl carrier domain and the biotin carboxylase domain in pyruvate carboxylase from Rhizobium etli.” *Biochemistry* 50, 9708-9723

Linne, U. & Marahiel, M.A. (2000) “Control of directionality in nonribosomal peptide synthesis: role of the condensation domain in preventing misinitiation and timing of epimerization.” Biochemistry 39, 10439–10447

Liu, Y., M. M. Budelier, K. Stine, and M. St Maurice. (2018) "Allosteric regulation alters carrier domain translocation in pyruvate carboxylase." *Nat Commun* 9 (1):1384. doi: 10.1038/s41467-018-03814-8.

Lowry, B., Li, X., Robbins, T., Cane, D. E., and Khosla, C. (2016) “A Turnstile Mechanism for the Controlled Growth of Biosynthetic Intermediates on Assembly Line Polyketide Synthases.” *ACS Cent. Sci.* 2, 14-20

Marahiel MA, Stachelhaus T, Mootz HD. (1997) “Modular Peptide Synthetases Involved in Nonribosomal Peptide Synthesis” *Chem Rev.* 97(7):2651-2674.

Marin-Valencia I, Roe CR, Pascual JM. (2010) “Pyruvate carboxylase deficiency: mechanisms, mimics and anaplerosis.” *Mol Genet Metab.* 101(1):9-17

Menefee, A. L., and Zeczycki, T. N. (2014) “Nearly 50 years in the making: defining the catalytic mechanism of the multifunctional enzyme pyruvate carboxylase.” *FEBS J.* 281, 1333-1354

Monod, J., Wyman, J., and Changeux, J. P. (1965) “On the Nature of Allosteric Transitions: A Plausible Model.” *J Mol Biol* 12, 88-118

Mootz, H.D. & Marahiel, M.A. (1997) “Biosynthetic systems for nonribosomal peptide antibiotic assembly.” Curr. Opin. Chem. Biol. 1, 543–551

Ogita, T., and J. R. Knowles. (1988) "On the intermediacy of carboxyphosphate in biotin-dependent carboxylations." *Biochemistry* 27 (21):8028-33.

Osmani, S. A., Marston, F. A., Selmes, I. P., Chapman, A. G., and Scrutton, M. C. (1981) "Pyruvate carboxylase from Aspergillus nidulans regulatory properties." *Eur. J. Biochem.* 118, 271-278

Patel, MS, Nemeria, NS, Furey, W, Jordan F. (2014) "The pyruvate dehydrogenase complexes: structure based function and regulation." *J Biol Chem.* 289(24): 16615–16623.

Perham, R. N. (2000) "Swinging arms and swinging domains in multifunctional enzymes: catalytic machines for multistep reactions." *Annu. Rev. Biochem.* 69, 961-1004

Perutz, M. F., M. G. Rossmann, A. F. Cullis, H. Muirhead, G. Will, and A. C. North. 1960. "Structure of haemoglobin: a three-dimensional Fourier synthesis at 5.5-A. resolution, obtained by X-ray analysis." *Nature* 185 (4711):416-22.

Phannasil P, Thuwajit C, Warnnissorn M, Wallace JC, MacDonald MJ, Jitrapakdee S. (2015) Pyruvate Carboxylase Is Up-Regulated in Breast Cancer and Essential to Support Growth and Invasion of MDA-MB-231 Cells. *PLoS One.* 10(6):e0129848. doi: 10.1371/journal.pone.0129848. eCollection 2015.

Prajapati, S, Haselbach, D, Wittig, S, Patel, MS, Chari, A, Schmidt, C, Stark, H, Tittmann, K. (2019) "Structural and functional analyses of the human PDH complex suggest a "Division of Labor" mechanism by local E1 and E3 clusters." *Structure*. 27(7): 1124-1136.

Robbins T, Liu YC, Cane DE, Khosla C. (2016) Structure and mechanism of assembly line polyketide synthases. *Curr Opin Struct Biol.* 41:10-18.

Rother D, Henrich HJ, Quentmeier A, Bardischewsky F, Friedrich CG (2001) "Novel genes of the sox gene cluster, mutagenesis of the flavoprotein SoxF, and evidence for a general sulfur-oxidizing system in Paracoccus pantotrophus GB17." *J Bacteriol* 183(15):4499–4508.

Samols D, Thornton CG, Murtif VL, Kumar GK, Haase FC, Wood HG. (1988) "Evolutionary conservation among biotin enzymes." *J. Biol. Chem.* 263:6461–64

Schär J, Stoll R, Schauer K, Loeffler DI, Eylert E, Joseph B, Eisenreich W, Fuchs TM, Goebel W. (2010) "Pyruvate carboxylase plays a crucial role in carbon metabolism of extra- and intracellularly replicating Listeria monocytogenes." *J Bacteriol.* 192(7):1774-84.

Scrutton MC, Keech DB, Utter MF. (1965) "Pyruvate carboxylase IV. Partial reactions and the locus of activation by acetyl coenzyme A." *J biol chem.* 240:574-81.

Shen, Y., Volrath, S. L., Weatherly, S. C., Elich, T. D., & Tong, L. (2004). "A mechanism for the potent inhibition of eukaryotic acetyl-coenzyme A carboxylase by soraphen A, a macrocyclic polyketide natural product." *Molecular Cell* 16, 881–891.

Sheng, X., Liu, Y. (2014) "QM/MM study of the reaction mechanism of the carboxyl transferase from *Staphylococcus aureus*." *Biochemistry*. 15;53 (27), 4455-66.

Sirithanakorn, C., Adina-Zada, A., Wallace, J. C., Jitrapakdee, S., and Attwood, P. V. (2014) "Mechanisms of inhibition of Rhizobium etli pyruvate carboxylase by L-aspartate*." Biochemistry* 53, 7100-7106

Sirithanakorn, C., S. Jitrapakdee, and P. V. Attwood. (2016) "Investigation of the Roles of Allosteric Domain Arginine, Aspartate, and Glutamate Residues of Rhizobium etli Pyruvate Carboxylase in Relation to Its Activation by Acetyl CoA." *Biochemistry* 55 (30):4220-4228. doi: 10.1021/acs.biochem.6b00548 [doi].

St Maurice, M., L. Reinhardt, K. H. Surinya, P. V. Attwood, J. C. Wallace, W. W. Cleland, and I. Rayment. (2007). "Domain architecture of pyruvate carboxylase, a biotin-dependent multifunctional enzyme." *Science* 317 (5841):1076-1079. doi: 10.1126/science.1144504.

Thoden, J. B., C. Z. Blanchard, H. M. Holden, and G. L. Waldrop. (2000). "Movement of the biotin carboxylase B-domain as a result of ATP binding." *The Journal of Biological Chemistry* 275 (21):16183-16190.

Tong, L. (2013) Structure and function of biotin-dependent carboxylases. *Cell. Mol. Life Sci.* 70, 863-891

Tong, L. (2017) "Striking Diversity in Holoenzyme Architecture and Extensive Conformational Variability in Biotin-Dependent Carboxylases." *Advances in*

protein chemistry and structural biology 109:161-194. doi: S1876-1623(17)30037-8 [pii].

Utter MF, Keech DB. (1963) “Pyruvate carboxylase I. Nature of the reaction.” *J Biol Chem.* 238:2603-8.

Utter, M. F., and D. B. Keech. (1960) "Formation of oxaloacetate from pyruvate and carbon dioxide." *The Journal of biological chemistry* 235:PC17-PC18.

Velazquez-Campoy A, Leavitt SA, Freire E. (2015) “Characterization of protein-protein interactions by isothermal titration calorimetry. Methods Mol Biol. 2015;1278:183-204.

Velyvis A, Yang YR, Schachman HK, Kay LE. (2007) “A solution NMR study showing that active site ligands and nucleotides directly perturb the allosteric equilibrium in aspartate transcarbamoylase.” *Proc Natl Acad Sci.* 104:8815-20.

Vogt, AD, Pozzi, N, Chen ,Z, Di Cera, E. (2014) “Essential role of conformational selection in ligand binding.” *Biophys Chem.* 0: 13–21. doi:10.1016/j.bpc.2013.09.003.

Waelbroeck, M. (2007) “An Alternative Presentation of Metabolism: Enzyme-catalyzed reactions can be viewed as atoms flowing through sluice gates” *Biochemistry and Molecular Biology Education* 35 (4): 233–237.

Waldrop, G. L., Holden, H. M., & St. Maurice, M. (2012) “The enzymes of biotin dependent CO2 metabolism: What structures reveal about their reaction mechanisms.” *Protein Science* 21, 1597–1619.

Waldrop, G. L., Rayment, I., & Holden, H. M. (1994). “Three-dimensional structure of the biotin carboxylase subunit of acetyl-CoA carboxylase.” *The Biochemist* 33, 10249–10256.

Wallace, JC, Jitrapakdee, S, Chapman-Smith, A. (1998) “Pyruvate carboxylase.” *The International Journal of Biochemistry and Cell Biology*. 30: 1-5

Wei, J., and L. Tong. (2015) "Crystal structure of the 500-kDa yeast acetyl-CoA carboxylase holoenzyme dimer." *Nature* 526 (7575):723-7. doi: 10.1038/nature15375.

Westerhold, L. E., Adams, S. L., Bergman, H. L., and Zeczycki, T. N. (2016) “Pyruvate Occupancy in the carboxyl transferase domain of pyruvate carboxylase facilitates product release from the biotin carboxylase domain through an intermolecular mechanism.” *Biochemistry* 55, 3447-3460

Westerhold, L. E., L. C. Bridges, S. R. Shaikh, and T. N. Zeczycki. (2017) "Kinetic and Thermodynamic Analysis of Acetyl-CoA Activation of Staphylococcus aureus Pyruvate Carboxylase." *Biochemistry* 56 (27):3492-3506. doi: 10.1021/acs.biochem.7b00383 [doi].

Westerhold, L. E., S. L. Adams, H. L. Bergman, and T. N. Zeczycki. 2016. "Pyruvate Occupancy in the Carboxyl Transferase Domain of Pyruvate Carboxylase Facilitates Product Release from the Biotin Carboxylase Domain through an Intermolecular Mechanism." *Biochemistry* 55 (24):3447-3460. doi: 10.1021/acs.biochem.6b00372 [doi].

Wood HG, Allen SH, Stjernholm R, Jacobson B. (1963) “Transcarboxylase III. Purification and properties of methylmalonyl oxaloacetic transcarboxylasecontaining tritiated biotin.” *J Biol Chem.* 238:547-56.

Xiang, S., and L. Tong. (2008) "Crystal structures of human and Staphylococcus aureus pyruvate carboxylase and molecular insights into the carboxyltransfer reaction." *Nature structural & molecular biology* 15 (3):295-302. doi: 10.1038/nsmb.1393.

Xu F, Wu H, Katritch V, Han GW, Jacobson KA, Gao ZG, Cherezov V, Stevens RC (2011) “Structure of an agonist-bound human A2A adenosine receptor.” *Science* 332:322-7.

Yu X, Hiromasa Y, Tsen H, Stoops JK, Roche TE, Zhou ZH. (2008) “Structures of the human pyruvate dehydrogenase complex cores: a highly conserved catalytic center with flexible N-terminal domains.” *Structure.* 16:104–114.

Yu, L. P., C. Y. Chou, P. H. Choi, and L. Tong. (2013) "Characterizing the importance of the biotin carboxylase domain dimer for Staphylococcus aureus pyruvate carboxylase catalysis." *Biochemistry* 52 (3):488-96. doi: 10.1021/bi301294d.

Yu, L. P., Xiang, S., Lasso, G., Gil, D., Valle, M., and Tong, L. (2009) “A symmetrical tetramer for S. aureus pyruvate carboxylase in complex with coenzyme A.” *Structure* 17, 823-832

Zeczycki, T. N., A. L. Menefee, A. Adina-Zada, S. Jitrapakdee, K. H. Surinya, J. C. Wallace, P. V. Attwood, M. St Maurice, and W. W. Cleland. (2011A) "Novel Insights into the Biotin Carboxylase Domain Reactions of Pyruvate Carboxylase from Rhizobium etli." *Biochemistry*. doi: 10.1021/bi2012788.

Zeczycki, T. N., A. L. Menefee, S. Jitrapakdee, J. C. Wallace, P. V. Attwood, M. St. Maurice, and W. W. Cleland. (2011B) "Activation and inhibition of pyruvate carboxylase from Rhizobium etli." *Biochemistry* 50:9694-9707.

Zeczycki, T. N., M. St Maurice, S. Jitrapakdee, J. C. Wallace, P. V. Attwood, and W. W. Cleland. (2009) "Insight into the carboxyl transferase domain mechanism of pyruvate carboxylase from Rhizobium etli." *Biochemistry* 48 (20):4305-4313. doi: 10.1021/bi9003759.

Zeczycki, T. N., M. St. Maurice, and P. V. Attwood. (2010) "Inhibitors of pyruvate carboxylase." *Open Enz. Inhib. J.* 3:8-26.

VIII. APPENDIX A: PRIMERS FOR MUTAGENESIS OF *Sa*PC

Table VIII-1 Forward Primers for *Sa*PC Mutagenesis

Mutation	Sequence
Q891C	5'-GGCACTTTATATGGTATGCAATGATCTTGATGAACAATC-3' (forward) 5'-GATTGTTCATCAAGATCATTGCATACCATATAAAGTGCC-3' (reverse)
N1102C	5'-GTGAAACTGTGAAAGCTTGTCAGCCGTTGCTAATTAC-3' (forward) 5'-GTAATTAGCAACGGCTGACAAGCTTTCACAGTTTCAC-3' (reverse)
D907C	5'-GGCTATAAATTATGTTTCCCAGAATCAG-3' (forward) 5'-CTGATTCTGGGAAACATAATTTATAGCC-3' (reverse)
Q1118C	5'-GAAACAACAATTTGCGCACCATTTG-3' (forward) 5'-CAAATGGTGCGCAAATTGTTGTTTC-3' (reverse)
K1112Q	5'-CTGAAGCTATGCAAATGGAAACAAC-3' (forward) 5'-GTTGTTTCCATTTGCATAGCTTCAG-3' (reverse)
Y621A	5'-GCTTCAAACGCAGTTGGTGCTAAAAACTATCCTGATAATG-3' (forward) 5'-CATTATCAGGATAGTTTTTAGCACCAACTGCGTTTGAAGC-3' (reverse)
T876A	5'-GGTGATATCGTAAAAGTAGCACCATCGTCTAAAGTAG-3' (forward) 5'-CTACTTTAGACGATGGTGCTACTTTTACGATATCACC-3' (reverse)
E243A	5'-CAAAAAGTTGTAGCAGTTGCACCATC-3' (forward) GATGGTGCAACTGCTACAACTTTTTG-3' (reverse)
V1062*	5'-GATGAAAATTAGCATACAAATGCG-3' (forward) 5'-CGCATTTGTATGCTAATTTTCATC-3' (reverse)
W808F	5'-GGAGTCACTTAGTCATTATTTCTCAACTGTACGTAC-3' (forward) 5'-GTACGTACAGTTGAGAAATAATGACTAAGTGACTCC-3' (reverse)